

**SYNTHON FORMATION IN INCLUSION COMPOUNDS OF  
PHENYLSUCCINIC ACID**

by

JEAN-EUDES ODOUNGA ODOUNGA

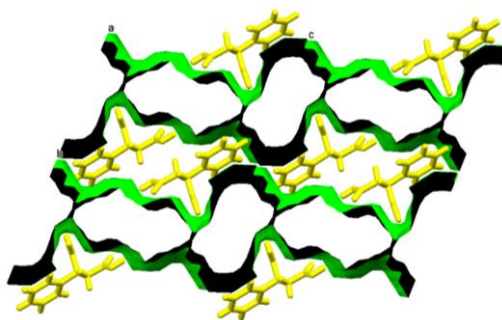
211211443

Thesis submitted in the fulfilment of the requirements for the degree

Master of Science in Chemistry

In the Faculty of Applied Sciences at

**CAPE PENINSULA UNIVERSITY OF TECHNOLOGY**



**Supervisor: Assoc. Prof. Nikoletta B. Báthori**

**2019**

The financial assistance of the National Research Foundation towards this research is acknowledged. Opinions expressed in this thesis and the conclusions arrived at, are those of the author, and are not necessarily to be attributed to the National Research Foundation

**CPUT copyright information**

The thesis may not be published either in part (in scholarly, scientific or technical journals) or in whole (as a monograph), unless permission has been obtained from the University

## DECLARARTION

I, Jean-Eudes ODOUNGA ODOUNGA, declare that this is my own original work and that all sources have been accurately reported and acknowledged, and that this document has not been previously in its entirety or in part submitted at any higher education institution for credit purposes.



.....  
Signature



.....  
Date

## ABSTRACT

The effect of chirality was investigated on selected physico-chemical properties by designing, synthesizing and analysing a series of racemic multicomponent crystals and their chiral counterparts. Eleven new crystalline materials were synthesised by combining phenylsuccinic acid (racemate or the *S*-enantiomer), a dicarboxylic acid, with primary or aromatic amines (aniline, pyridine, 4-picoline, 2,4-lutidine, 3,4-lutidine and 3,5-lutidine) and a drug pyrazine carboxamide (PCA). The carboxylic acids were combined with the amines to ensure the formation of the multicomponent crystals via acid-base heterosynthons. The varied positions of the functional groups on the aromatic amines gave rise to fine tune the packing of the crystals. The multicomponent crystals formed were examined by differential scanning calorimetry, thermogravimetric analysis, powder and single crystal X-ray diffraction. Fourier transform infrared spectroscopy was also performed for the complete characterisation of the new compounds. Ten out of the eleven novel compounds afforded multicomponent crystals with the expected composition, i.e. both the acid and the base were included in the crystal. These crystallisations resulted in a variety of different crystal forms, such as a true salt ( $[(R,S)\text{-PSA}^-][\text{ANI}^+]$ ), a salt solvate ( $[(S)\text{-PSA}^{2-}][2\text{ANI}^+]\cdot\text{ANI}$ ), solvates ( $(R,S)\text{-PSA}\cdot 2\text{PYR}$ ,  $(R,S)\text{-PSA}\cdot 2(4\text{PIC})$ ,  $(R,S)\text{-PSA}\cdot 2(2,4\text{LUT})$ ,  $(R,S)\text{-PSA}\cdot 2(3,4\text{LUT})$  and  $2(S\text{-PSA})\cdot 4(3,4\text{LUT})$ ), co-crystal salts ( $[(R,S)\text{-PSA}^{2-}]_2[3,5\text{LUT}^+]\cdot 2(R,S)\text{-PSA}$  and  $2[(S)\text{-PSA}^{2-}]_4[3,5\text{LUT}^+]\cdot 4(S)\text{-PSA}$ ) and a co-crystal  $(R,S)\text{-PSA}\cdot\text{PCA}$ . In these crystals, the phenylsuccinic acid showed great conformational variety. The analysis of the crystal packing ( $Z$  and related parameters, void analysis, etc.) highlighted the complexity of the packing of the multicomponent crystals and the significant differences between the racemic multicomponent crystals and their chiral counterparts. The acid-base heterosynthon, depicted as  $R_2^2(7)$ , was formed between the carboxylic acid and the pyridine moiety only in five of the multicomponent crystals. Interestingly, in the co-crystal of  $(R,S)\text{-PSA}\cdot\text{PCA}$  the carboxylic acid formed hydrogen bonds via the amide functional group of the PCA instead of via the nitrogen atom in the aromatic ring. The occurrence of the  $R_2^2(7)$  synthon was investigated with the aid of the Cambridge Structural Database and the statistical analysis showed that the heterosynthon is formed only in 25-30% of the cases. It was also concluded that formation of the  $R_2^2(7)$  synthon is less expected when crystallising enantiopure crystals because the limitations of the packing of chiral compounds adds an extra constraint to the packing of the crystal.

## ACKNOWLEDGEMENTS

### **I wish to thank:**

- My supervisor, Professor Nikoletta Bathori. The door to Prof. Bathori's office was always open whenever I had question about my research or writing. She steered me in the right direction whenever she thought I needed it.
- The staff of the Chemistry Department, CPUT. Without their participation and input, this research would not have been possible.
- The Barbour Group at Stellenbosch University, led by Professor Len Barbour, and the diffraction laboratory manager Dr. Leigh Loots.
- My parents, friends and colleagues for providing me with unfailing support and continuous encouragement throughout my years of study and through the process of researching and writing this thesis. This accomplishment would not have been possible without them. Thank you!

## **DEDICATION**

I dedicated my thesis to my family.

## TABLE OF CONTENTS

Declaration of own work	ii
Abstract	iii
Acknowledgement	iv
Dedication	v
List of figures	x
List of tables	xii
Glossary	xiii
Atom colours	xiv
Curve colours	xiv

## CHAPTER I: INTRODUCTION

1.1	Supramolecular chemistry .....	2
1.2	Multicomponent crystals .....	3
1.3	Pharmaceutical co-crystals .....	5
1.4	Salt versus co-crystal formation .....	7
1.5	Supramolecular synthons .....	8
1.6	Racemic versus chiral crystals .....	9
1.7	Crystal packing .....	10
1.8	Aspects of this study .....	11

## CHAPTER II: EXPERIMENTAL AND MATERIALS

<b>2.1</b>	<b>Experimental methods</b> .....	<b>16</b>
<b>2.1.1</b>	<b>Crystallisation and crystal growth</b> .....	<b>16</b>
<b>2.1.2</b>	<b>Crystallisation procedure</b> .....	<b>16</b>
<b>2.1.3</b>	<b>Thermal analysis</b> .....	<b>17</b>
	<b>(a) Differential scanning calorimetry (DSC)</b> .....	<b>17</b>
	<b>(b) Thermogravimetric analysis (TGA)</b> .....	<b>18</b>
<b>2.1.4</b>	<b>Fourier transform infrared spectroscopy (FTIR)</b> .....	<b>18</b>
<b>2.1.5</b>	<b>X-ray diffraction</b> .....	<b>18</b>
	<b>(a) Powder X-ray diffraction (PXRD)</b> .....	<b>19</b>
	<b>(b) Single crystal X-ray diffraction (SCXRD)</b> .....	<b>19</b>
<b>2.1.6</b>	<b>Computing components</b> .....	<b>21</b>
<b>2.2</b>	<b>Materials</b> .....	<b>23</b>
	<b>2.2.1 Dicarboxylic acids</b> .....	<b>23</b>
	<b>2.2.2 Coformers</b> .....	<b>24</b>
	<b>References</b> .....	<b>27</b>

## CHAPTER III: CRYSTAL STRUCTURES

<b>3.1</b>	Multicomponent crystal formation of phenylsuccinic acid with primary amines .....	<b>29</b>
<b>3.1.1</b>	<i>tert</i> -Butylammonium carbonate: $[2tBa^+][COO^{2-}]$ .....	<b>29</b>
<b>3.1.2</b>	Anilinium phenylsuccinate: $[(R,S)\text{-PSA}^-][ANI^+]$ .....	<b>31</b>
<b>3.1.3</b>	Anilinium (S)-phenylsuccinate aniline solvate: $[(S)\text{-PSA}^{2-}][2ANI^+]\cdot ANI$ .....	<b>32</b>
<b>3.2</b>	Multicomponent crystal formation of phenylsuccinic acid with aromatic amines .....	<b>34</b>
<b>3.2.1</b>	(R,S)-Phenylsuccinic acid pyridine solvate: (R,S)-PSA $\cdot$ 2PYR .....	<b>34</b>
<b>3.2.2</b>	(R,S)-Phenylsuccinic acid 4-picoline solvate: (R,S)-PSA $\cdot$ 2(4PIC) .....	<b>37</b>
<b>3.2.3</b>	(R,S)-Phenylsuccinic acid 2,4-lutidine solvate: (R,S)-PSA $\cdot$ 2(2,4LUT) .....	<b>38</b>
<b>3.2.4</b>	(R,S)-Phenylsuccinic acid 3,4-lutidine solvate: (R,S)-PSA $\cdot$ 2(3,4LUT) .....	<b>40</b>
<b>3.2.5</b>	(S)-Phenylsuccinic acid 3,4-lutidine solvate: 2(S-PSA) $\cdot$ 4(3,4LUT) .....	<b>45</b>
<b>3.2.6</b>	(R,S)-Phenylsuccinic acid 3,5-lutidine co-crystal salt: $[(R,S)\text{-PSA}^{2-}]_2[3,5LUT^+]_2\cdot 2(R,S)\text{-PSA}$ .....	<b>46</b>
<b>3.2.7</b>	(S)-Phenylsuccinic acid 3,5-lutidine co-crystal salt: $2[(S)\text{-PSA}^{2-}]_4[3,5LUT^+]_4\cdot 4(S)\text{-PSA}$ .....	<b>48</b>
<b>3.3</b>	Multicomponent crystal formation of phenylsuccinic acid with pyrazine carboxamide .....	<b>50</b>
<b>3.3.1</b>	(R,S)-Phenylsuccinic acid pyrazine carboxamide co-crystal: (R,S)-PSA $\cdot$ PCA .....	<b>50</b>
<b>References</b>	.....	<b>53</b>



## CHAPTER IV: BULK PROPERTY ANALYSIS

4.1	Conformation analysis of the phenylsuccinic acid moiety .....	55
4.2	Protonation state of PSA and the coformers in the multicomponent crystals .....	58
4.3	Z parameters of the multicomponent crystals .....	60
4.4	Structure-property relationships in PSA crystals .....	61
4.5	Occurrence of the $R_2^2(7)$ heterosynthon between carboxylic acid and aromatic amine moieties .....	67
	References .....	70

## CHAPTER V: SUMMARY AND CONCLUSION

5.	Summary and conclusion .....	72
----	------------------------------	----

## LIST OF FIGURES

<b>Figure 1.1</b> Schematic description of molecular and supramolecular chemistry .....	2
<b>Figure 1.2</b> Schematic representation of a salt, co-crystal, solvate, hydrate and polymorphs .....	3
<b>Figure 1.3</b> Classification diagram of multicomponents crystal .....	4
<b>Figure 1.4</b> Drug development pathway for MCCs .....	6
<b>Figure 1.5</b> Chemical structure of salt hydrate Entresto .....	6
<b>Figure 1.6</b> Differentiation of a co-crystal and a salt .....	7
<b>Figure 1.7</b> Supramolecular homosynthon and heterosynthon .....	8
<b>Figure 1.8</b> Representation of dimer and catemer motifs .....	10
<b>Figure 1.9</b> Structural line diagrams of acids and bases .....	12
<b>Figure 2.1</b> Chemical structures of (R,S) and (S)-Phenylsuccinic acid .....	23
<b>Figure 2.2</b> Chemical structures of coformers .....	24
<b>Figure 2.3</b> Work flow chart for crystallisation experiments .....	25
<b>Figure 3.1</b> Crystal structure of $[2\text{tBa}^+][\text{COO}^{2-}]$ .....	30
<b>Figure 3.2</b> Crystal structure of $[(\text{R,S})\text{-PSA}^-][\text{ANI}^+]$ .....	32
<b>Figure 3.3</b> Crystal structure of $[(\text{S})\text{-PSA}^{2-}][2\text{ANI}^+]\cdot\text{ANI}$ .....	33
<b>Figure 3.4</b> Crystal structure of (R,S)-PSA·2PYR .....	35
<b>Figure 3.5</b> Crystal structure of (R,S)-PSA·2(4PIC) .....	38
<b>Figure 3.6</b> Crystal structure of (R,S)-PSA·2(2,4LUT) .....	39
<b>Figure 3.7</b> Crystal structure of (R,S)-PSA·2(3,4LUT) .....	41
<b>Figure 3.8</b> Crystal structure of 2(S)-PSA·4(3,4LUT) .....	46
<b>Figure 3.9</b> Crystal structure of $[(\text{R,S})\text{-PSA}^{2-}]_2[3,5\text{LUT}^+]\cdot 2(\text{R,S})\text{-PSA}$ .....	47

<b>Figure 3.10</b> Crystal structure of 2[(S)-PSA <sup>2-</sup> ] <sub>4</sub> [3,5LUT <sup>+</sup> ] <sub>4</sub> ·4(S)-PSA .....	<b>49</b>
<b>Figure 3.11</b> Crystal structure of (R,S)-PSA·PCA .....	<b>51</b>
<b>Figure 4.1</b> Schematic representation of torsion angles of PSA .....	<b>55</b>
<b>Figure 4.2</b> $\Delta pK_a$ values for PSA and coformers .....	<b>59</b>
<b>Figure 4.3</b> Change in topology with crystallisation temperature .....	<b>61</b>
<b>Figure 4.4</b> Colour coded bar chart of melting points of PSA MCCs .....	<b>66</b>
<b>Figure 4.5</b> The $R_2^2(7)$ heterosynthon formed in co-crystals and salts .....	<b>67</b>
<b>Figure 4.6</b> Occurrence of carboxylic acid and pyridine moieties, and their combination in the CSD .....	<b>69</b>
<b>Figure 4.7</b> Occurrence of carboxylate and pyridinium moieties, and their combination in the CSD .....	<b>69</b>

## LIST OF TABLES

<b>Table 1.1</b> Summary of the main and subclasses of multicomponent crystals .....	<b>5</b>
<b>Table 2.1</b> List of successful solvents including polarity ( <i>P</i> ) and molecular size ( <i>N</i> , Å) .....	<b>16</b>
<b>Table 2.2</b> Physical properties of the dicarboxylic acids (PSA) .....	<b>23</b>
<b>Table 2.3</b> Physical properties of coformers .....	<b>25</b>
<b>Table 3.1</b> Summary of crystallisation experiments .....	<b>29</b>
<b>Table 3.2</b> Crystal data for [2tBa <sup>+</sup> ][COO <sup>2-</sup> ], [(R,S)-PSA <sup>-</sup> ][ANI <sup>+</sup> ] and [(S)-PSA <sup>2-</sup> ][2ANI <sup>+</sup> ].ANI .....	<b>30</b>
<b>Table 3.3</b> Hydrogen bonds in [2tBa <sup>+</sup> ][COO <sup>2-</sup> ], [(R,S)-PSA <sup>-</sup> ][ANI <sup>+</sup> ] and [(S)-PSA <sup>2-</sup> ][2ANI <sup>+</sup> ].ANI .....	<b>31</b>
<b>Table 3.4</b> Crystal data for (R,S)-PSA·2PYR, (R,S)-PSA·2(4PIC) and (R,S)-PSA·2(2,4LUT) .....	<b>36</b>
<b>Table 3.5</b> Hydrogen bonds in (R,S)-PSA·2PYR, (R,S)-PSA·2(4PIC) and (R,S)-PSA·2(2,4LUT) .....	<b>36</b>
<b>Table 3.6</b> Crystal data for (R,S)-PSA·2(3,4LUT), 2(S)-PSA·4(3,4LUT), [(R,S)-PSA <sup>2-</sup> ][2(3,5LUT <sup>+</sup> )·2(R,S)-PSA] and 2[(S)-PSA <sup>2-</sup> ][4(3,5LUT <sup>+</sup> )·4(S)-PSA] .....	<b>42</b>
<b>Table 3.7</b> Hydrogen bonds in (R,S)-PSA·2(3,4LUT), 2(S)-PSA·4(3,4LUT), [(R,S)-PSA <sup>2-</sup> ][2(3,5LUT <sup>+</sup> )·2(R,S)-PSA] and 2[(S)-PSA <sup>2-</sup> ][4(3,5LUT <sup>+</sup> )·4(S)-PSA] .....	<b>43</b>
<b>Table 3.8</b> Crystal data for (R,S)-PSA·PCA .....	<b>52</b>
<b>Table 3.9</b> Hydrogen bonds in (R,S)-PSA·PCA .....	<b>52</b>
<b>Table 4.1</b> Torsion angles and molecular conformations of PSA in MCCs .....	<b>56</b>
<b>Table 4.2</b> Δ <i>pK<sub>a</sub></i> values for PSA and selected coformers .....	<b>59</b>
<b>Table 4.3</b> Space groups and <i>Z</i> parameters for PSA MCCs .....	<b>60</b>
<b>Table 4.4</b> Densities, voids, solvent percentages for PSA MCCs .....	<b>62</b>
<b>Table 4.5</b> Thermoanalytical data for PSA MCCs .....	<b>66</b>

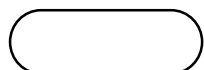
## GLOSSARY

<b>Terms/Acronyms/Abbreviations</b>	<b>Definitions/Explanation</b>
<b>a, b, c</b>	<b>Unit cell axes</b>
<b><math>\alpha</math></b>	<b>Angle between b and c unit cell axes</b>
<b><math>\beta</math></b>	<b>Angle between a and c unit cell axes</b>
<b><math>\gamma</math></b>	<b>Angle between a and b unit cell axes</b>
<b>V</b>	<b>Unit cell volume</b>
<b>Z</b>	<b>Number of formula units per cell</b>
<b>ANI</b>	<b>Aniline</b>
<b>API</b>	<b>Active pharmaceutical ingredient</b>
<b>C<sub>arom</sub></b>	<b>Aromatic carbon</b>
<b>CSD</b>	<b>Cambridge Structural Database</b>
<b>DSC</b>	<b>Differential scanning calorimetry</b>
<b>GFSC</b>	<b>Generated from single crystal</b>
<b>LUT</b>	<b>Lutidine</b>
<b>MCC</b>	<b>Multicomponent crystal</b>
<b>N<sub>arom</sub></b>	<b>Aromatic nitrogen</b>
<b>PI</b>	<b>Polarity index</b>
<b>PCA</b>	<b>Pyrazine carboxamide</b>
<b>PIC</b>	<b>Picoline</b>
<b>PXRD</b>	<b>Powder X-ray diffraction</b>
<b>PYR</b>	<b>Pyridine</b>
<b>(R,S)-PSA</b>	<b>Racemic phenylsuccinic acid</b>
<b>(S)-PSA</b>	<b>S-phenylsuccinic acid</b>
<b>S.O.F</b>	<b>Site occupancy factor</b>
<b>TBA</b>	<b>Tertbutylamine</b>
<b>TGA</b>	<b>Thermogravimetric analysis</b>
<b>T<sub>on</sub></b>	<b>Onset temperature</b>
<b>T<sub>peak</sub></b>	<b>Peak temperature</b>
<b><math>\epsilon</math></b>	<b>Dielectric constant</b>

## ATOM COLOURS



Carbon



Hydrogen



Oxygen



Nitrogen

## CURVE COLOURS



(R,S)/(S)-PSA



PCA



GRINDING



CO-CRYSTAL/SALT (BULK)



CO-CRYSTAL/SALT (SINGLE CRYSTAL)

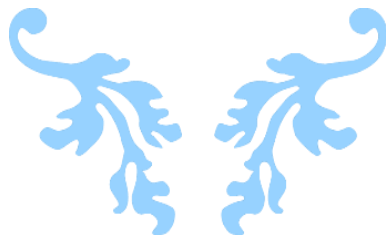


---

# CHAPTER I

---

## INTRODUCTION



## Introduction

### 1.1 Supramolecular chemistry

Nobel Laureate Jean-Marie Lehn described supramolecular chemistry as “the chemistry of molecular associations and of the intermolecular bond”.<sup>1</sup> The need to comprehend the making of electrical activities through charged species of sodium and potassium in the body nerve system<sup>2</sup> led to his research in the area of supramolecular chemistry. In 1806, the first multicomponent crystal, chlorine hydrate, was isolated by Humphrey Davy, but it was only later, in 1896 with Emil Fischer’s investigation on the functioning of enzymes that a specific approach in supramolecular chemistry truly began, and was further conducted by the study of Lehn on host-guest compounds.<sup>3</sup>

Supramolecular chemistry developed at high rate during the last decade, shown by a large number of publications. Nowadays, it has progressed into an interdisciplinary field linking physics, biology and chemistry and its development had a significant impact on the synthesis of crystalline structures of distinctive forms and sizes with the required functions. These supramolecular compounds are formed by linking molecules via intermolecular interactions that are described by their capacity to contribute in directional or non-directional forces (Figure 1.1). Although nondirectional interactions have a significant part to play in the spacing and conformation of supramolecular elements, directional forces usually are important for the geometry and spatial arrangement of component molecules.<sup>4,5,6</sup> The general purpose of supramolecular chemistry, is the synthesis of supermolecules using hydrogen bonding,  $\pi$ - $\pi$  stacking, charge transfer, Van der Waals and/or dipole-dipole interactions with desired properties or functions.<sup>7</sup>

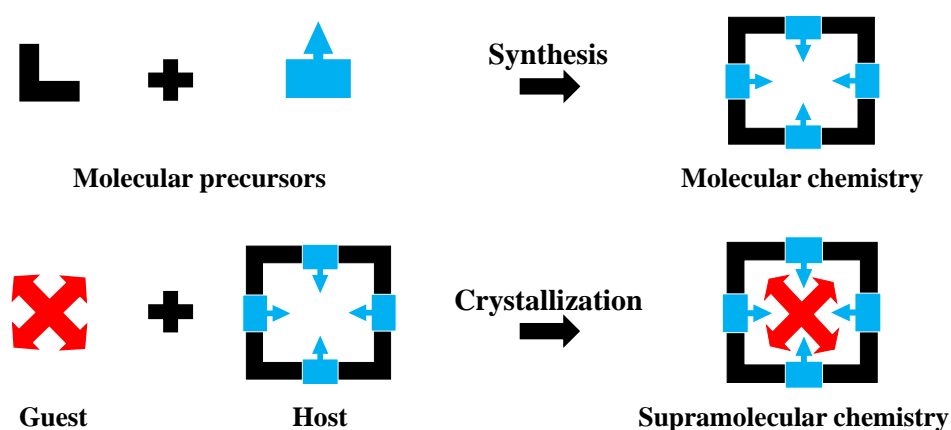


**Figure 1.1** Schematic description of molecular and supramolecular chemistry.



## 1.2 Multicomponent crystals

Multicomponent crystals (MCCs) have a minimum of two distinct chemical entities and can be categorised as co-crystals, salts, solvates or hydrates. The earliest multicomponent crystal reported in 1844 by Friedrich Wöhler was quinhydrone, a green solid resulting from mixing solutions of benzoquinone and hydroquinone, in a 1:1 ratio.<sup>8</sup> Over the years co-crystals have been denoted and categorised as molecular complexes<sup>9</sup>, multicomponent molecular crystals<sup>10,11</sup>, and ionic co-crystals.<sup>12</sup> In 2012, forty six authors<sup>13</sup> issued a viewpoint article entitled, “Polymorphs, Salts, and Co-crystals: What’s in a name” defining the term co-crystal as “solid crystals made from at least two distinctive molecular and/or ionic compounds usually in a stoichiometric ratio”. The components present in crystals are all organic species but the presence of specific elements in the structure of these supermolecules, such as charged species, water, solvent and neutral species is used to distinguish the type of crystals but also to classify them as salt, hydrate, solvate or co-crystal, respectively. Another important occurrence in supramolecular architecture is polymorphism, which is the formation of different packing arrangements of the same compound (Figure 1.2).<sup>14</sup>

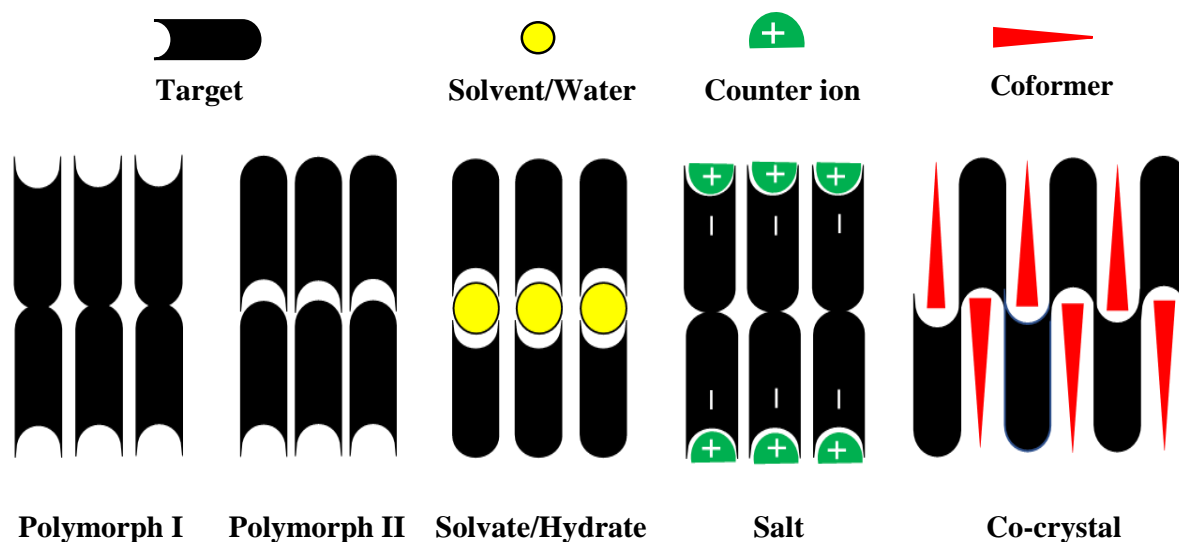


**Figure 1.2** Schematic representation of a salt, co-crystal, solvate, hydrate and polymorphs.

The classification of crystal structures brought some disagreement between the Food and Drug Administration (FDA) and the academic community in order to find the most appropriate classification. Back in 2011, the FDA agency announced draft guidelines regarding the definition and classification of co-crystals as “dissociable API-excipient molecular

complexes".<sup>15</sup> In reference to the work of Aitipamula et al. contesting the FDA classification by suggesting the combination of co-crystals with salts, the classification of multicomponents crystals was re-examined. The authors claimed that co-crystals and salts cannot have different sets of rules and regulations since the differentiation of these crystals is at times challenging and cofomers which are similarly behaving like ions, frequently behave more like APIs than like an inactive substance. However, the concept of Aitipamula et al. was further reviewed by Grothe et al.<sup>16</sup> For example, looking at the multicomponent crystal of isonicotinamide pyromellic acid hydrate containing two ions and a solvent, the classification proposed by Aitipamula et al. does not provide a group for this kind of crystals. However, the Venn diagram proposed by Grothe et al. does provide a name, a salt solvate which requires the asymmetric unit to have a solvent molecule and either a cofomer or a minimum of two ions (Figure 1.3). The incomplete categorisation of Aitipamula et al. led to a reconsideration of the three main classes, listed in Table 1.1, as well as their seven subclasses. By definition multicomponent crystals are crystals with a minimum of two distinctive residues in the crystal lattice. The amount of residues present in the asymmetric unit is represented by the symbol  $Z^R$  and these elements can be of different kind, a solvent, a co-former or a charged species. The types of residues are important to determine the subclasses of crystals which is well described by the classification system recommended by Grothe et al. Originating from the Venn diagram, three main classes and seven subclasses are observed (Figure 1.3).

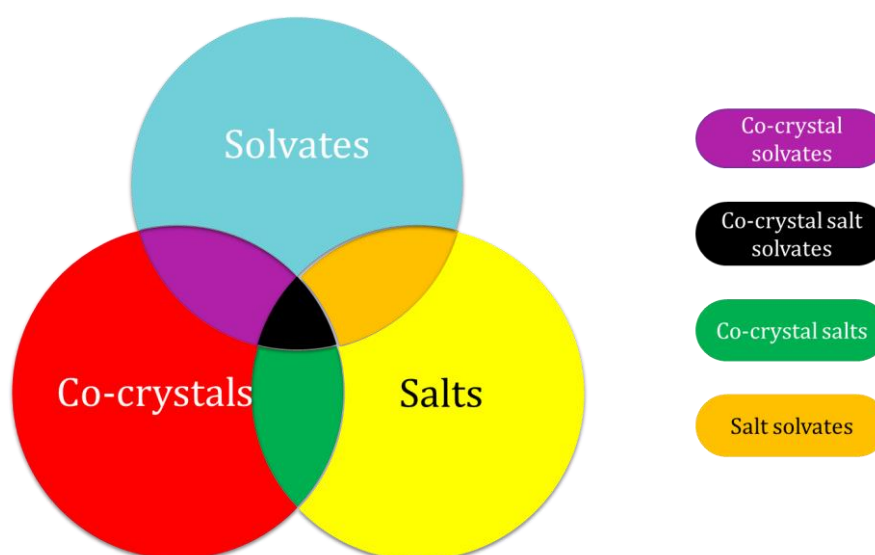


**Figure 1.3** Classification diagram of multicomponents crystal.

**Table 1.1** Summary of the main and subclasses of multicomponent crystals.

<b>3 MAIN CLASSES</b>	<b>SALT</b>	Crystal with a minimum of two ions
	<b>CO-CRYSTAL</b>	Crystal containing a coformer molecule and either an extra coformer or a minimum of two ions
	<b>SOLVATE</b>	Crystal containing a solvent molecule and either a coformer or a minimum of two ions
<b>7 SUBCLASSES</b>	<b>TRUE SALT</b>	Only ions
	<b>TRUE CO-CRYSTAL</b>	Only coformers
	<b>TRUE SOLVATE</b>	At least one solvent and precisely one coformer, but no ions
	<b>CO-CRYSTAL SALT</b>	At least one coformer and a minimum of two ions, but no solvents
	<b>CO-CRYSTAL SOLVATE</b>	At least one solvent and a minimum of two coformers, but no ions
	<b>SALT SOLVATE</b>	At least one solvent and a minimum of two ions, but no coformers
	<b>CO-CRYSTAL SALT SOLVATE</b>	At least one solvent, and a minimum of two ions, with one or more coformers

The concept of Aitipamula et al., that salt and co-crystals are alike in some circumstances to one another and to recommend that co-crystals and salts have to fall under the same group, is acceptable to the scientific community. Nevertheless, even though some crystals are very similar, others are very distinct due to the type of interactions present in salts (ionic) which can vary significantly from those in co-crystals.<sup>32</sup>

### 1.3 Pharmaceutical co-crystals

Pharmaceutical co-crystals are multicomponent crystals containing at least one active pharmaceutical ingredient (API) and one coformer compound, where the latter is typically selected from a list of chemicals generally regarded as safe (GRAS).<sup>17,18</sup> These molecular constituents fuse through secondary interactions, typically hydrogen bonds, in a definite ratio in the lattice. The particular attention towards pharmaceutical co-crystals before and in present days is due to their possible usefulness as substitute drug elements with upgraded physico-chemical properties. APIs frequently have unfavourable solid-state properties<sup>19</sup>, but these

properties can be changed by altering the solid state structure of the API with a coformer to improve its properties without compromising the therapeutic efficacy of the drug. However, the path to take to obtain a medicine is a major assignment and usually, developing a therapeutic co-crystal as the API into a medication may be separated to eight steps (see Figure 1.4).<sup>20</sup>

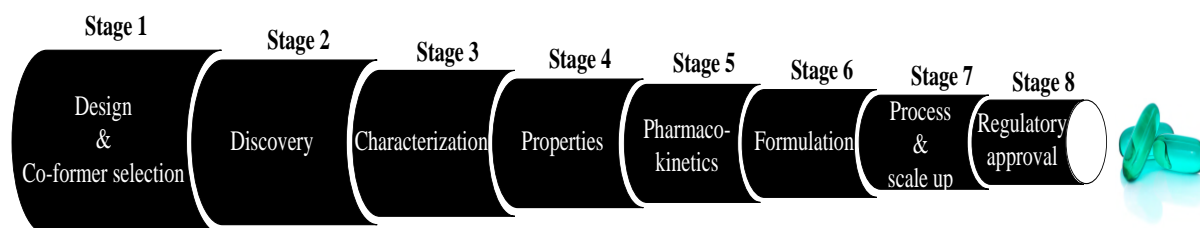


**Figure 1.4** Drug development pathway for MCCs

Through these manipulations medicines were improved. To date, only a few pharmaceutical multicomponent crystals have been approved by the FDA as medication. As an example the salt hydrate Entresto<sup>™</sup>, a product of Novartis for the treatment of chronic heart failure<sup>21</sup>, was approved in 2015. The salt hydrate is a mixture of sacubitril and valsartan with molecular formula  $C_{96}H_{120}N_{12}Na_6O_{21}$  (see Figure 1.5). Many other cases are under study such as metaxalone, the API present in Skelaxin<sup>®</sup>, prescribed for relief related to musculoskeletal soreness.<sup>22</sup> The multicomponent crystals of metaxalone with succinic and fumaric acid known as GRAS compounds gave results with better bioavailability than metaxalone only.<sup>23</sup>

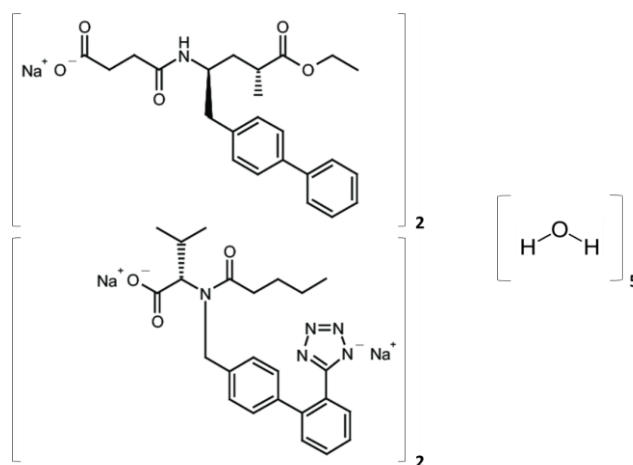


**Figure 1.5** Chemical structure of the salt hydrate Entresto<sup>™</sup>

### 1.4 Salt versus co-crystal formation

If the constituents of the multicomponent crystals have ionizable functional groups such as carboxylic acid or amine moieties, it is possible to form a salt of the target compound by the displacement of the hydrogen atom from an acidic group to a basic moiety<sup>24</sup>. Co-crystals do not essentially display fixed stoichiometries but salts must exhibit fixed ratios due to their charged nature. A typical example to describe this problem occurs when carboxylic acids are co-crystallised with aromatic amines (Figure 1.6). In this case, the proton of the carboxylic acid can stay on the acid, forming a co-crystal, or occasionally, it transfers to the base to form a salt. The differentiation between these two extremes by X-ray diffraction methods locating the position of the hydrogen atom, can be challenging because of the low X-ray scattering power of the hydrogen.<sup>25</sup> In some cases, the displacement of the proton might then be considered as a “continuum” from one extreme to the other.<sup>26</sup> The geometrical analysis of the heavy atoms, i.e. the bond length of the C-O bonds, is often used to aid the decision on the question of co-crystal vs. salt formation. (Importantly, the observation of the X-ray analysis should be supported by spectroscopic measurements, typically Fourier Transform Infrared spectrometry.)

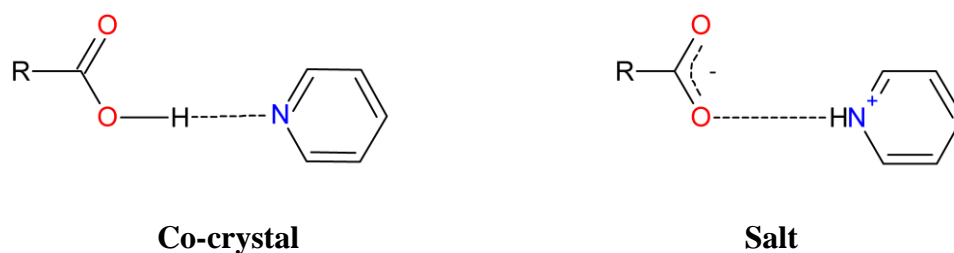


**Figure 1.6** Differentiation of a co-crystal and a salt

The outcome of the co-crystallisation of an acidic and a basic component, i.e. the formation of a salt or a co-crystal, is based on the  $pK_a$  differences between the two parties. Nangia et al. defined the so called “ $pK_a$ -rule” after investigating large amount of crystals obtained from co-crystallisations of carboxylic acids and substituted pyridines as acid-base pairs.<sup>27</sup> When calculating the  $\Delta pK_a$  values for each pairs of compounds crystallised together ( $\Delta pK_a = pK_a$  (base) –  $pK_a$  (acid))<sup>28</sup> the following pattern was observed: compound pairs that resulted in negative  $\Delta pK_a$  values will most likely form co-crystals and when the difference is greater than 2-3  $pK_a$  units, salt formation is expected. For a  $pK_a$  difference in the range of 0 to 3, the outcome of the crystallisation is unpredictable. This rule of thumb was quantitated by Cruz Cabeza, who studied more than six thousand crystalline complexes with acid-base pairs obtained from the Cambridge Structural Database.<sup>29</sup> Three areas were delimited and examined

individually due to their distinct occurrences. When the  $\Delta pK_a < -1$  (defined as zone 1) it is almost certain to obtain a co-crystal; if the  $\Delta pK_a > 4$  (zone 3) nearly all compounds formed are salts. When the  $\Delta pK_a$  value is between -1 and 4 (zone 2) both a co-crystal or a salt can be formed. It is also essential to note that  $pK_a$  values may be influenced and are subject to change in various solvents, therefore the selection of a solvent is crucial, especially in syntheses of organic salts.<sup>30, 31</sup>

### 1.5 Supramolecular synthons

Multicomponent crystal design is based on the use of supramolecular synthons where the latter is defined as a linear assembly between molecular building units.<sup>32</sup> Synthons are formed following the association or assembly of two molecules via their functional groups by interacting with one another in an expected manner by non-covalent interactions. Based on the interacting functional groups, there are two principal types of synthons that can be defined: the homosynthon and heterosynthon (Figure 1.7). Homosynthons are formed between two identical functional groups, while heterosynthons are built from the interaction of different but complementary moieties. The functional groups in carboxylic acids, amides or alcohols are self-complementary due to the presence of both hydrogen bond donors and acceptors and are consequently capable of building homosynthons. Other functionalities have exclusively hydrogen bond donors or acceptors, thus these compounds are likely to form heterosynthons with compounds that have complementary functional groups.<sup>33</sup> Nevertheless, all groups are capable to build heterosynthons with other corresponding functional groups. As an example, carboxylic acid functional groups, are self-complementary and can assemble together to form a homosynthon, whereas the same acid reacting with pyridine, which has a different functional group, will result in the formation of a heterosynthon.

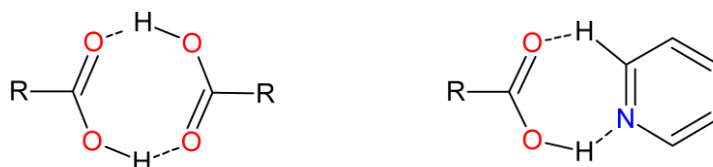


**Figure 1.7** Supramolecular homosynthon (left) and heterosynthon (right).

## 1.6 Racemic versus chiral crystals

A Large number of drug targets are enzymes that have chiral active sites, therefore a significant number of currently used small molecule drugs are chiral. Chiral drugs, containing at least one chiral centre, are extensively considered, but most of the drugs are consumed as racemic blends with the same amount of R and S enantiomers. These individual drug enantiomers exhibit distinctive pharmacological actions in a chiral domain, like the human body. The fact, that in a drug only one of the two enantiomers is responsible for the effectiveness of a treatment, and that its counterpart has an unknown pharmacological activity or may present a danger for some organs, highlights the fundamental importance of the racemic and the enantiopure formulations.<sup>34</sup> When new formulations are planned for a selected API, such as co-crystal formation or polymorph screening to improve some of the physicochemical properties, (melting temperature, solubility, etc.), it is vital to investigate the packing arrangement of the new racemic and chiral crystalline solids and understand the differences or similarities of the synthon formation of these compounds.<sup>35</sup>

According to Wallach's rule (an empirically deduced rule), the pure enantiomer forms a less dense crystal structure than the racemic counterpart.<sup>36</sup> From this deduction, Brock ascribed this inclination of the racemate to be more stable and denser than their chiral partners, to their ideal packing arrangements in racemic space groups in contrast with chiral ones, and not a result of any special sorts of interactions between opposite enantiomers.<sup>37</sup> While Brock's conclusion was based on single component crystals, Lemmerer et al. examined the single crystal structures of two series of co-crystals of chiral carboxylic acids (2-phenylbutyric acid (PBA)), 2-phenylpropionic (PPA) with isonicotinamide (INA). (R)-PPA and (S)-PPA formed catemers (see Figure 1.8).<sup>36</sup> (R,S)-PBA rather formed the dimer motif, due to the longer chain of the butyric acid in comparison with the propionic acid, requiring a change in motif from catemer to dimer, which is the favoured conformation for carboxylic acids with large substituents.<sup>38</sup> The melting point of the racemic co-crystals was found to be higher than the chiral ones, while the crystal densities and packing efficiencies shows that the chiral structures pack less closely and therefore are expected to have a lower stability and be less thermally stable.

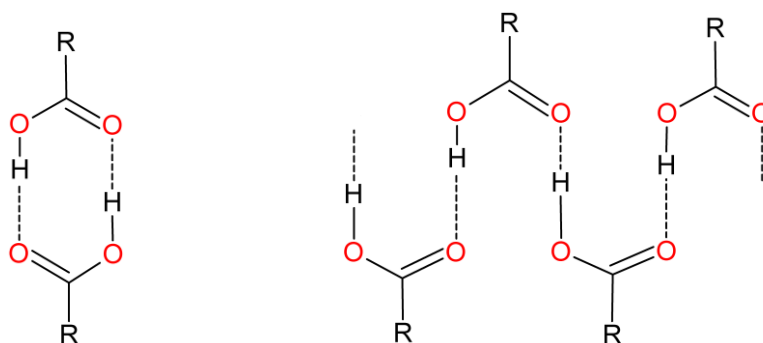


**Figure 1.8** Representation of dimer (left) and catemer (right) motifs.

### 1.7 Crystal packing

The number of molecules in the entire unit cell is denoted as  $Z$ , and the symbol  $Z'$  is defined as the number of formula units in the crystallographic unit cell divided by the number of independent general positions<sup>39</sup>, which is the amount of molecules in the unit cell divided by the group multiplicity or the number of independent general positions.<sup>40</sup> The molecules being free to bond together in three dimensions in the asymmetric unit is the reason for the complexity of that same asymmetric unit, which is different from asymmetric units constrained to operate through specific symmetry operations. Besides, the interpretation of what comprises the formula unit can be challenging, especially in multicomponent crystals, such as the salt of a doubly protonated amine *o*-phenylenediamine (PDA), with the parameter  $Z''$  (the sum of chemical entities within the asymmetric unit<sup>41,42</sup>) being equal to 26 molecules or charged species comprising eight independent *o*-PDA cations in the asymmetric unit. Therefore, the value that must be assigned to  $Z'$ , regardless of the large value of  $Z''$ , is 2. The right value was found by neutron diffraction that showed the precise position of the protons. The predicament is even more equivocal for nonstoichiometric solvates and inclusion compounds where the exact contents of the asymmetric unit may not even be determined.<sup>39</sup> Additionally, it is fundamental to understand that the  $Z'$  parameter emerges from computational summary of real diffraction information and this portrayal might embody an unreliable description of the real laboratory condition. For example, crystals with low symmetry space groups, like  $P1$  and  $Cc$  with  $Z' > 1$ , were found to be afterwards defined by a greater symmetry model with accordingly reduced  $Z'$  number.<sup>43</sup>

The parameter  $Z''$ , is very important especially for complex crystal structures with ratio that cannot be divided in order to give a smaller integer ratio. For instance, the  $C_{60}$  calixarene



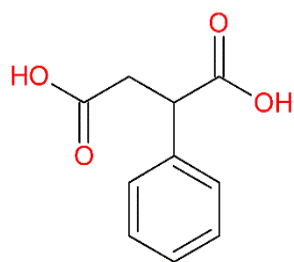
toluene co-crystal is, a remarkable inclusion complex of formula (calix[5]arene)<sub>4</sub>·(C<sub>60</sub>)<sub>5</sub>·(toluene)<sub>2</sub>.<sup>44</sup> The structure has a  $Z'$  with the value of 1 and a ratio of 4:5:2 that cannot be divided to obtain a smaller common denominator, but the  $Z'' = 11$  points out the complexity of structure. Apart from the mentioned parameters, a third one,  $Z'$ , is the quantity of distinct kinds of residues (solvents, charged species and neutral compounds).<sup>45</sup> To explain the crystal packing phenomena of complex structures it is crucial to list explicitly the parameters  $Z'$ ,  $Z''$  and  $Z'$ .<sup>46</sup> Approximately 9.3% of crystals in the CSD crystallise with  $Z' > 1$ .<sup>47</sup> Some types of compounds, especially chiral molecules show a preference of forming structures with high  $Z'$ .<sup>48</sup> The trend observed was associated with a “frustration” of at least two interactions competing during the nucleation process and growth.<sup>38</sup> Nevertheless, from previous research<sup>49,50,51,52</sup> it was concluded that despite the fact that these two factors (frustration and nucleation) are important, it is obvious that the variety of structures with high  $Z'$  is too large to allow for any extensive generalisation.<sup>40</sup>

## 1.8 Aspects of this study

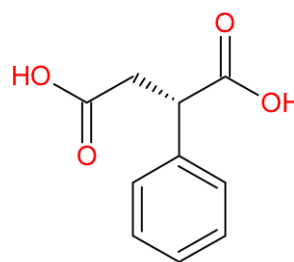
Based on the literature review presented here and our previous experience in crystal engineering, the introduction of chirality when forming new multicomponent crystals is a suitable way to alter the crystal packing and eventually the physicochemical properties of the new multicomponent crystals.

The purpose of this research was to design and synthesise first, a set of multicomponent crystals where the drug molecule was replaced by a simple chemical unit (phenylsuccinic acid) which has limited auxiliary interaction options and conformational motions, while the co-crystallising compounds were tertbutylamine, aniline, pyridine, 4-picoline, 2,4-lutidine, 3,4 and 3,5 lutidine (Figure 1.9). The mentioned acids and bases were selected due to their capacity to hydrogen bond via O-H···N interactions. The second section of the study focused on the synthesis of pharmaceutical co-crystals using pyrazinamide (pyrazine carboxamide), an important drug that shortens tuberculosis therapy<sup>53</sup> as an API while the co-crystallising compound or cofomer was phenylsuccinic acid. Phenylsuccinic acid was used in the form of a racemic mixture, and in an optically active enantiomer (S) form, for both model and pharmaceutical co-crystals. After obtaining the desired single crystals, the aim was the examination of the synthesised crystalline structures via the synthons formed within them to understand the effect of the racemic and chiral crystal arrangement.

## ACIDS

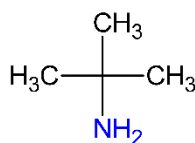


(R,S)-PSA

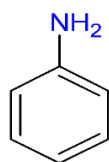


(S)-PSA

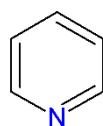
## BASES



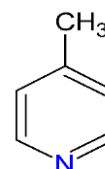
TBA



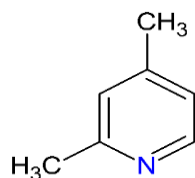
ANI



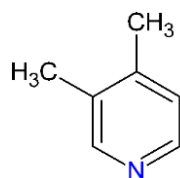
PYR



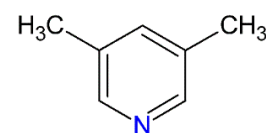
4-PIC



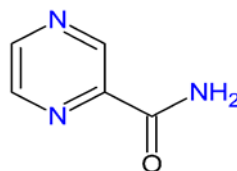
2,4 LUT



3,4 LUT



3,5-LUT



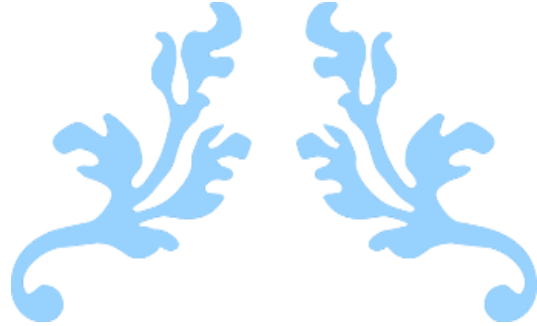
PCA

**Figure 1.9** Structural line diagrams of acids (rac-phenylsuccinic acid: (R,S)-PSA; S-phenylsuccinic acid: (S)-PSA), and bases (Tertbutylamine: TBA; Aniline: ANI; pyridine: PYR; 4-methylpyridine: 4-PIC; 2,4-dimethylpyridine: 2,4-LUT; 3,4-dimethylpyridine: 3,4-LUT; 3,5-dimethylpyridine: 3,5-LUT; pyrazine carboxamide: PCA).

## References

- <sup>1</sup> Lehn J. M. 1978. *Pure Appl. Chem.* 50 (9-10), 871-892.
- <sup>2</sup> Lehn J. M. 1992. Supramolecular chemistry - scope and perspectives molecules - supermolecules - molecular devices. In *Nobel lectures, chemistry 1981-1990*, Frängsmyr, T.; Malmström, B. G., Eds. World Scientific: Singapore; p 708.
- <sup>3</sup> Desiraju G.R., Vittal J.J. & Ramanan A. 2011. *Crystal engineering: A textbook*, Mainland Press, Singapore; p 57-58.
- <sup>4</sup> Steed J. W., & Atwood, J. L. 2009. *Supramolecular chemistry*. 2nd ed.; John Wiley & Sons, Ltd: Chichester.
- <sup>5</sup> Desiraju G. R. 1989. *Crystal engineering the design of organic solids*. Elsevier: New York.
- <sup>6</sup> Novoa J. J., D'Oria, E. & Carvajal, M. A. 2007. *Understanding the nature of the intermolecular interactions in molecular crystals. A theoretical perspective*. Wiley-VCH Verlag GmbH & Co. KGaA; p 25-57.
- <sup>7</sup> Dunitz J. D. 1991. Phase transitions in molecular crystals from a chemical viewpoint. *Pure Appl. Chem.* 63 (2), 177-185.
- <sup>8</sup> Wohler F. 1844. *Chem. Pharm.* 51, 145-163.
- <sup>9</sup> Desiraju G. R. 2003. *CrystEngComm.* 5, 466-467.
- <sup>10</sup> Bond A. D. 2007. *CrystEngComm.* 9, 833-834.
- <sup>11</sup> Dunitz J. D. 2003. *CrystEngComm.* 5, 506.
- <sup>12</sup> Braga D., Grepioni F., Maini L., Prosperi S., Gobetto R. & Chierotti M. R., *Chem. Commun.*, 2010, 46, 7715-7717.
- <sup>13</sup> Aitipamula S., Banerjee R., Bansal A. K., Biradha K., Cheney M. L., Choudhury A. R., Desiraju G. R., Dikundwar A. G., Dubey R., Duggirala N., Ghogale P. P., Ghosh S., Goswami P. K., Goud N. R., Jetti R. R. K. R., Karpinski P., Kaushik P., Kumar D., Kumar V., Moulton B., Mukherjee A., Mukherjee G., Myerson A. S., Puri, A. Ramanan, T. Rajamannar, C. M. Reddy, N. Rodriguez-Hornedo, R. D. Rogers, T. N. Guru Row, P. Sanphui V., Shan N., Shete G., Singh A., Sun C. C., Swift J. A., Thaimattam R., Thakur T. S., Thaper R. K., Thomas S. P., Tothadi S., Vangala V. R., Variankaval N., Vishweshwar P., Weyna D. R. & Zaworotko M. J. 2012. *Cryst. Growth Des.* 12, 2147-2152.
- <sup>14</sup> Moulton B. & Zaworotko M.J. 2001. *Chem Rev.* 101(6):1629-1658.
- <sup>15</sup> Guidance for Industry: Regulatory Classification of Pharmaceutical co-crystals; U.S. FDA: Silver Spring, MD, 2011.
- <sup>16</sup> Grothe E., Meekes H., Vlieg E. ter Horst J. H. & de Gelder R. 2016. *Cryst. Growth Des.* 16, 3237-3243.
- <sup>17</sup> Generally Recognized as Safe. <http://www.fda.gov/food/ingredientspackaginglabeling/gras/default.html>. [February 2019]
- <sup>18</sup> Bolla G. & Nangia A. 2016. *CrystEngComm*, 52, 8342-8360.
- <sup>19</sup> Viertelhaus M. & Hafner A. 2015. *Chemistry Today*. Vol 33: 23-26.
- <sup>20</sup> Duggirala N.K., Perry M.L., Almarsson O. & Zaworotko M.J. 2016. *CrystEngComm*, 52, 640-655.
- <sup>21</sup> <https://www.novartis.com/news/media-releases/novartis-new-heartfailure-medicine-lcz696-now-called-entrestotm-approved-fda>.
- <sup>22</sup> Toth P.E. & Urtis J. 2004 *Clin. Ther.* 26, 1355-1367.
- <sup>23</sup> Holland J., Frampton C., Chorlton A. & Gooding D. 2014. *US Pat.* 8,871,793 B2.
- <sup>24</sup> Lide. D. R. 2000. *CRC Handbook of Chemistry and Physics*. 81st, CRC Press: Boca Raton; 2-55.
- <sup>25</sup> Childs S. L., Stahly G. P. & Park A. 2011. *Mol. Pharm.*, 4, 323-338.
- <sup>26</sup> Ramon G., Davies K. & Nassimbeni L. R. 2014. *CrystEngComm*, 16, 5802-5810
- <sup>27</sup> Bhogala. B. R, Basavoju. S & Nangia. A. 2005. *CrystEngComm.*, 7, 551-562.
- <sup>28</sup> Stahl P. H. & Wermuth. C. G. 2002. *Handbook of Pharmaceutical Salts: Properties, Selection and Use*. International Union of Pure and Applied Chemistry, VHCA: Wiley-VCH: Weinheim, New York.
- <sup>29</sup> Cruz-Cabeza, A. J. 2012. *CrystEngComm*, 14: 6362-6365.
- <sup>30</sup> Black S. N., Collier E. A., Davey R. J. & Roberts R. J. 2007. *J. Pharm. Sci.* 96, 1053-1068.
- <sup>31</sup> Cox B. 2014. *Acids and Bases*. Oxford: OUP Oxford.
- <sup>32</sup> Desiraju, G.R. 1995. *Angew. Chem, Int Ed. Engl.*, 34, 2311-2327.
- <sup>33</sup> Vijayaraj S. & Saravana Kumar A. 2013. *IJPDT*, 3 (1), 35-40.
- <sup>34</sup> Mohan S.J., Mohan E.C. & Yamsani M.R. 2009. *IJPSN*. Vol 1: 309-316.
- <sup>35</sup> Ayamane A. 2015. *Melting point structure relationships of multicomponent crystals*, Master thesis, Cape Peninsula University of Technology, Cape Town South Africa.
- <sup>36</sup> Lemmerer A., Bathori N.B. & Bourne S.A. 2008. *Acta Cryst, B64*, 780-790.
- <sup>37</sup> Brock C. P., Schweizer, W. B. & Dunitz, J. D. 1991. *J. Am. Chem. Soc.* 113, 9811-9820.

- 
- <sup>38</sup> Das D. & Desiraju, G. R. 2006. *CrystEngComm*, 8, 674–679.
- <sup>39</sup> Steed K.M. & Steed J.W. 2015. *Chem. Rev.* 115, 2895–2933
- <sup>40</sup> Brock C.P. 2016. *Acta Cryst.* B72, 807–821
- <sup>41</sup> Van Eijck B. P. & Kroon J. 2000. *Acta Cryst. Sect. B*, 56, 535-542.
- <sup>42</sup> Clegg W. & Nichol G. S. 2006. *Cryst. Growth Des.* 6, 451-460.
- <sup>43</sup> Marsh R. E. 2005. *Acta Cryst. Sect. B*, 61, 359.
- <sup>44</sup> Atwood J. L.; Barbour L. J. & Raston, C. L. 2002. *Cryst. Growth Des.* 2, 3-6.
- <sup>45</sup> Anderson K. M., Probert M. R., Whiteley C. N., Rowland A. R. Goeta A. E. & Steed J. W. 2009. *Cryst. Growth. Des.* 9, 1082-1087.
- <sup>46</sup> Thakuria R.; Cherukuvada S. & Nangia A. 2012. *Cryst. Growth Des.* 12, 3944-3953.
- <sup>47</sup> Cambridge Structural Database search version 5.39 (March 2019).
- <sup>48</sup> Steiner T. 2000. *Acta Cryst. Sect. B*, 56, 673-676.
- <sup>49</sup> Koutentis P. A., Haddon R. C., Oakley R. T., Cordes A.W. & Brock C. P. (2001). *Acta Cryst.* B57, 680–691.
- <sup>50</sup> Bakus II R. C., Atwood D. A., Parkin S., Brock C. P. & Petricek V. 2013. *Acta Cryst.* B69, 496–508.
- <sup>51</sup> Hao X., Chen J., Cammers A., Parkin S. & Brock C. P. 2005. *Acta Cryst. Sect. B*, 61, 218–226.
- <sup>52</sup> Wachter E., Glazer E. C., Parkin S. & Brock C. P. 2016. *Acta Cryst.* B72, 223–231.
- <sup>53</sup> Zhang Y., Wade M. M., Scorpio A., Zhang H. & Sun Z. 2003. *J. Antimicrob. Chemoter.* 52, 790-795.

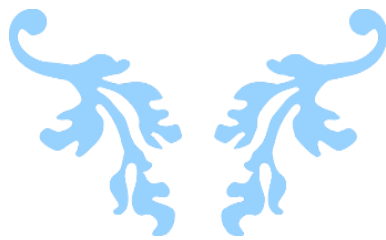


---

## CHAPTER II

---

### EXPERIMENTAL METHODS AND MATERIALS



## 2.1 Experimental methods

### 2.1.1 Crystallisation and crystal growth

Crystallisation is a supramolecular process, therefore a crystal is a product of a supramolecular reaction and essentially a kinetic phenomenon. There are different crystallisation techniques for molecular solids, such as sublimation, mechanochemistry, melt cooling and solvent evaporation, which is the technique that was mostly used. The process of crystallisation is a complicated one and can be split into two main steps, known as nucleation and crystal growth.

### 2.1.2 Crystallisation procedure

The multicomponents crystals were synthesised by dissolving the solid acid (R,S-PSA or S-PSA) in the liquid bases, while the pharmaceutical co-crystal was synthesised by dissolving the 1:1 mixture of the solid API (pyrazine carboxamide) and the solid acid (rac-PSA or S-PSA) in different solvents with known properties such as, polarity ( $P$ ) and molecular size ( $N$ , Å), see Table 2.1. The mixtures were gently heated to 40-50°C on a hot plate while stirring for the solutions to be clear. After homogenisation, the solutions were allowed to cool down before filtration through a 0.45µm syringe filter into new vials and left for slow evaporation.

**Table 2.1** List of successful solvents including polarity ( $P$ ) and molecular size ( $N$ , Å).<sup>1</sup>

Solvent	Polarity ( $P$ )	Molecular size ( $N^a$ )
Dichloromethane	3.4	0.460
Methanol	5.1	0.408
Tetrahydrofuran	4.2	0.504

<sup>a</sup>Molecular size ( $N$ ) indicates the real size of solvent molecules. Data taken from reference 1.

### 2.1.3 Thermal Analysis

Differential scanning calorimetry and thermogravimetry were done on a Perkin-Elmer<sup>®</sup> DSC 6000 series and a Perkin-Elmer<sup>®</sup> Pyris 6 series respectively. DSC and TG instruments were run with the inert gas N<sub>2</sub> with a flow rate of 30 mL.min<sup>-1</sup> and constant heating rate of 10°C.min<sup>-1</sup>. The multicomponent crystals were extracted from their respective solvents, cautiously dried with a filter paper, reduced to powder with a pestle and mortar and placed in closed pan with holes for DSC analysis and open pan for TGA analysis.

#### a. Differential scanning calorimetry (DSC)

DSC is a thermoanalytical technique which measures the temperatures and heat flows related with changes in material as a function of time and temperature in a controlled environment. The results give qualitative and quantitative details about chemical and physical changes involving exothermic or endothermic events. DSC can be used for determination of crystallinity, melting point, kinetic studies, or glass and phase transition.

When running a DSC measurement, the sample is placed in a vented pan and further closed with a lid. The sample holder is placed next to a reference material and they are both subjected to the same temperatures. The result of a DSC analysis is a curve, with the temperature shown on the x-axis (°C or K) and the amount of heat transferred presented on the y-axis (mW) displaying peaks and troughs to show the distinctive endothermic and exothermic changes, respectively.<sup>2</sup> The enthalpy of transition can be calculated using the curve with the following formula:

$$\Delta H = KA$$

Where:                       $\Delta H$  = the enthalpy of transition  
                                    K= the calorimetric constant  
                                    A= the area below the curve

**b. Thermogravimetric analysis (TGA)**

TGA is a method that is used for the determination of compounds experiencing mass variation when exposed to thermal stress.<sup>3</sup> It is used to analyse the decomposition, kinetics and thermal stability of a sample under a diversity of conditions controlled by the equipment. Thermogravimetry was used in this work to check the absence or presence of solvents in the different multicomponent crystals synthesised.

**2.1.4 Fourier Transform Infrared Spectroscopy (FTIR)**

FTIR spectroscopy is a highly reliable and well-known analytical method for bulk property analysis. One of the advantages of FTIR spectroscopy is its capacity as an analytical technique to acquire spectra from an extensive variety of fluids, gases and solids. FTIR is useful in organic chemistry because it allows identification of functional groups due to their absorptions with diverse intensities at specific regions of the infra-red spectrum. Identifying the absorptions of the functional groups and understanding the spectrum is crucial and will support further examinations of the new multicomponent crystals.

Spectra were collected by a universal attenuated total reflectance infrared spectrometer (ATR-FTIR) by Perkin Elmer<sup>®</sup> spectrum 2.

**2.1.5 X-ray diffraction**

Diffraction takes place when X-rays are scattered by a periodic array with long-range order, generating at specific angles constructive interference. The atoms present in a crystal diffract because they are periodically arranged. The distance between the atoms is similar to the wavelength of X-ray. Powder X-ray diffraction techniques use this theory to reveal the composition of the crystalline materials. The scattering of X-rays from atoms generate a diffraction pattern holding details concerning the crystal atomic arrangement.<sup>4</sup>

The diffraction is described by Bragg's law:

$$n\lambda = 2d \sin\theta$$



Where:  $\theta$  = angle of incidence  
 $\lambda$  = wavelength of the rays  
 $d$  = spacing between layers of atoms  
 $n$  = integer

When Bragg's law is satisfied, "reflected" beams are in phase and interfere constructively

The powder X-ray diffractometer measurements were performed at the Cape Peninsula University of Technology and the single crystal structure measurements were performed at the University of Cape Town because of the availability of the instrument.

**a. Powder X-ray diffraction (PXRD)**

PXRD is a powerful and quick technique principally employed for phase determination of a crystal structure and able to provide information regarding the size of the unit cell. Bulk amount of crystals of interest is carefully reduced to powder and an average portion is analysed. To analyse the crystalline material and phases the PXRD at disposal was a Bruker® D2 phaser fitted a graphite-monochromated Cu K $\alpha$  radiation ( $\lambda = 1.5418$  Å) at room temperature.<sup>5</sup> The obtained pattern of the bulk material was compared to the PXRD pattern of the pure starting material and conclusion was drawn based on the level of similarity of the two PXRD pattern.

**b. Single crystal X-ray diffraction (SCXRD)**

Single crystal diffraction data were collected on a Bruker® Duo APEX II diffractometer with a graphite-monochromated Mo K $\alpha$  radiation ( $\lambda = 0.71073$  Å) at 173K using an Oxford Cryostream 700.<sup>6</sup>

Structures were solved using SHELXL-2016<sup>7</sup> which was run under a graphical user interface, X-seed<sup>8</sup>. The space groups were determined by using the collected intensities and pre-determined cell parameters as inputs to program XPREP.<sup>9</sup> SHELXL-2016<sup>6</sup> was used to resolve all crystals by direct methods and refinement was done with SHELXL-2016<sup>6</sup> by employing full matrix least-squares against  $F^2$  for unique reflection.

$$\sum w (F_0^2 - kF_c^2)^2$$

The agreement between the observed structure factors ( $F_o$ ) and the calculated structure factors ( $F_c$ ) was monitored by assessing the residual index  $R$ . The residual index  $R_1$  is the agreement between the observed and calculated structure factors based on  $F$ , while the residual index,  $R_2$ , is the agreement based on  $F^2$ .

$$R_1 = \frac{\sum ||F_o| - |F_c||}{\sum |F_o|} \quad R_2 = \left[ \frac{\sum w (F_o^2 - F_c^2)^2}{\sum w (F_o^2)^2} \right]^{\frac{1}{2}}$$

The weighting scheme  $w$  was used to yield a constant distribution in terms of  $a$  and  $b$ , and further refined in the final cycles of structure refinement.

$$w = \frac{1}{\sigma^2 (F_o^2) + (aP)^2 + bP}$$

where:

$$P = \frac{\max(0, F_o^2) + 2 F_c^2}{3}$$

SHELXL-2016<sup>6</sup> refines against  $F^2$ , which leads to greater deviation of the Goodness of Fit ( $S$ ) from unity than the refinement against  $F$ . The Goodness of Fit expression is:

$$S = \left[ \frac{\sum w (|F_o|^2 - |F_c|^2)^2}{(N - n_p)^2} \right]^{\frac{1}{2}}$$

The hydrogen atoms bound to carbon atoms were placed at idealised positions and refined as riding atoms with  $U_{iso}(\text{H}) = 1.2 U_{eq}(\text{Ar-H, CH}_2)$  or  $1.5 U_{eq}(\text{CH}_3)$  of the atom to which the H is bound. If it was possible, the H atoms bonded to carboxylic acid, amine or amide groups were located in the difference electron density map and their coordinates refined freely but their isotropic displacement parameters were fixed ( $U_{iso}(\text{H}) = 1.2 U_{eq}(\text{O})$  or  $U_{eq}(\text{N})$ ) if it was necessary.

X-ray powder patterns were calculated using LAZY PULVERIX<sup>10</sup> and compared to experimental powder patterns for comparison. All crystal packing diagrams were generated with POV-RAY<sup>11</sup>. The program LAYER<sup>12</sup> was utilised to test systematic absences and space group symmetry. X-Seed was used as a graphical interface for the program SHELXL-2016, LAZY PULVERIX, POV-RAY and LAYER.

### 2.1.6 Computing components

**ConQuest:** Search engine using the Cambridge Structural Database (CSD) for informative and comparative structure details.<sup>13</sup>

**Platon:** A multipurpose analytical tool for crystal structure analysis; calculates all molecular parameters for the structures.<sup>14</sup>

**SADABS** (Siemens Area Detector Absorption Corrections): an application in the APEX suite used to scale and correct data for absorption collected on a Bruker AXS area detector.<sup>15</sup> The program is designed to exploit data redundancy, corrects for errors resulting from the variation in the volume of crystal, absorption by the crystal support and crystal decay during the measurement.

**XPREP:** This program determines the space group by reading the raw data file (.raw) and the parameter file (.p4p) written by the diffractometer control program, also write the instruction file (.ins) and reflection data (hkl).<sup>16</sup>

**X-Seed:** graphical user interface for crystallography and graphical program.<sup>8</sup>

**Layer** is a component of X-Seed. It displays simulated precession photographs of the reciprocal lattice levels using the intensity data.<sup>12</sup>

**LAZY PULVERIX:** software which calculates the theoretical powder X-ray diffraction pattern from single crystal X-ray diffraction data.<sup>10</sup>

**Pov-Ray:** program which generates graphics.<sup>11</sup>

**Pov-Label:** allows controlling the atom labels on an image rendered using Pov-Ray.<sup>11</sup>

**Mercury:** Analysis software which provides options to aid the investigation and analysis of crystal structures. It can import chemical bond types, 2D connection tables and present them in 3D illustration, generates packing diagrams, defines and visualises Miller planes and take a slice through a crystal in any direction and also displays space group symmetry elements, calculates voids based either on contact surface or solvent accessible surface and intermolecular potentials, it can also be used to perform a basic gas phase calculation.<sup>17</sup>

## 2.2 Materials

### 2.2.1 Dicarboxylic acids

(R,S)-Phenylsuccinic acid and (S)-Phenylsuccinic acid were used in this research (Figure 2.1). The chemical structures, molar masses and melting points of these weak acids are listed in Table 2.2.



a) (R,S)-Phenylsuccinic acid, (rac-PSA)

b) (S)-Phenylsuccinic acid, (S-PSA)

**Figure 2.1** Chemical structures of (R,S) and (S)-Phenylsuccinic acid

**Table 2.2** Physical properties of the dicarboxylic acids (PSA)

Host	Formula	Mr (g.mol <sup>-1</sup> )	Mp (°C)
(R,S)-PSA	C <sub>10</sub> H <sub>10</sub> O <sub>4</sub>	194.19	165-168
(S)-PSA	C <sub>10</sub> H <sub>10</sub> O <sub>4</sub>	194.19	173-176

### 2.2.2 Coformers

Tertbutylamine (TBA), aniline (ANI), pyridine (PYR), 4-picoline (4PIC), 2,4-Lutidine (2,4LUT), 3,4-lutidine (3,4LUT), 3,5-lutidine (3,5LUT) and pyrazine carboxamide (PCA) were bought from Sigma-Aldrich and Merck & Co (Figure 2.2). The chemical structures as well as the molecular mass, boiling and melting point of the amines and the amide PCA are listed in Table 2.3. The amines are used for the synthesis of the multicomponent crystals while the amide PCA is used for the synthesis of pharmaceutical co-crystals. The amines used for this research are derivatives of pyridine and differ by the position and number of the methyl groups on the phenyl ring to study their effect on the crystal packing. The chemical structures of the coformers are shown in Figure 2.2.

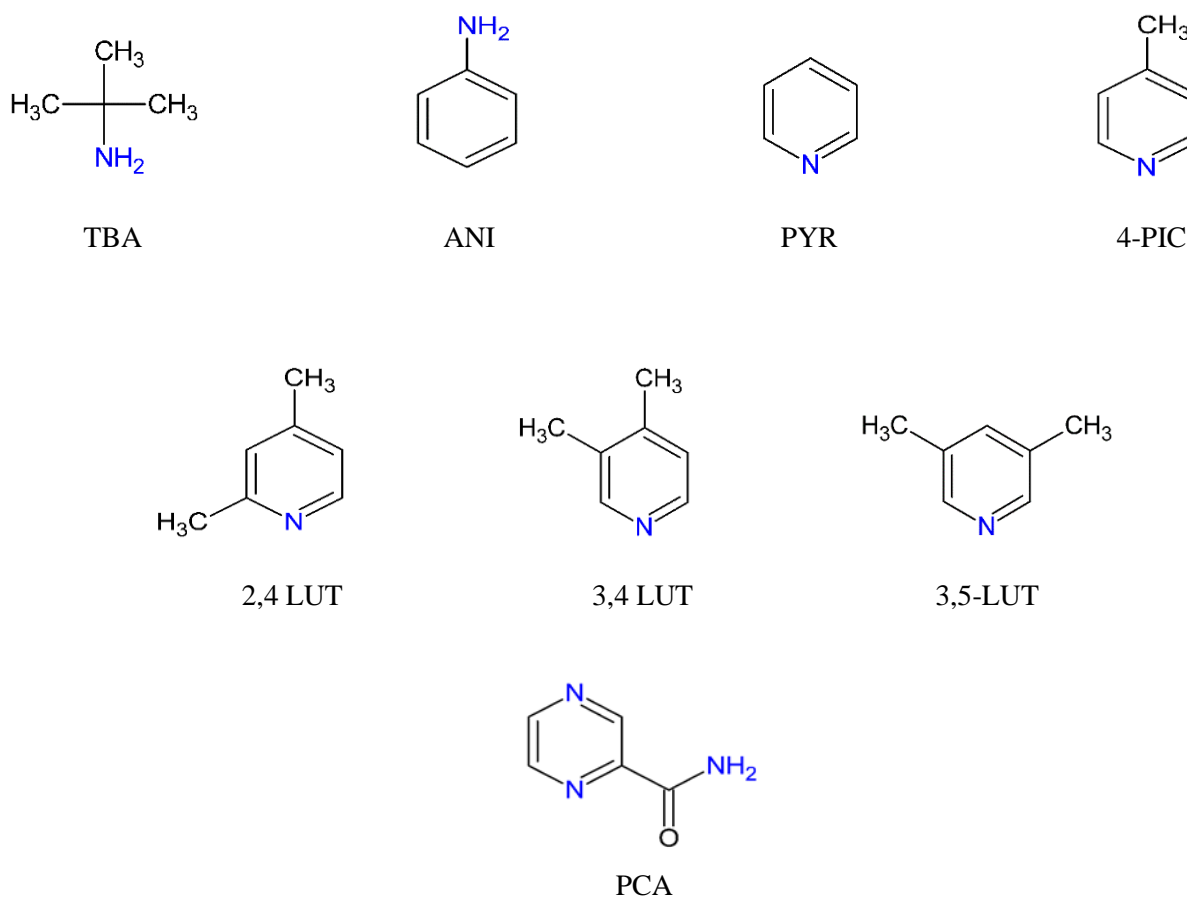


**Figure 2.2** Chemical structures of coformers (Tertbutylamine: TBA; Aniline: ANI; pyridine: PYR; 4-methylpyridine: 4-PIC; 2,4-dimethylpyridine: 2,4-LUT; 3,4-dimethylpyridine: 3,4-LUT; 3,5-dimethylpyridine: 3,5-LUT) and the API (pyrazine carboxamide: PCA).

**Table 2.3** Physical properties of cofomers

<b>Cofomer</b>	<b>Formula</b>	<b>Mr (g.mol<sup>-1</sup>)</b>	<b>Bp (°C)</b>	<b>Mp (°C)</b>
TERTBUTYLAMINE	C <sub>4</sub> H <sub>11</sub> N	73.14	44-46	n/a
ANILINE	C <sub>6</sub> H <sub>7</sub> N	93.13	183-184	n/a
PYRIDINE	C <sub>5</sub> H <sub>5</sub> N	79.10	115-116	n/a
4-PICOLINE	C <sub>6</sub> H <sub>7</sub> N	93.13	144-145	n/a
2,4-LUTIDINE	C <sub>7</sub> H <sub>9</sub> N	107.15	160-161	n/a
3,4-LUTIDINE	C <sub>7</sub> H <sub>9</sub> N	107.15	163-164	n/a
3,5-LUTIDINE	C <sub>7</sub> H <sub>9</sub> N	107.15	169-170	n/a
PYRAZINE CARBOXAMIDE	C <sub>5</sub> H <sub>5</sub> N <sub>3</sub> O	123.11	n/a	357

*#: Amines and amide are damaging to skin, eyes and respiratory tract. They are dangerous if swallowed; if in contact with skin and if breathed in. Important signs for eyes are redness and pain, for skin is redness and scalded feeling while following ingestion the effects on central nervous system can be delayed.*

The successfulness of all the crystallisation experiments between (R,S)-PSA, (S)-PSA and the cofomers would have resulted in the formation of sixteen novel crystal structures. However due to the cost of (S)-PSA and the lower probability to obtain crystals with the enantiopure compared to the racemate, the work plan (Figure 2.3) was first, attempt to obtain crystals with the racemic acid, and second, to try with the enantiopure acid. When no crystals were obtained from (R,S)-PSA, there was no attempt with (S)-PSA.

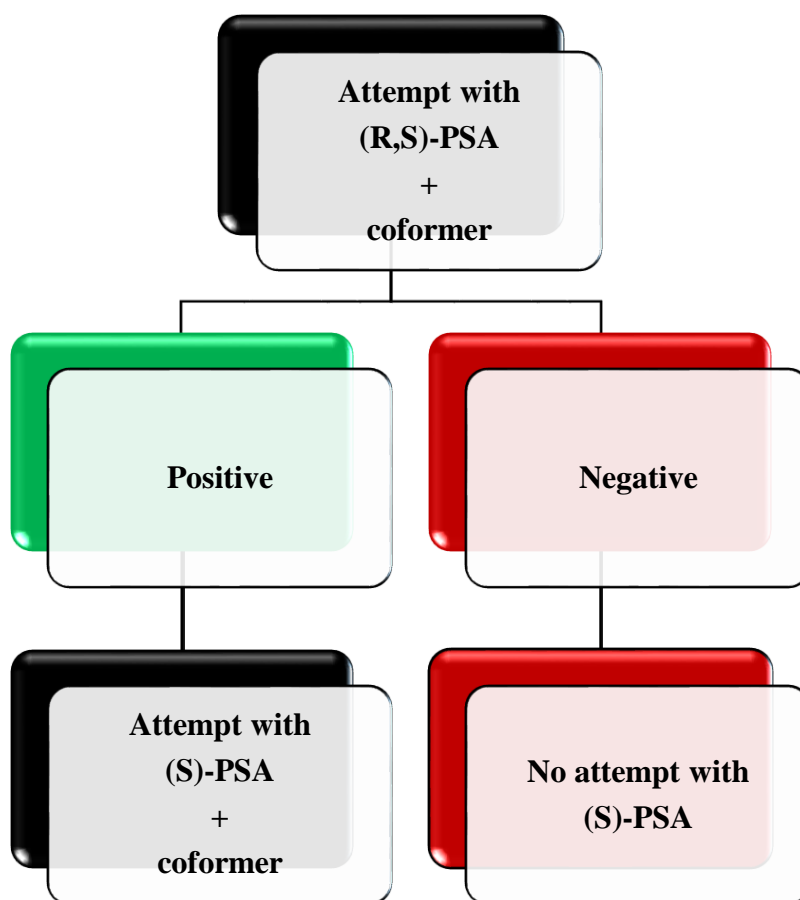
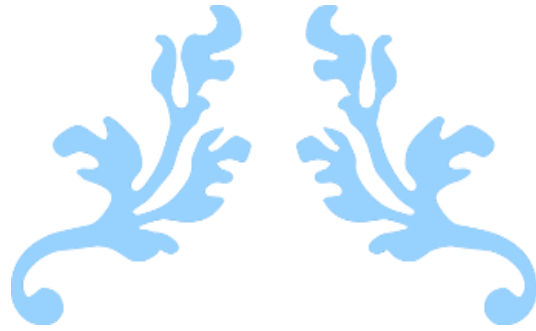


**Figure 2.3** Work flow chart for crystallisation experiments.

## References:

- 
- <sup>1</sup> Marcus Y. 1998. *The properties of solvents*, Wiley, Chichester.
- <sup>2</sup> Gabbott P. 2007. *The Principles and Applications of Thermal Analysis*, Wiley-Blackwell, London.
- <sup>3</sup> Brown, M.E. 1998. *Introduction to thermal analysis*. Chapman & Hall, London.
- <sup>4</sup> Stout, G. H. & Jensen L. H. 1965. *X-ray structure determination: a practical guide*. The MacMillan Company, New York.
- <sup>5</sup> Bruker 2005. *APEX2*. Version 1.0-27. Bruker AXS Inc., Madison, Wisconsin, USA
- <sup>6</sup> Rissanen, K. 2014. X-ray Crystallography. *Encyclopaedia of supramolecular chemistry*, 2: 1586-1591.
- <sup>7</sup> Sheldrick, G.M. 2015. Crystal refinement with SHELXL *Acta. Cryst.* C71, 3-8
- <sup>8</sup> Barbour, L.J. 2001, X-Seed Graphical Interface for SHELX program. *J. Supramol. Chem*, 1: 189-191.
- <sup>9</sup> XPREP, Data preparation and reciprocal space preparation, Version 5.1/NT © 1997, Bruker Analytical X-Ray and Systems.
- <sup>10</sup> Yvon, K., Jeitschoko, W. & Parthe E.J. 1990. LAZY RPULVERIX, a computer program, for calculating X-Ray and neutron diffraction powder patterns. *J. Appl. Cryst.*, 10: 73-74
- <sup>11</sup> POV-Ray for Windows, Version 3.1e.watcom.win32. The persistence of vision development team, © 1991-1999.
- <sup>12</sup> Barbour L.J. 1999. LAYER, A computer program for the graphic display of intensity data as simulated precession photographs *J. Appl. Cryst.*, 32: 351.
- <sup>13</sup> Bruno I., Cole J., Edgington P., Kessler M., Macrae C., McCabe P., Pearson J. & Taylor R. 2002. *Acta Cryst. Sect. B*, 58(3), 389-397.
- <sup>14</sup> Spek, A. L. PLATON, A multipurpose crystallographic tool, Version 10500, © 1980-2000.
- <sup>15</sup> Bruker 2010, D2 PHASER. Version 3-07. Bruker AXS GmbH, Karlsruhe, Germany.
- <sup>16</sup> Aulton, M.E. 2002. *Pharmaceutics: the science of dosage form design*. Second edition, Churchill Livingstone, Edinburgh.
- <sup>17</sup> Sheldrick, G.M. 2002. University of Göttingen, Germany.



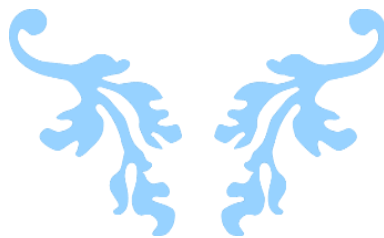


---

# CHAPTER III

---

## CRYSTAL STRUCTURES



This chapter presents all the multicomponent crystals obtained from the crystallisations of racemic or enantiopure phenylsuccinic acids with the selected bases (Table 3.1). The naming convention of the compounds follows the system, where first the anion and secondly the cation is listed. The reason for this somewhat unorthodox style of naming is to keep the common item, i.e. the phenylsuccinic acid, in the first place, followed by the actual base, which aids the clarity of discussion.

	tBa	ANI	PYR	4-PIC	2,4-LUT	3,4-LUT	3,5-LUT	PCA
(R,S)-PSA	●	●	●	●	●	●	●	●
(S)-PSA	●	●	●	●	●	●	●	●

● Successful  
● Unsuccessful

**Table 3.1** Summary of crystallisation experiments

### 3.1 Multicomponent crystal formation of phenylsuccinic acid with primary amines

(*R,S*)-PSA and (*S*)-PSA were exposed to primary amines with bulky functional groups (*tert*-butylamine and aniline) to aid the crystallisation process.

#### 3.1.1 *tert*-Butylammonium carbonate: $[2\text{tBa}^+][\text{COO}^{2-}]$

Co-crystallisation of (*R,S*)-PSA with *tert*-butylamine (tBa) under atmospheric conditions produced crystals with unexpected chemical composition. The amine reacted with the atmospheric  $\text{CO}_2$  and formed a carbonate salt. This behaviour is not uncommon in primary amines.<sup>1,2,3</sup> The  $[2\text{tBa}^+][\text{COO}^{2-}]$  crystallised in the trigonal  $R\bar{3}c$  space group (No. 167) with  $\frac{1}{3}$  tBa<sup>+</sup> and  $\frac{1}{6}$  COO<sup>2-</sup> in the ASU (Figure 3.1a). Each oxygen atom hydrogen bonds to two neighbouring tBa<sup>+</sup> ions via the N3-H1...O5 interaction and its symmetry generated counterparts (Figure 3.1b). The hydrophobic and ionic layers are alternating down the [001] direction (Figure 3.1c). The crystallographic details and hydrogen bonds for  $[2\text{tBa}^+][\text{COO}^{2-}]$  are summarised in Tables 3.2 and 3.3. Although great effort was invested in the experimental work, the crystallisation of the *S*-enantiomer of the phenylsuccinic acid with *tert*-butylamine was unsuccessful.

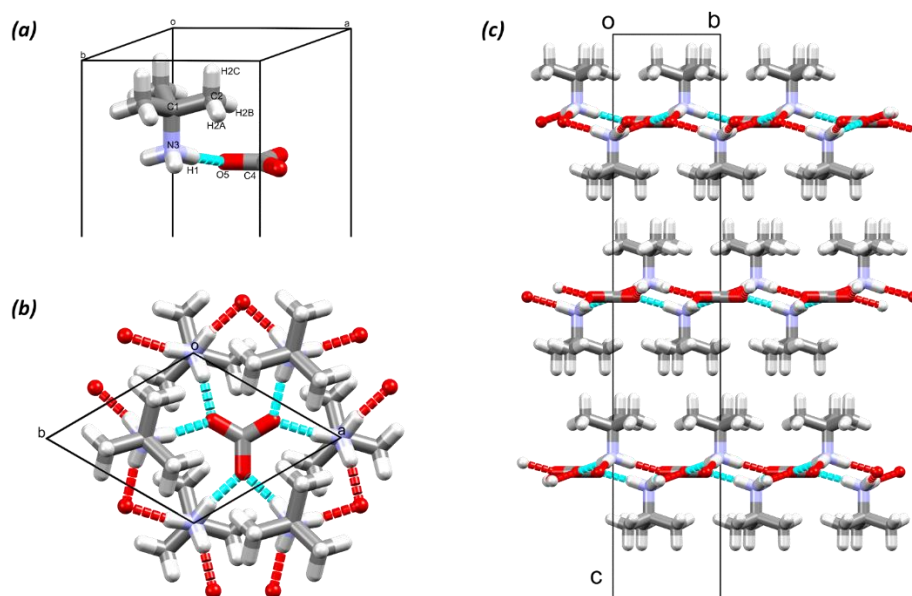


Figure 3.1  $[2tBa^+][COO^{2-}]$  crystal structure with labelled atoms in the ASU (a), hydrogen bonds between the ions (b) and crystal packing view down  $[100]$  (c).

Table 3.2 Crystal data for  $[2tBa^+][COO^{2-}]$ ,  $[(R,S)\text{-PSA}^-][ANI^+]$  and  $[(S)\text{-PSA}^{2-}][2ANI^+]\cdot ANI$ .

Crystal data			
Compounds	$[2tBa^+][COO^{2-}]$	$[(R,S)\text{-PSA}^-][ANI^+]$	$[(S)\text{-PSA}^{2-}][2ANI^+]\cdot ANI$
Molecular formula	$C_9H_{24}N_2O_3$	$C_{16}H_{17}NO_4$	$C_{28}H_{31}N_3O_4$
Formula weight ( $g\cdot mol^{-1}$ )	208.30	287.30	473.56
Crystal system	Trigonal	Monoclinic	Orthorhombic
Space group	$R\bar{3}c$ (167)	$Pn(7)$	$P2_1$ (18)
a (Å)	6.3212(9)	9.5310(19)	25.731(5)
b (Å)	6.3212(9)	8.3030(17)	8.2594(17)
c (Å)	53.448(11)	9.885(2)	12.118(2)
$\alpha$ (°)	90	90	90
$\beta$ (°)	90	111.82(3)	90
$\gamma$ (°)	120	90	90
V (Å <sup>3</sup> )	1849.5(6)	726.2(3)	2575.3(9)
Z	6	2	4
$\rho_{calc}/g\cdot cm^{-3}$	1.122	1.314	1.221
$\mu$ (MoK $\alpha$ ) / $mm^{-1}$	0.083	0.095	0.082
F (000)	696	304	1008
Crystal size (mm)	0.07 × 0.38 × 0.40	0.04 × 0.240 × 0.300	0.093 × 0.328 × 0.334
Temperature (K)	173(2)	173(2)	173(2)
Radiation [Å]	MoK $\alpha$ (0.71073 Å)	MoK $\alpha$ (0.71073 Å)	MoK $\alpha$ (0.71073 Å)
Theta min-max [°]	2.286, 28.417	2.453, 28.389	1.583, 27.175
Dataset	-8:7, -8:8, -70:70	-12:12, -11:11, -13:13	-33:32, -10:10, -15:15
Final R indices [I > 2.0 (I)]	$R_1 = 0.0331$ , $wR_2 = 0.0922$	$R_1 = 0.0392$ , $wR_2 = 0.0810$	$R_1 = 0.0415$ , $wR_2 = 0.0996$
R indices (all data)	$R_1 = 0.0359$ , $wR_2 = 0.0946$	$R_1 = 0.0500$ , $wR_2 = 0.0862$	$R_1 = 0.0473$ , $wR_2 = 0.1028$
Tot., uniq.data, R (int)	4739, 484, 0.0280	10213, 3039, 0.0316	28838, 5209, 0.0375
$N_{ref}$ , $N_{par}$	528, 26	3608, 206	5734, 394
S	1.118	0.992	1.068
Max. ans av. Shift/error	0.000, 0.000	0.000, 0.000	0.000, 0.000
Min. and max. resd. Dens (Å <sup>3</sup> )	-0.135, 0.287	-0.179, 0.152	-0.223, 0.177

**Table 3.3 Hydrogen bonds in [2tBa<sup>+</sup>][COO<sup>2-</sup>], [(R,S)-PSA<sup>-</sup>][ANI<sup>+</sup>] and [(S)-PSA<sup>2-</sup>][2ANI<sup>+</sup>].ANI.**

D-H...A	d(D-H) (Å)	d(H...A) (Å)	d(D...A) (Å)	D-H...A (°)	Symmetry operator
<b>[2tBa<sup>+</sup>][COO<sup>2-</sup>]</b>					
N3-H1...O5	0.95	1.79	2.730	170.0	
<b>[(R,S)-PSA<sup>-</sup>][ANI<sup>+</sup>]</b>					
N15-H15A...O10	1.02	1.67	2.675	168.5	
N15-H15B...O13	0.87	2.36	2.937	124.2	x, y, z+1
N15-H15B...O14	0.87	2.34	2.937	126.1	x-1/2, -y+1, z+1/2
N15-H15C...O11	0.94	1.77	2.714	177.4	x+1/2, -y+1, z+1/2
O14-H14...O11	0.91	1.61	2.523	173.5	x+1/2, -y+1, z-1/2
<b>[(S)-PSA<sup>2-</sup>][2ANI<sup>+</sup>].ANI</b>					
C17-H17...O13	0.95	2.50	3.265	138.1	
N15-H15A...O13	0.94	2.51	3.024	114.5	
N15-H15A...O14	0.94	1.81	2.721	163.5	
N15-H15B...O11	0.93	1.85	2.743	160.4	x, y+1, z
N22-H22C...O10	0.95	1.79	2.736	174.0	x, y+1, z
N22-H22C...O11	0.95	2.55	3.083	116.0	x, y+1, z
N22-H22A...O13	0.91	1.78	2.684	174.4	
N22-H22B...O10	0.95	1.78	2.723	175.8	-x+1/2, y+1/2, -z
N29-H29A...O11	0.87	2.22	3.089	175.4	
N15-H15C...O14	0.94	1.77	2.709	176.0	-x+1/2, y+1/2, -z+1
C17-H17...O13	0.95	2.50	3.265	138.1	

### 3.1.2. Anilinium phenylsuccinate: [(R,S)-PSA<sup>-</sup>][ANI<sup>+</sup>]

The crystallisation of the *racemic*-phenylsuccinic acid from aniline resulted in the [(R,S)-PSA<sup>-</sup>][ANI<sup>+</sup>] salt that crystallised in the monoclinic *Pn* space group (No. 7) with one mono-deprotonated PSA<sup>-</sup> and one ANI<sup>+</sup> in the ASU. (The ASU was selected to contain the S-enantiomer of the PSA. This was done in all of the following racemic structures of PSA to aid the easy comparison of molecular conformations.) The deprotonation happened on the propanoate end of the molecule (Figure 3.2a) and the N15-H15A...O10 charge assisted hydrogen bond is formed. The acid molecules hydrogen bond to each other via the O14-H12...O11 interaction and the anilinium ions are linking the acid chains by forming three hydrogen bonds with neighbouring carboxylic acid and carboxylate functional groups (Figure 3.2b). The alternating aromatic rings of the hydrogen bonded acids and anilinium ions interlock to form the third dimension of the crystal (Figure 3.2c and d). The data collection and refinement details as well as hydrogen bonds for [(R,S)-PSA<sup>-</sup>][ANI<sup>+</sup>] are summarised in tables 3.2 and 3.3.

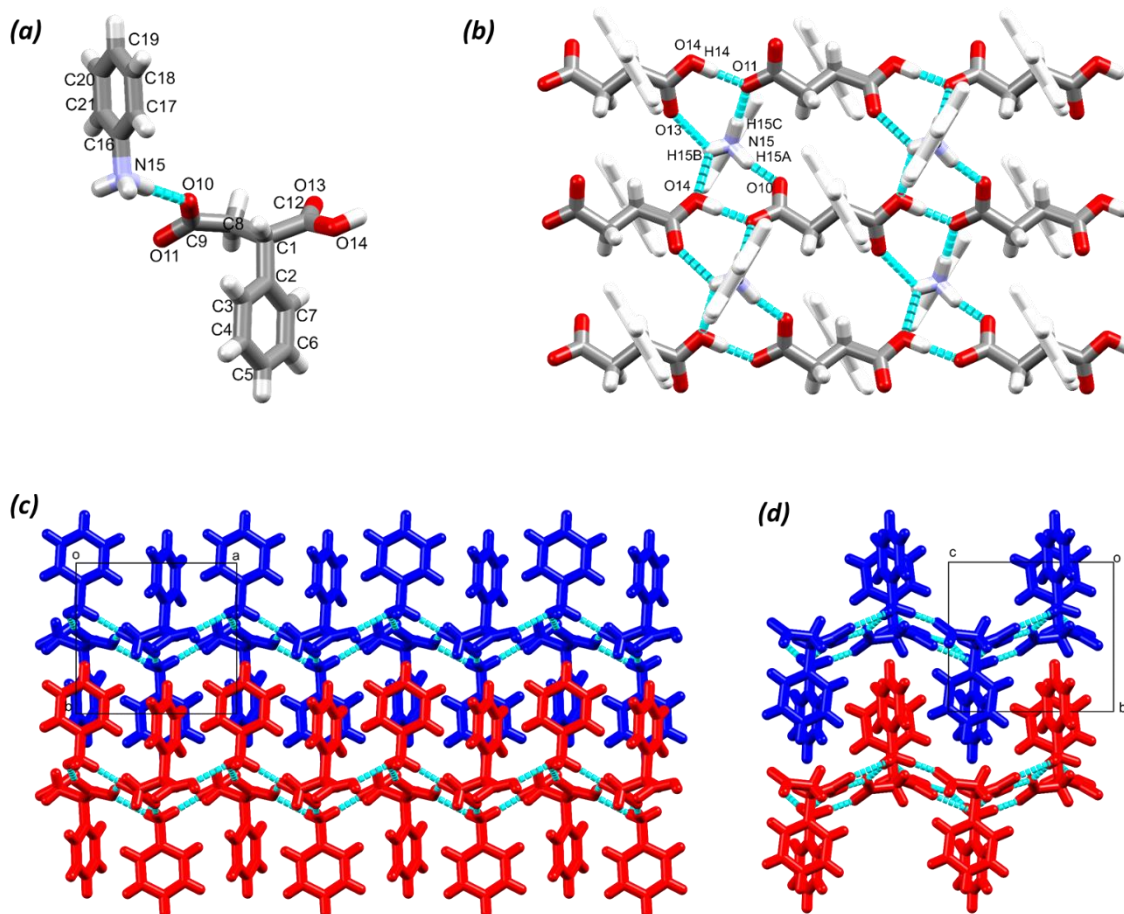


Figure 3.2 Crystal structure of  $[(R,S)\text{-PSA}^-][\text{ANI}^+]$  with labelled atoms of the ASU (a), hydrogen bonds between the ions (b, the aromatic rings are faded out to aid a better viewing of the prominent hydrogen bonds) and crystal packing showing the interlocking aromatic layers, (c) view down  $[001]$  and (d)  $[100]$ .

### 3.1.3. Anilinium (S)-phenylsuccinate aniline solvate: $[(S)\text{-PSA}^{2-}][2\text{ANI}^+]\cdot\text{ANI}$

The crystallisation of the enantiopure (S)-phenylsuccinic acid from aniline yielded crystals with different stoichiometry than observed during the crystallisation of the racemic acid. The structure may be classified as a salt-solvate since it contains a double deprotonated phenylsuccinic acid  $[(S)\text{-PSA}^{2-}]$ , two anilinium ions and one neutral aniline in the ASU (Figure 3.3a). The  $[(S)\text{-PSA}^{2-}][2\text{ANI}^+]\cdot\text{ANI}$  crystallised in the orthorhombic  $P2_12_12$  space group (No. 18). Crystal data, refinement details and hydrogen bonds of  $[(S)\text{-PSA}^{2-}][2\text{ANI}^+]\cdot\text{ANI}$  are summarised in Tables 3.2 and 3.3

The  $\text{PSA}^{2-}$  ion is disordered in two positions in a 70-30% distribution. The minor disorder is shown with light blue colouring on Figure 3.3a and is omitted from the following packing diagrams for clarity. The  $\text{PSA}^{2-}$  ions are hydrogen bonding to neighbouring anilinium ions via

N-H $\cdots$ O interactions and forming rings that may be described by the  $R_4^4(12)$  graph set (Figure 3.3b). The hydrogen bonding extends via the  $-\text{NH}_3^+$  moiety to form layers of ions (Figure 3.3b, green arrows). The neutral aniline molecules are interacting with the carboxylate groups via N29-H29A $\cdots$ O11 interactions that are not ideal geometrically. These loosely bonding solvent molecules are embedded between the aromatic rings of the hydrogen bonded ions (Figure 3.3c, yellow space fill model). Contrary to the racemic structure, here, the layers that are formed from the hydrogen bonded ions and the neutral aniline molecules, do not interlock with each other and form non-polar layers built from two layers of aromatic rings in the crystal (Figure 3.3d).

The difference between the crystal structures of the racemic and the chiral salts obtained from crystallisation of PSA from aniline, [(R,S)-PSA $^-$ ][ANI $^-$ ] and [(S)-PSA $^{2-}$ ][2ANI $^+$ ] $\cdot$ ANI is significant. The structures differ in (1) the deprotonation of the acid, (2) the stoichiometric ratio of crystallisation and (3) the hydrogen bonds formed in the crystals. While packing differences between racemic and their chiral counterparts are expected to occur because of the different molecular shapes of these molecular building blocks, the difference in their deprotonation is unexpected, since the  $\text{p}K_a$  values of the enantiomers are the same.

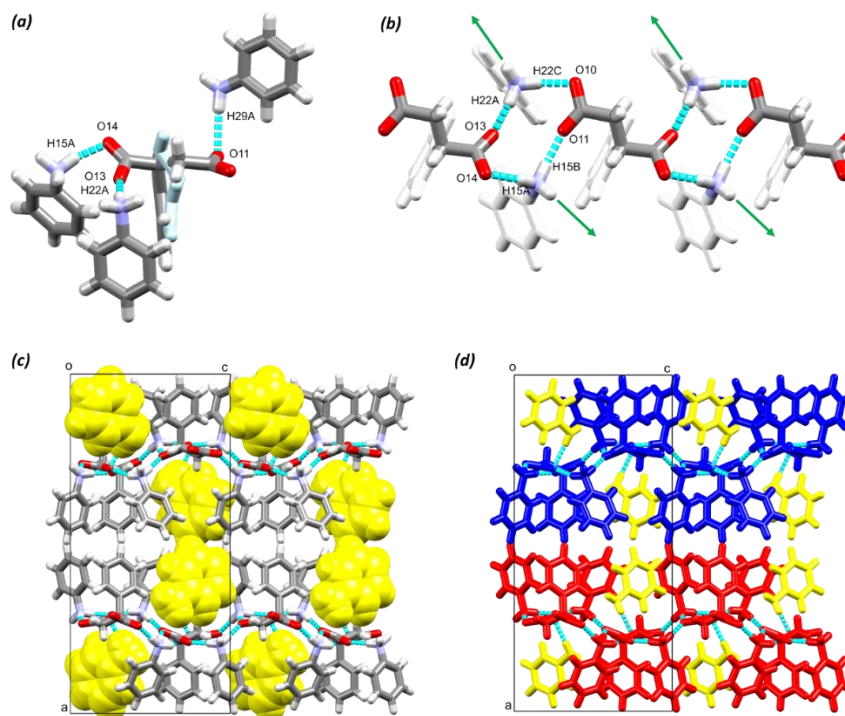


Figure 3.3 Crystal structure of [(S)-PSA $^{2-}$ ][2ANI $^+$ ] $\cdot$ ANI with labelled contact atoms of the ASU (a) and the hydrogen bonds between the ions (b, the aromatic rings are faded out to aid a better viewing of the prominent hydrogen bonds and green arrow represent the extending hydrogen bonds). The aniline molecules are embedded between the aromatic rings of the hydrogen bonded ions (c, yellow space fill model). The aromatic rings of the hydrogen bonded layers (d, blue and red) do not interlock with neighbouring ones.

### 3.2 Multicomponent crystal formation of phenylsuccinic acid with aromatic amines

(*R,S*)-PSA and (*S*)-PSA were exposed to pyridine and a series of methyl substituted aromatic amines. The racemic acid was crystallised successfully with pyridine (PYR), 4-picoline (4PIC) and 2,4-lutidine (2,4LUT). Crystallisation from 3,4-lutidine (3,4LUT) and 3,5-lutidine (3,5LUT) was successful with both the racemic and the *S*-enantiomer of PSA.

#### 3.2.1 (*R,S*)-Phenylsuccinic acid pyridine solvate: (*R,S*)-PSA·2PYR

(*R,S*)-PSA crystallised with two equivalent of PYR in the centrosymmetric  $P\bar{1}$  (No. 2) space group (Figure 3.4a). The crystal data and hydrogen bonds for (*R,S*)-PSA·2PYR are listed in Tables 3.4 and 3.5. The PSA molecule is in a different conformation when compared to the previously described structures. The succinic acid backbone was linear in the previous cases, while here, this moiety takes up a ‘bent’ conformation. The details of the conformational changes observed in all the multicomponent crystals of PSA presented in this thesis are discussed in chapter 4. There was no proton transfer observed between the acid and the base and the formation of the acid-base heterosynthon via two hydrogen bonds, described as  $R_2^2(7)$  graph set, was noted. Molecule A of the PYR is coplanar with the related carboxylic acid group ( $\neq 17.2^\circ$ ) but molecule B is  $31.7^\circ$  out of plane with the related acid moiety. Nevertheless, the interaction between molecule B and the acid occurred through two hydrogen bonds, between the ortho hydrogen (H22) and the carbonyl oxygen atom (2.66 Å). The neighbouring acids interact via C8-H8A $\cdots$ O11 hydrogen bond and its symmetry generated counterpart, forming  $R_2^2(8)$  rings. There are also weak C17-H17 $\cdots$ O10 hydrogen bonds formed between the adjacent base-acid-base (BAB) units (Figure 3.4b). Overall, the crystal has a layered structure, where the alternating sheets of the solvent molecules and the acids form layers parallel to the (010) plane (Figure 3.4c).

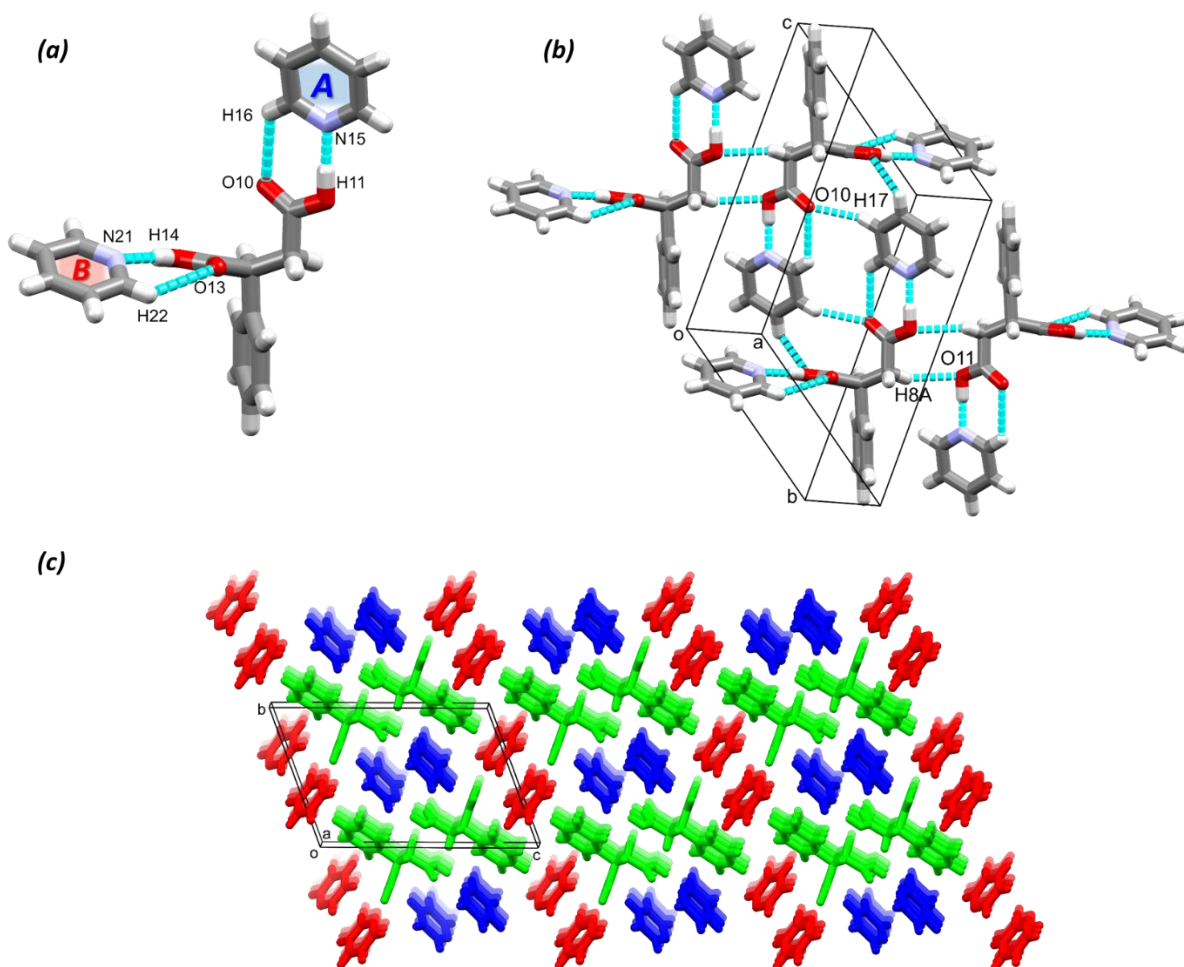


Figure 3.4 Crystal structure of (R,S)-PSA-2PYR with hydrogen bonds and labelled contact atoms of the ASU (a). The neighbouring base-acid-base (BAB) units hydrogen bond via C8-H8A...O11 and its symmetry generated counterpart and weak C17-H17...O10 interactions between the pyridine and the carbonyl oxygen atoms (b). The solvent molecules (blue and red) are packed in layers that are parallel with the (010) and (001) planes (c).



Table 3.4 Crystal data for (R,S)-PSA·2PYR, (R,S)-PSA·2(4PIC) and (R,S)-PSA·2(2,4LUT).

Crystal data			
Compounds	(R,S)-PSA·2PYR	(R,S)-PSA·2(4PIC)	(R,S)-PSA·2(2,4LUT)
Molecular formula	C <sub>20</sub> H <sub>20</sub> N <sub>2</sub> O <sub>4</sub>	C <sub>22</sub> H <sub>24</sub> N <sub>2</sub> O <sub>4</sub>	C <sub>24</sub> H <sub>28</sub> N <sub>2</sub> O <sub>4</sub>
Formula weight (g.mol <sup>-1</sup> )	352.38	380.43	408.48
Crystal system	Triclinic	Monoclinic	Monoclinic
Space group	<i>P</i> $\bar{1}$ (2)	<i>P</i> 2 <sub>1</sub> / <i>c</i> (14)	<i>P</i> 2 <sub>1</sub> / <i>c</i> (14)
a (Å)	5.6697(4)	22.906(5)	11.773(2)
b (Å)	10.5672(6)	5.7441(11)	8.4930(17)
c (Å)	15.5754(10)	15.376(3)	22.318(5)
$\alpha$ (°)	109.3480(10)	90	90
$\beta$ (°)	96.6060(10)	100.98(3)	96.22(3)
$\gamma$ (°)	91.6060(10)	90	90
V (Å <sup>3</sup> )	872.44(10)	1986.1(7)	2218.4(8)
Z	2	4	4
$\rho_{\text{calc}} / \text{g.cm}^{-3}$	1.341	1.272	1.223
$\mu$ (MoK $\alpha$ ) / mm <sup>-1</sup>	0.094	0.088	0.083
F (000)	372	808	872
Crystal size (mm)	0.010×0.010×0.010	0.080×0.110×0.210	0.180×0.380×0.570
Temperature (K)	173(2)	173(2)	173(2)
Radiation [Å]	MoK $\alpha$ (0.71073 Å)	MoK $\alpha$ (0.71073 Å)	MoK $\alpha$ (0.71073 Å)
Theta min-max [°]	1.398, 27.532	1.811, 27.131	1.740, 28.452
Dataset	-7:7, -13:13, -20:20	-29:29, -7:3, -19:19	-15:15, -11:11, -28:29
Final R indices [I > 2.0 (I)]	R <sub>1</sub> =0.0359, wR <sub>2</sub> =0.0885	R <sub>1</sub> =0.0782, wR <sub>2</sub> =0.1954	R <sub>1</sub> =0.0545, wR <sub>2</sub> =0.1303
R indices (all data)	R <sub>1</sub> =0.0389, wR <sub>2</sub> =0.0907	R <sub>1</sub> =0.1345, wR <sub>2</sub> =0.2287	R <sub>1</sub> =0.0822, wR <sub>2</sub> =0.1464
Tot., uniq.data, R (int)	23333, 3681, 0.0223	11159, 2529, 0.0316	25976, 3832, 0.0242
N <sub>ref</sub> , N <sub>par</sub>	4011, 243	4367, 278	5492, 353
S	1.059	1.035	1.025
Max. ans av. Shift/error	0.001, 0.000	0.000, 0.000	0.000, 0.000
Min. and max. resd. Dens (Å <sup>3</sup> )	-0.135, 0.287	-0.283, 0.473	-0.270, 0.256

Table 3.5 Hydrogen bonds in (R,S)-PSA·2PYR, (R,S)-PSA·2(4PIC) and (R,S)-PSA·2(2,4LUT).

D-H...A	d(D-H) (Å)	d(H...A) (Å)	d(D...A) (Å)	D-H...A (°)	Symmetry operator
(R,S)-PSA·2PYR					
C8-H8A...O11	0.99	2.55	3.356	138.7	-x+2, -y+2, -z+1
O11-H11...N15	0.95	1.68	2.625	174.4	
O14-H14...N21	0.91	1.80	2.700	174.6	
C17-H17...O10	0.95	2.53	3.427	158.6	-x+1, -y+1, -z+1
C22-H22...O13	0.95	2.66	3.308	126.1	
(R,S)-PSA·2(4PIC)					
C23-H23...O11Bb	0.84	2.43	2.974	123.5	
O11Aa-H14A...N22	0.84	1.77	2.597	166.5	
O14Aa-H14A...N15	0.84	1.87	2.704	177.0	
O11Bb-H11B...N22	0.84	2.33	2.938	129.2	
(R,S)-PSA·2(2,4LUT)					
O11-H11...N23	1.03	1.59	2.610	168.2	
O14-H14...N15	1.03	1.56	2.587	174.2	
C19-H19...O10	0.95	2.50	3.379	154.3	x+1, y, z
C20-H20...O13	0.95	2.64	3.305	127.6	
C27d-H27d...O13	0.95	2.53	3.463	167.3	x+1, y, z

## 3.2.2. (R,S)-Phenylsuccinic acid 4-picoline solvate: (R,S)-PSA·2(4PIC)

(R,S)-PSA crystallised with two equivalents of 4PIC in the centrosymmetric  $P2_1/c$  (No. 14) space group (Figure 3.5a). (For crystallographic details and hydrogen bonds see Tables 3.4 and 3.5.) The succinic acid backbone is linear but disordered in two positions and the major disorder occupies 82% of the positions. Both of the carboxylic acid groups are disordered in two positions also and their site occupancy was set the same as the disorders of the backbone. (The minor disorder is represented in wireframe style on Figure 3.5a.) The structure is a solvate, i.e. no proton has been transferred from the acid to the base. This decision was made based on the analysis of the C-O bond length. Some of these bond lengths were close to 1.3 Å (in case of C9-O11A, C9-O11B, C12-O14A and C12-O14B), thus these were treated as C-OH groups and hydrogen atoms were added with the appropriate restrains. The length of the complementary C-O bonds was closer to 1.2 Å that are in the region of the C=O double bond (C9-O10A, C9-O10B, C12-O13A and C12-O13B). To support the decision based on the C-O bond length, there was no protonation observed of the nitrogen atoms of the 4-picolines. The minor disorders of the carboxylic acid groups are not representing chemically meaningful positions; therefore, structural description of the crystal will focus on the interactions of the main disorder model.

The PSA molecule forms the well-known acid-amine<sub>(ar)</sub> heterosynthon via O11A-H11A...N22 and C23-H23...O10A, described with  $R_2^2(7)$  graph set, and forms a single hydrogen bond via O14A-H14A...N15 with the other 4PIC. These T-shape molecular base-acid-base (BAB) units form molecular tapes where the distance between the planes fitted to the 4PICs are 3.25 Å and 3.58 Å (Figure 3.5b, green and yellow highlights, respectively). These values are in the region of the typical  $\pi \cdots \pi$  interactions and although the 4PIC molecules are parallel to one another the rings are offset. These molecular tapes are in a 45.9° angle when view down [001] (Figure 3.5c). The two symmetry independent 4PIC molecules are packed in a slightly different manner in the crystal when forming the layered structure. One of the 4PIC (molecule A, represented with blue on Figure 3.5d) shows better overlap with neighbouring molecules than the other 4PIC (molecule B, red on Figure 3.5d). This subtle difference in the packing environment cannot be clearly seen on the thermal behaviour of the crystal; the release of the two 4PIC molecules happen in one step during the TGA analysis (Figure E.2, Appendix).

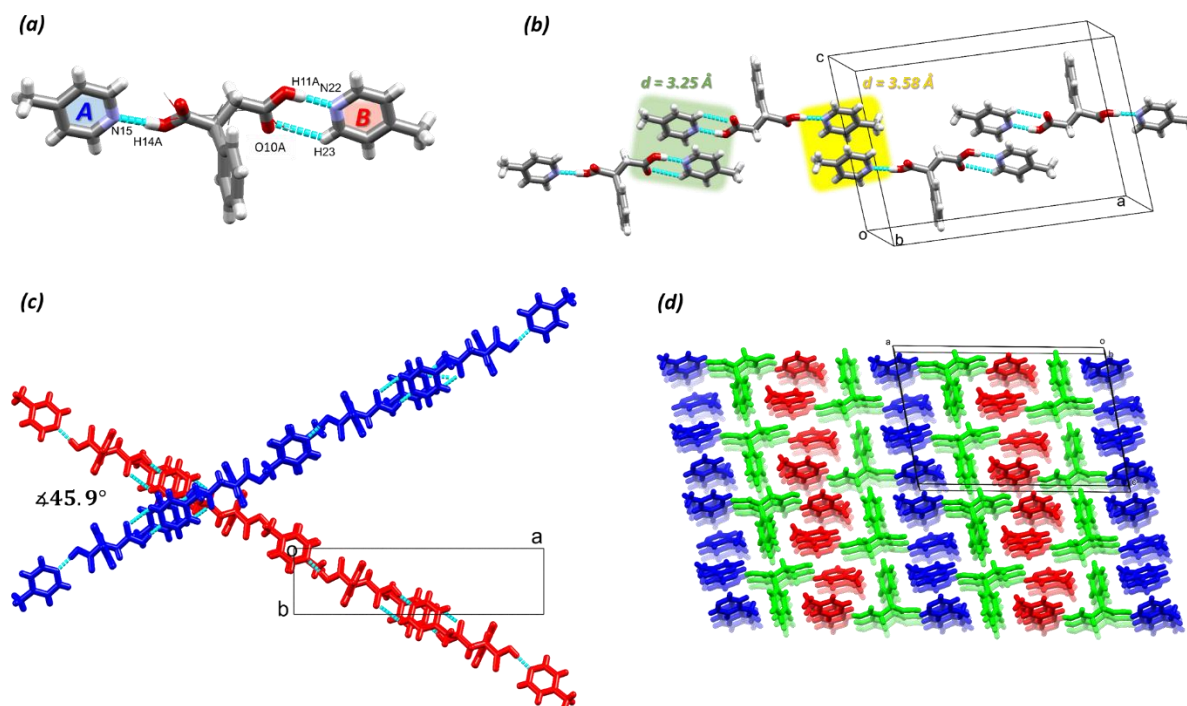


Figure 3.5 Crystal structure of (R,S)-PSA·2(4PIC) with labelled contact atoms of the ASU and showing the minor disorder of the acid with wireframe presentation (a). The T-shape base-acid-base (BAB) units form molecular tapes (b) that are in  $45.9^\circ$  angle (c) when view down [001]. The layered structure of the crystal (d) where molecules are coloured according to symmetry equivalence.

### 3.2.3 (R,S)-Phenylsuccinic acid 2,4-lutidine solvate: (R,S)-PSA·2(2,4LUT)

(R,S)-PSA crystallised with two equivalent of 2,4LUT in the centrosymmetric  $P2_1/c$  (No. 14) space group (Figure 3.6a). (For crystal structure data and hydrogen bonds see tables 3.4 and 3.5.) The structure is a solvate, i.e. no proton has been transferred from the acid to the base. The conformation of the succinic acid backbone is linear, similar to that seen in the previous crystal structure, and disordered in two positions. The major disorder occupies ca. 75% of the positions. (The minor disorder is represented in wireframe style on Figure 3.6a.) Contrary to (R,S)-PSA·2(4PIC), the carboxylic acid groups are ordered in this structure and their hydroxyl hydrogens were located in the electron density map. (H11 and H14 were restrained during the refinement process to reach convergence.) The two carboxylic acid groups form acid-amine<sub>(ar)</sub> heterosynthons with 2,4LUT molecules via pairs of hydrogen bonds (O14-H14...N15 and C20-H20...O13 with molecule A, and O11A-H11A...N23 and C28-H28...O10 with molecule B) that can be described with the  $R_2^2(7)$  graph set (Figure 3.6a). Three out of the four methyl groups of the 2,4LUT molecules are disordered and were refined using appropriate restraints (two positions were refined with equal site occupancies).

The neighbouring T-shape BAB units interact via hydrogen bonds formed between the carbonyl oxygen of the acid and the C-H hydrogen atoms of the 2,4LUT molecules (C19-H19 $\cdots$ O10 and C27-H27 $\cdots$ O13, Figure 3.6b). Also, similarly to the (R,S)-PSA $\cdot$ 2(4PIC) structure, the BAB units interact with neighbouring ones via  $\pi\cdots\pi$  interactions formed between their overlapping symmetrically identical 2,4LUT molecules with a centroid distance of 3.51 Å (Figure 3.6c, green highlights between two molecules A, coloured blue).  $\pi\cdots\pi$  interactions occurs only between these pairs of molecules. The overlap is not perfect between the symmetry independent 2,4LUT molecules because of the lack of their parallel arrangement and the offset positions. The layered nature of the crystal packing is similar to the (R,S)-PSA $\cdot$ 2(4PIC) structure but the symmetrically independent 2,4LUT molecules are in the same layer (Figure 3.6d).

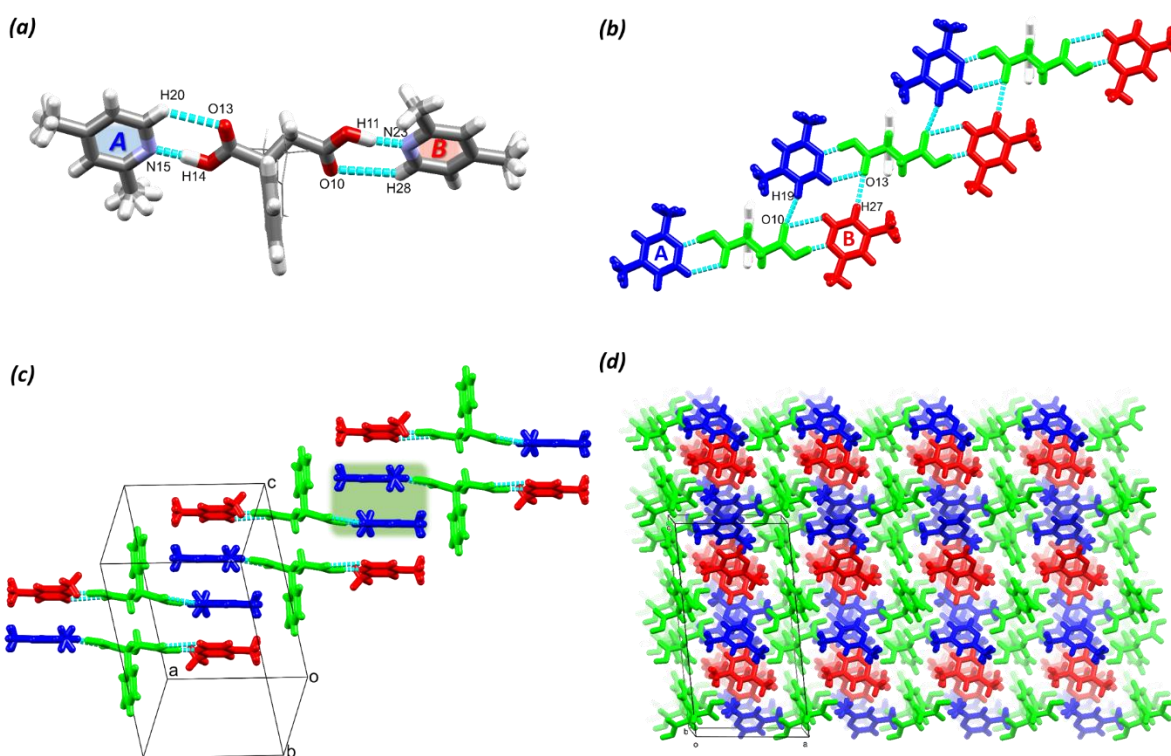


Figure 3.6 Crystal structure of (R,S)-PSA $\cdot$ 2(2,4LUT) with labelled contact atoms of the ASU and showing the minor disorder of the acid with wireframe presentation (a). The T-shape base-acid-base (BAB) units form hydrogen bonded molecular tapes (b) and aromatic interactions (c) with neighbouring counterparts. The layered structure of the crystal (d) where molecules are coloured according to symmetry equivalence.

### 3.2.4 (R,S)-Phenylsuccinic acid 3,4-lutidine solvate: (R,S)-PSA·2(3,4LUT)

(R,S)-PSA crystallised with two equivalent of 3,4LUT in the centrosymmetric  $P\bar{1}$  (No. 2) space group (Figure 3.7a). The succinic acid backbone of the PSA molecule is ‘bent’. There was no proton transfer observed between the acid and the base, and the formation of the acid-base heterosynthon with one of the base molecules (B) via two hydrogen bonds, described as  $R_2^2(7)$  graph set, was noted. The other base (molecule A) forms only a single hydrogen bond with the acid. (See tables 3.6 and 3.7 for crystallographic data and hydrogen bonds.) The structural arrangement of the ASU resembles (R,S)-PSA·2PYR, but one of the base (molecule A) forms only a single hydrogen bond with the related carboxylic acid moiety because they are out of plane ( $\neq 22.3^\circ$ ). Subsequently, a longer distance was observed between the carbonyl oxygen and the ortho hydrogen atom (2.79 Å). The two structures also differ in the next level of interactions formed between the BAB units with neighbouring symmetry equivalents. The units interact via the formation of  $\pi$ -stacking between like lutidine moieties (see blue and red pair of molecules on Figure 3.7b). The pair of lutidines (molecule A, blue) are parallel to one another (3.45 Å) but positioned in slightly offset with the two centroids distanced to 3.87 Å, while the other pair (molecule B, red) are situated showing a better overlap (plane distance: 3.42 Å, distance of centroids: 3.52 Å). The crystal has a layered structure, where the alternating sheets of the symmetrically identical solvent molecules and the acids form layers parallel to the (010) plane (Figure 3.7c).

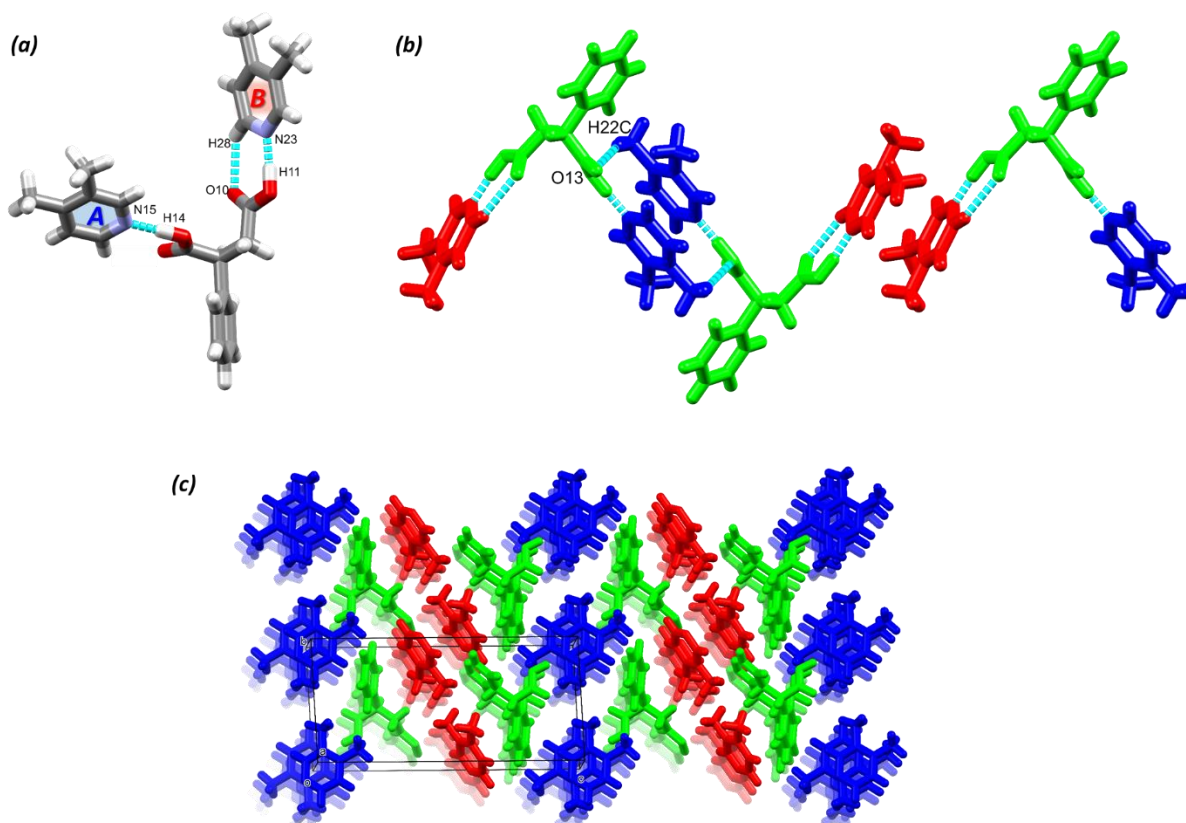


Figure 3.7 Crystal structure of (R,S)-PSA·2(3,4LUT) with hydrogen bonds and labelled contact atoms of the ASU (a). The neighbouring base-acid-base (BAB) units hydrogen bond via C22-H22C...O14 and its symmetry generated counterpart and  $\pi$ -interactions between the 3,4LUTs (b). The solvent molecules (blue and red) are packed in separate layers that are parallel with the (001) plane (c).

**Table 3.6 Crystal data for (R,S)-PSA·2(3,4LUT), 2(S)-PSA·4(3,4LUT), [(R,S)-PSA<sup>2-</sup>]  
2[3,5LUT<sup>+</sup>]<sup>2</sup>·2(R,S)-PSA and 2[(S)-PSA<sup>2-</sup>]<sup>4</sup>·4(3,5LUT<sup>+</sup>)<sup>4</sup>·4(S)-PSA.**

Crystal data				
Compounds	(R,S)-PSA·2(3,4LUT)	2(S)-PSA·4(3,4LUT)	[(R,S)-PSA <sup>2-</sup> ] 2[3,5LUT <sup>+</sup> ] <sup>2</sup> ·2(R,S)-PSA	2[(S)-PSA <sup>2-</sup> ] 4[3,5LUT <sup>+</sup> ] <sup>4</sup> ·4(S)-PSA
Molecular formula	C <sub>24</sub> H <sub>28</sub> N <sub>2</sub> O <sub>4</sub>	C <sub>28</sub> H <sub>28</sub> N <sub>2</sub> O <sub>4</sub>	C <sub>24</sub> H <sub>28</sub> N <sub>2</sub> O <sub>4</sub>	C <sub>88</sub> H <sub>96</sub> N <sub>4</sub> O <sub>24</sub>
Formula weight (g.mol <sup>-1</sup> )	408.48	408.48	408.48	1593.68
Crystal system	Triclinic	Triclinic	Monoclinic	Triclinic
Space group	<i>P</i> $\bar{1}$ (2)	<i>P</i> 1 (1)	<i>P</i> 2 <sub>1</sub> / <i>c</i> (14)	<i>P</i> 1 (1)
a (Å)	7.0626(14)	7.1918(14)	12.222(2)	8.3469(17)
b (Å)	8.7704(18)	8.7570(18)	14.926(3)	12.268(3)
c (Å)	18.630(4)	18.766(4)	22.984(5)	20.595(4)
α (°)	90.98(3)	89.75(3)	90	84.66(3)
β (°)	100.42(3)	79.83(3)	103.42(3)	86.58(3)
γ (°)	107.25(3)	72.07(3)	90	76.63(3)
V (Å <sup>3</sup> )	1080.8(4)	1105.2(4)	4078.4(15)	2041.2(8)
Z	2	2	4	1
ρ <sub>calc</sub> / g.cm <sup>-3</sup>	1.255	1.227	1.298	1.296
μ (MoKα) / mm <sup>-1</sup>	0.086	0.084	0.095	0.095
F (000)	436	436	1688	844
Crystal size (mm)	0.140 × 0.220 × 0.480	0.100 × 0.100 × 0.100	0.100 × 0.200 × 0.240	0.200 × 0.240 × 0.500
Temperature (K)	173(2)	173(2)	173(2)	173(2)
Radiation [Å]	MoKα (0.71073 Å)	MoKα (0.71073 Å)	MoKα (0.71073 Å)	MoKα (0.71073 Å)
Theta min-max [°]	2.229, 28.450	4.015, 26.707	1.640, 27.610	1.712, 28.361
Dataset	-9:9, -11:10, -24:24	-9:9, -11:11, -23:23	-14:15, -19:19, -29:29	-11:11, -16:16, -27:26
Fin. R ind. [I > 2.0 (I)]	R <sub>1</sub> = 0.0513, wR <sub>2</sub> = 0.1213	R <sub>1</sub> = 0.0647, wR <sub>2</sub> = 0.1511	R <sub>1</sub> = 0.0696, wR <sub>2</sub> = 0.1655	R <sub>1</sub> = 0.0768, wR <sub>2</sub> = 0.1977
R indices (all data)	R <sub>1</sub> = 0.0683, wR <sub>2</sub> = 0.1313	R <sub>1</sub> = 0.1152, wR <sub>2</sub> = 0.1786	R <sub>1</sub> = 0.1101, wR <sub>2</sub> = 0.1906	R <sub>1</sub> = 0.1012, wR <sub>2</sub> = 0.2177
Tot., uniq.data, R (int)	12233, 4166, 0.0265	9225, 5940, 0.075	51410, 6132, 0.0506	46913, 14901, 0.0269
N <sub>ref</sub> , N <sub>par</sub>	5423, 284	9225, 546	9432, 609	19773, 1062
S	1.057	1.023	1.030	1.019
Max. ans av. Shift/error	0.000, 0.000	0.000, 0.000	0.000, 0.000	0.000, 0.000
Min. and max. resd. Dens (Å <sup>3</sup> )	-0.277, 0.535	-0.338, 0.428	-0.432, 0.933	-0.503, 0.725

**Table 3.7 Hydrogen bonds in (R,S)-PSA·2(3,4LUT), 2(S)-PSA·4(3,4LUT), [(R,S)-PSA<sup>2-</sup>]<sub>2</sub>[3,5LUT<sup>+</sup>]<sub>2</sub>(R,S)-PSA and 2[(S)-PSA<sup>2-</sup>]<sub>4</sub>[3,5LUT<sup>+</sup>]<sub>4</sub>(S)-PSA.**

D-H...A	d(D-H) (Å)	d(H...A) (Å)	d(D...A) (Å)	D-H...A (°)	Symmetry operator
<b>(R,S)-PSA·2(3,4LUT)</b>					
N15-H15...O10	0.92	2.58	3.192	123.9	
N15-H15...O11	0.92	1.83	2.756	176.0	
C16-H16...O10	0.95	2.50	3.150	125.3	
C16-H16...O10Y	0.95	2.26	3.148	155.8	x-1, y, z
C20-H20...O13Y	0.95	2.35	3.204	148.7	
N23-H23...O14	0.92	2.60	3.210	124.3	
N23-H23...O14	0.92	1.80	2.722	179.3	
C24-H24...O10X	0.95	2.31	3.143	146.4	-x, y-1/2, -z+1/2
C28-H28...O13	0.95	2.46	3.132	127.3	
C28-H28...O13X	0.95	2.39	3.267	152.5	-x+1, y-1/2, -z+1/2
C1Aa-H1A...O14Y	1.00	2.51	3.342	153.8	
C8Aa-H8A1...O11X	0.99	2.43	3.342	152.6	-x, y-1/2, -z+1/2
C1Bb-H1B...O11X	1.00	2.34	3.292	158.5	-x, y-1/2, -z+1/2
C8Bb-H8B1...O14Y	0.99	2.48	3.428	160.6	
O14Y-H14Y...O11	0.87	1.73	2.586	170.7	
O14X-H14X...O13	0.91	1.69	2.593	176.9	-x+1, y+1/2, -z+1/2
O11Y-H11Y...O10	0.89	1.73	2.611	171.3	x+1, y, z
O11X-H11X...O14	0.98	1.62	2.600	174.4	-x, y+1/2, -z+1/2
<b>2(S)-PSA·4(3,4LUT)</b>					
C1A-H1A...O11X	1.00	2.41	3.356	157.6	
C8A-H8B...O11Y	0.99	2.46	3.246	135.9	x, y-1, z
N15A-H15A...O13A	0.88	1.82	2.692	173.3	
N15A-H15A...O14A	0.88	2.62	3.208	124.7	
C16A-H16A...O10Y	0.95	2.38	3.238	149.5	x, y-1, z
C20A-H20A...O14A	0.95	2.54	3.180	125.0	
C20A-H20A...O13Y	0.95	2.38	3.235	149.4	
N23A-H23A...O14A	0.88	1.85	2.717	170.2	
C24A-H24A...O10A	0.95	2.51	3.168	126.3	
C24A-H24A...O13X	0.95	2.34	3.212	153.0	x, y-1, z
C28A-H28A...O10X	0.95	2.39	3.232	147.9	
N15B-H15B...O10X	1.10	1.56	2.631	165.1	
C16B-H16B...O10Z	0.95	2.33	3.194	150.3	
C20B-H20B...O13Z	0.95	2.31	3.183	155.7	x, y-1, z
N23B-H23B...O11B	0.76	1.92	2.667	171.8	
C24B-H24B...O10W	0.95	2.31	3.209	158.7	
C28B-H28B...O13W	0.95	2.22	3.059	146.5	x, y-1, z
O11W-H11W...O10B	0.84	1.82	2.656	176.8	
O14W-H14W...O11B	0.84	1.82	2.654	173.6	x, y+1, z
O11X-H11X...O11A	0.84	1.72	2.558	174.6	
O14X-H11X...O10A	0.84	1.78	2.612	170.1	x, y+1, z
O11Y-H11Y...O13A	0.84	1.74	2.573	174.4	x, y+1, z
O14Y-H11Y...O14A	0.84	1.73	2.566	174.0	
O11Z-H11Z...O13B	0.84	1.79	2.611	165.5	
O14Z-H14Z...O14B	0.84	1.88	2.709	170.2	x, y+1, z



[(R,S)-PSA <sup>2-</sup> ] <sub>2</sub> [3,5LUT <sup>+</sup> ] <sub>2</sub> ·2(R,S)-PSA					
N15-H15...O10	0.92	2.58	3.192	123.9	
N15-H15...O11	0.92	1.83	2.756	176.0	
C16-H16...O10	0.95	2.50	3.150	125.3	
C16-H16...O10Y	0.95	2.26	3.148	155.8	x-1, y, z
C20-H20...O13Y	0.95	2.35	3.204	148.7	
N23-H23...O13	0.92	2.60	3.210	124.3	
N23-H23...O14	0.92	1.80	2.722	179.3	
C24-H24...O10X	0.95	2.31	3.143	146.4	
C28-H28...O13	0.95	2.46	3.132	127.3	
C28-H28...O13X	0.95	2.39	3.267	152.5	x+1, y, z
C1Aa-H1A...O14Y	1.00	2.51	3.342	153.8	
C8Aa-H8A1...O11X	0.99	2.43	3.342	152.6	
C1Bb-H1B...O11X	1.00	2.34	3.292	158.5	
C8Bb-H8B1...O14Y	0.99	2.48	3.428	160.6	
O14Y-H14Y...O11	0.87	1.73	2.586	170.7	
O14X-H14X...O13	0.91	1.69	2.593	176.9	x-1, y, z
O11Y-H11Y...O10	0.89	1.73	2.611	171.3	x+1, y, z
O11X-H11X...O14	0.98	1.62	2.600	174.4	
2[(S)-PSA <sup>2-</sup> ] <sub>4</sub> [3,5LUT <sup>+</sup> ] <sub>4</sub> ·4(S)-PSA					
C1A-H1A...O11X	1.00	2.41	3.356	157.6	x, y+1, z
C8A-H8B...O11Y	0.99	2.46	3.246	135.9	x, y-1, z
N15A-H15A...O13A	0.88	1.82	2.692	173.3	
N15A-H15A...O14A	0.88	2.62	3.208	124.7	
C16A-H16A...O10Y	0.95	2.38	3.238	149.5	x, y-1, z
C20A-H20A...O14A	0.95	2.54	3.180	125.0	
C20A-H20A...O13Y	0.95	2.38	3.235	149.4	
N23A-H23A...O11A	0.88	1.85	2.717	170.2	
C24A-H24A...O10A	0.95	2.51	3.168	126.3	
C24A-H24A...O13X	0.95	2.34	3.212	153.0	
C28A-H28A...O10X	0.95	2.39	3.231	147.9	x, y+1, z
N15B-H15B...O13B	1.10	1.56	2.631	165.1	
C16B-H16B...O10Z	0.95	2.33	3.194	150.3	x, y+1, z
C20B-H20B...O13Z	0.95	2.31	3.183	155.7	
N23B-H23B...O11B	0.76	1.92	2.667	171.8	
C24B-H24B...O10W	0.95	2.31	3.209	158.7	
C28B-H28B...O13W	0.95	2.22	3.059	146.5	x, y-1, z
O11W-H11W...O10B	0.84	1.82	2.656	176.8	
O14W-H14W...O11B	0.84	1.82	2.654	173.6	x, y+1, z
O11X-H11X...O11A	0.84	1.72	2.558	174.6	x, y-1, z
O14X-H11X...O10A	0.84	1.78	2.612	170.1	
O11Y-H11Y...O13A	0.84	1.74	2.573	174.4	x, y+1, z
O14Y-H11Y...O14A	0.84	1.73	2.566	174.0	
O11Z-H11Z...O13B	0.84	1.79	2.611	165.5	x, y-1, z
O14Z-H14Z...O14B	0.84	1.88	2.709	170.2	

## 3.2.5 (S)-Phenylsuccinic acid 3,4-lutidine solvate: 2(S-PSA)·4(3,4LUT)

(S)-PSA crystallised with two equivalent of 3,4LUT in the non-centrosymmetric *P1* (No. 1) space group. The ASU contains two PSA and four 3,4LUT neutral molecules (Figure 3.8a). Similar to the racemic structure, the succinic acid backbone of both PSA molecules is ‘bent’. The two symmetrically independent BAB units (Figure 3.8a) differ slightly in their hydrogen bonding. The unit that is formed by molecule A of (S)-PSA is disordered in the position of one of the 3,4LUT (58% S.O.F. for the main disorder) and the related acid moiety (60% occupied by the main disorder). This unit has only single hydrogen bonds formed between the acid and the bases. The other BAB unit (formed by molecule B of (S)-PSA) is ordered and the hydrogen bonding formed between the acid and the base moieties can be described as the  $R_2^2(7)$  graph set. (For crystallographic details of the structure and hydrogen bonds see Tables 3.6 and 3.7.) The structural arrangement of the crystal resembles the (R,S)-PSA·2(3,4LUT) in that the BAB units are interacting via the formation of  $\pi$ -stacking between the lutidine moieties (see dark and lighter blue and dark and lighter red pairs of molecules on Figure 3.8b). The 3,4LUT molecules are not parallel to one another in these dimers but their average ring distance is ca. 3.5 Å. The crystal structure bears a resemblance to the racemic equivalent (R,S)-PSA·2(3,4LUT) with the common understanding that in this structure all PSA molecules are in the S-configuration (Figure 3.8c).

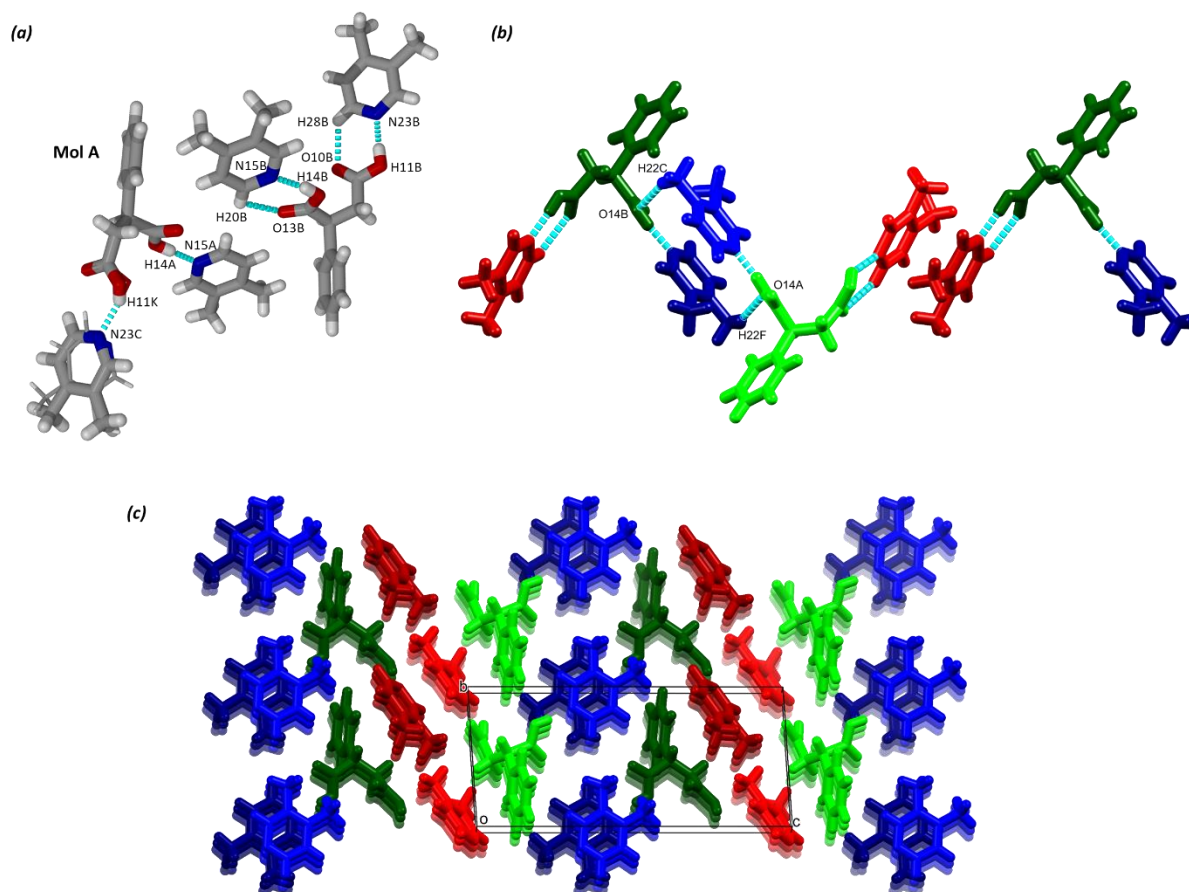


Figure 3.8 The ASU of 2(S-PSA)-4(3,4LUT) with hydrogen bonds and labelled contact atoms (a). The symmetry independent base-acid-base (BAB) units interact via hydrogen bonds and  $\pi$ -interactions between the 3,4LUT molecules (b), colouring based on symmetry equivalence). The packing of the crystal mimics the racemic structure (c).

### 3.2.6 (R,S)-Phenylsuccinic acid 3,5-lutidine co-crystal salt: [(R,S)PSA<sup>2-</sup>]<sub>2</sub>[3,5LUT<sup>+</sup>]<sub>2</sub>·2(R,S)-PSA

(R,S)-PSA crystallised from the solvent 3,5LUT in the centrosymmetric  $P2_1/c$  (No. 14) space group with three molecules of PSA and two molecules of 3,5LUT in the ASU (Figure 3.9a), dubbed as a pentamer. All three PSA molecules have linear succinic acid backbones but they differ in their protonation states. One of the PSA is deprotonated on both ends, and thus the hydrogen bonded 3,5LUT molecules are protonated to form the charged BAB unit [(R,S)-PSA<sup>2-</sup>]<sub>2</sub>[3,5LUT<sup>+</sup>]. In these units, the PSA is disordered in two positions, with the main disorder occupying 70% of the positions. (The minor disorder is shown with wireframe representation on Figure 3.9a. In the following figures the atoms of the minor disorder are omitted for clarity.) The other two neutral PSA molecules hydrogen bond between two neighbouring BAB units (shown yellow and grey on Figure 3.9b). The data collection and refinement details as well as hydrogen bonds for [(R,S)-PSA<sup>2-</sup>]<sub>2</sub>[3,5LUT<sup>+</sup>]<sub>2</sub>·2(R,S)-PSA are listed

in tables 3.6 and 3.7. The protonation states of the molecules were established based on evaluating the C-O bond lengths and also locating the hydrogen atoms in the electron density map. The C-O bond lengths for the C=O groups were found in the region of 1.17-1.20 Å, while they were found around 1.3 Å for the C-O groups. For the deprotonated carboxylate groups these values were between 1.22-1.26 Å. Subsequently, the protonation of the lutidines were proven by locating the hydrogen atoms from the aromatic nitrogen atoms at a distance of 0.92 Å. Therefore, this crystal can be described as a co-crystal salt based on Grothe et al.<sup>4</sup>

The hydrogen bonded pentamers, i.e. the ionic BAB units and the linking neutral PSA molecules, form tapes and these interact with neighbouring counterparts via weak aromatic interactions formed between the lutidinium ions (Figure 3.9c). They are in offset positions with the ring distance of ca. 3.5 Å and the plane of the rings are in ca. 2° incline (inset of Figure 3.9c).

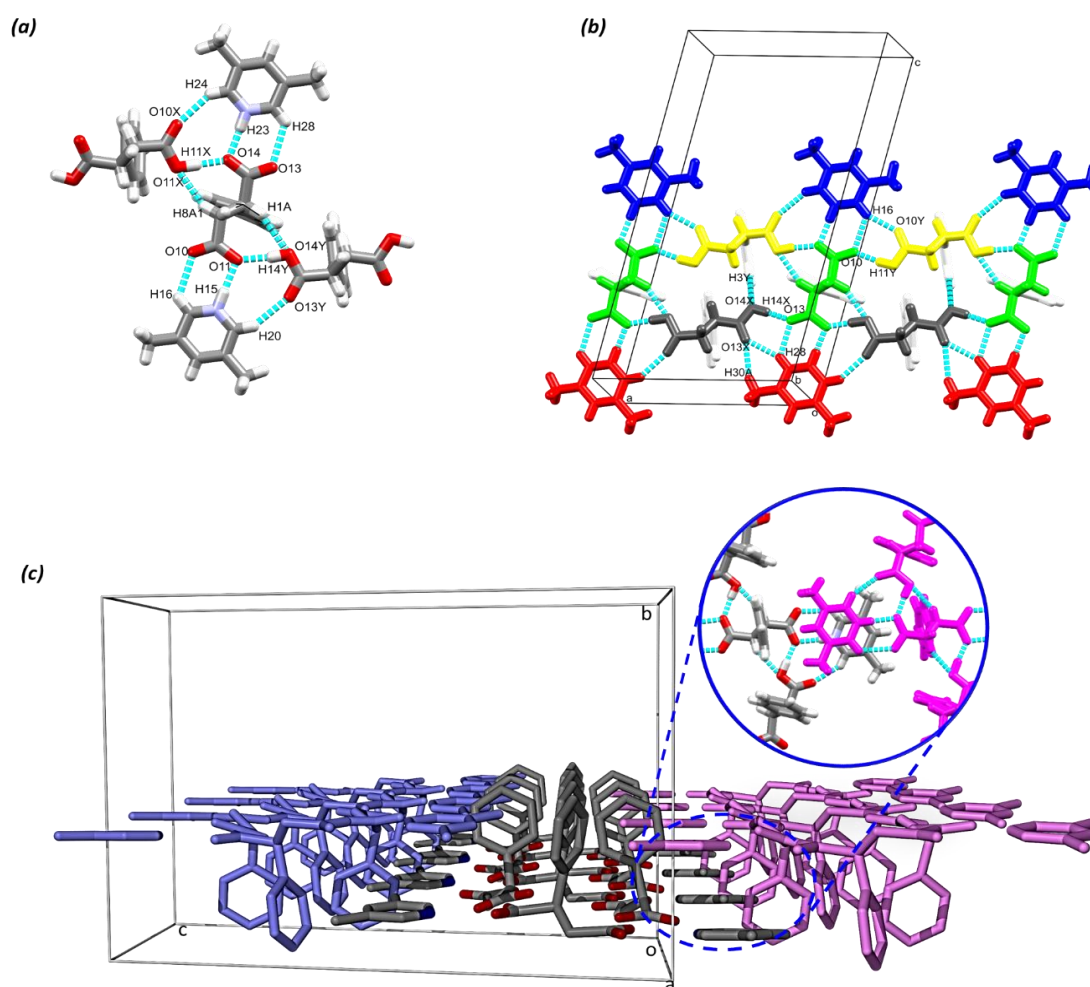


Figure 3.9 The ASU of  $[(R,S)\text{-PSA}^{2-}]_2[3,5\text{LUT}^+] \cdot 2(R,S)\text{-PSA}$  with hydrogen bonds and labelled contact atoms (a). The hydrogen bonds between the neighbouring supramolecular units (equivalent of ASU) (b, colouring based on symmetry equivalence). The hydrogen bonded columns running down [100] direction interact via weak aromatic interactions formed between the lutidinium cations (inset, c).

3.2.7 (S)-Phenylsuccinic acid 3,5-lutidine co-crystal salt:  $2[(S)\text{-PSA}^{2-}]_4[3,5\text{LUT}^+] \cdot 4(S)\text{-PSA}$ 

(S)-PSA crystallised from the solvent 3,5LUT in the non-centrosymmetric *P1* (No. 1) space group with six molecules of PSA and four molecules of 3,5LUT in the ASU. This ASU is mimicking the ASU of the racemic crystal,  $[(R,S)\text{-PSA}^{2-}]_2[3,5\text{LUT}^+] \cdot 2(R,S)\text{-PSA}$ , but contains two pentamers (Figure 3.10a). Basically, this ASU is double that of the ASU seen in the racemic crystal. The possibility of disordered ionic PSAs was investigated but the refinement was unstable after the atoms were split. (See details in the relevant checkCIF report.). Crystal data, refinement details and hydrogen bonds of  $2[(S)\text{-PSA}^{2-}]_4[3,5\text{LUT}^+] \cdot 4(S)\text{-PSA}$  are summarised in Tables 3.6 and 3.7. The protonation states of the molecules, and subsequently the pentamers, were established by following the method explained in the case of the  $[(R,S)\text{-PSA}^{2-}]_2[3,5\text{LUT}^+] \cdot 2(R,S)\text{-PSA}$  crystal and found to be identical to it. The overall arrangement of the molecules in the two pentamers in the ASU are similar but not identical. The difference between the pentamers is shown in Figure 3.10b, where the deprotonated PSA ions are overlaid (central blue and yellow molecules) and their hydrogen bonded neighbours are presented with the same colour as the central PSA. It is clearly seen that the molecular fit of the central PSA ions is good and the obvious difference is noted between the positions of the hydrogen bonded lutidinium ions and also hydrogen bonded neutral PSA molecules. The overall packing of the chiral crystal is very similar to the racemic crystal; both have a layered structure where the hydrogen bonded units interact with neighbouring units via the weak interactions between the lutidinium ions. In the case of  $2[(S)\text{-PSA}^{2-}]_4[3,5\text{LUT}^+] \cdot 4(S)\text{-PSA}$ , the offset is more prominent between the aromatic rings. This offset  $\pi$ -stacking arrangement causes the subsequent layers to be shifted in the structure of  $2[(S)\text{-PSA}^{2-}]_4[3,5\text{LUT}^+] \cdot 4(S)\text{-PSA}$ . The overlap of the crystal structures of  $[(R,S)\text{-PSA}^{2-}]_2[3,5\text{LUT}^+] \cdot 2(R,S)\text{-PSA}$  (black, Figure 3.10c) and  $2[(S)\text{-PSA}^{2-}]_4[3,5\text{LUT}^+] \cdot 4(S)\text{-PSA}$  (red, Figure 3.10c) shows good agreement in the packing when compared layer by layer, but also shows the molecular shift between the subsequent layers in the chiral structure.

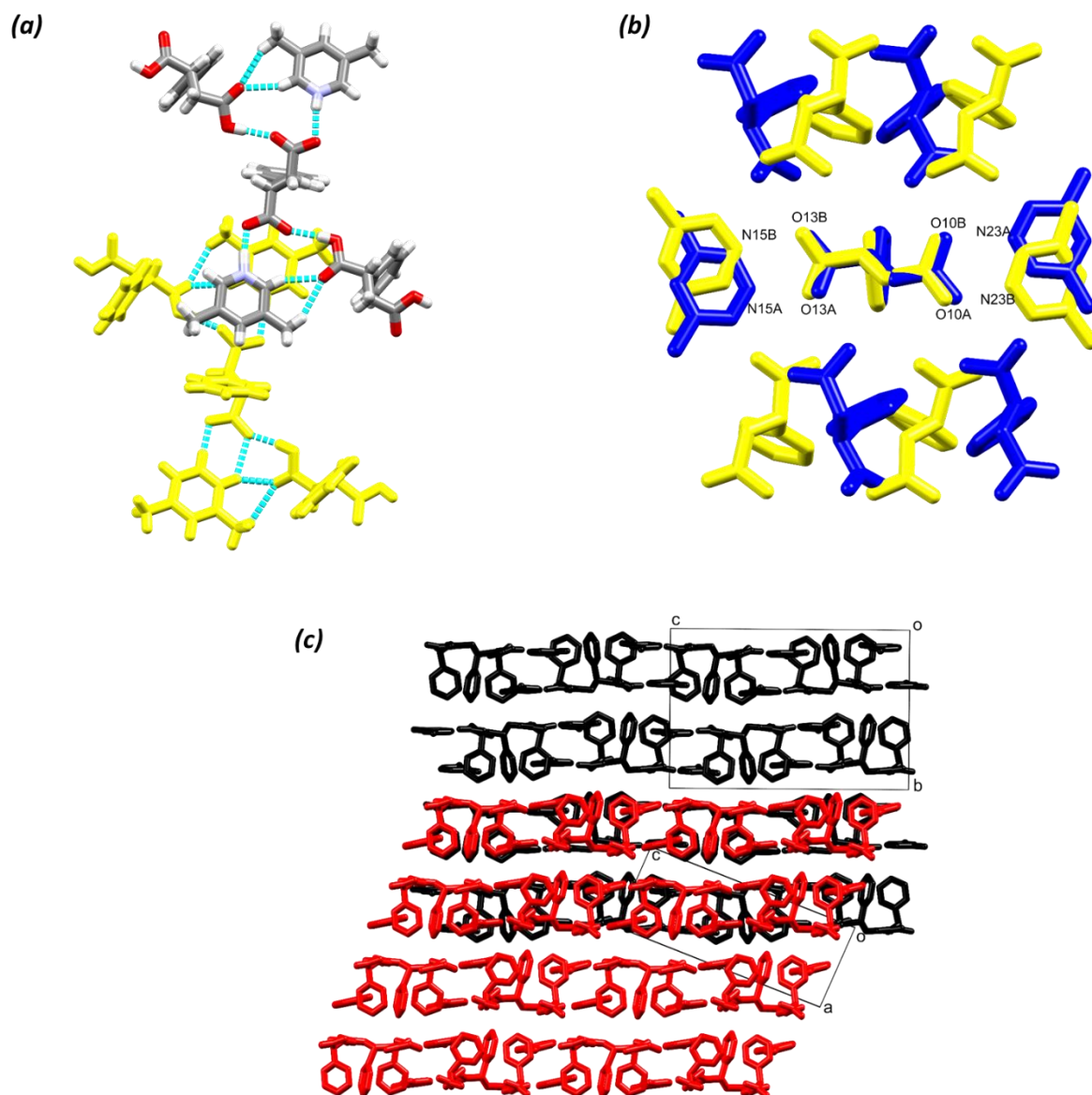


Figure 3.10 The ASU of  $2[(S)\text{-PSA}^2]4[3,5\text{LUT}^+]-4(S)\text{-PSA}$  (half of the unit is coloured with yellow for clarity) (a). The overlap of the two pentamer subunits of the ASU (b). Overlap of the crystal structures of  $[(R,S)\text{-PSA}^2]2[3,5\text{LUT}^+]-2(R,S)\text{-PSA}$  (black) and  $2[(S)\text{-PSA}^2]4[3,5\text{LUT}^+]-4(S)\text{-PSA}$  (red) shows good agreement in the packing when compared layer by layer but also shows the molecular shift between the subsequent layers (c).

### 3.3 Multicomponent crystal formation of phenylsuccinic acid with pyrazine carboxamide

Both (R,S)-PSA and (S)-PSA were exposed to pyrazineamide (pyrazine carboxamide, PCA), a first-line antituberculous drug, but only the racemic acid was co-crystallised successfully with PCA.

#### 3.3.1 (R,S)-Phenylsuccinic acid pyrazine carboxamide co-crystal: (R,S)-PSA·PCA

Co-crystallisation of racemic PSA and PCA in a 1:1 ratio resulted a co-crystal with the same stoichiometry. The compound crystallised in the centrosymmetric  $P\bar{1}$  (No. 2) space group and contains one molecule of PSA and one molecule of PCA in the ASU (Figure 3.11a). The succinic acid backbone of the PSA is bent and there was no proton transfer observed between the acid and the drug coformer. The PSA forms (1) an acid-amide heterodimer with the PCA that can be described with  $R_2^2(8)$  graph set (Figure 3.11a) and (2) an acid-acid homodimer via O11-H11...O10 and its symmetry generated counterpart. (This interaction can be described with the same graph set notation as the acid-amide heterodimer.) Based on intermolecular potential calculations<sup>5,6</sup> the strongest interaction in the crystal is the acid-acid homodimer ( $-41.8 \text{ kJ mol}^{-1}$ ) and the second strongest interaction is the acid-amide heterodimer ( $-39.0 \text{ kJ mol}^{-1}$ ). Therefore, it may be concluded that the supramolecular building unit of the crystal is the PCA-PSA-PSA-PCA tetramer (highlighted on Figure 3.11b with yellow). The tetramers interact with neighbouring units via the PCA moieties forming C20-H20...N22 and C23-H23...N19 hydrogen bonds (Figure 3.11b) and also weak hydrogen bonds are formed between the adjacent coplanar acid dimers (C6-H6...O10 and C7-H7...O11, Figure 3.11c). The crystal packing has a layered nature in the direction of [001] with alternating PSA and PCA layers (Figure 3.11d). The crystallographic details and hydrogen bonds for (R,S)-PSA·PCA are summarised in Tables 3.8 and 3.9.

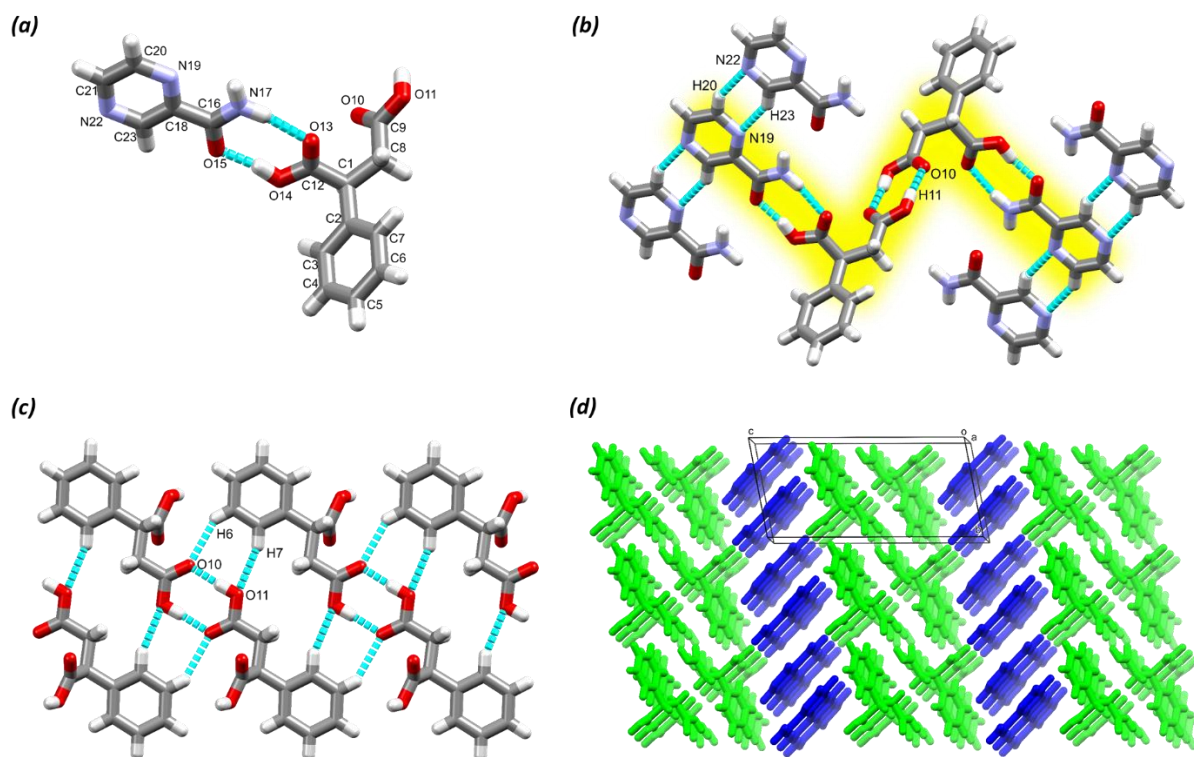


Figure 3.11 The ASU of (R,S)-PSA·PCA with labelled heavy atoms and the acid-amide dimer formation between PCA and PSA (a). Hydrogen bonds between the adjacent PCA molecules and the acid dimer formation between neighbouring PSA molecules (b). Hydrogen bonds between neighbouring acid dimers (c). Layered nature of the structure (PCA molecules with blue, PSA molecules with green colouring) (d).



Table 3.8 Crystal data for (R,S)-PSA•PCA.

Crystal data	
Compounds	(R,S)-PSA•PCA
Molecular formula	C <sub>15</sub> H <sub>15</sub> N <sub>3</sub> O <sub>5</sub>
Formula weight (g.mol <sup>-1</sup> )	317.30
Crystal system	Triclinic
Space group	<i>P</i> $\bar{1}$ (2)
a (Å)	5.7726(12)
b (Å)	7.9815(16)
c (Å)	16.594(3)
$\alpha$ (°)	99.36(3)
$\beta$ (°)	99.28(3)
$\gamma$ (°)	97.44(3)
V (Å <sup>3</sup> )	734.9(3)
Z	2
$\rho_{\text{calc}} / \text{g.cm}^{-3}$	1.434
$\mu$ (MoK $\alpha$ ) / mm <sup>-1</sup>	0.110
F (000)	332
Crystal size (mm)	0.040 × 0.220 × 0.900
Temperature (K)	173(2)
Radiation [Å]	MoK $\alpha$ (0.71073 Å)
Theta min-max [°]	1.266, 28.353
Dataset	-7:7, -10:10, -22:22
Final R indices [I > 2.0 (I)]	R <sub>1</sub> = 0.0403, wR <sub>2</sub> = 0.0898
R indices (all data)	R <sub>1</sub> = 0.0553, wR <sub>2</sub> = 0.0971
Tot., uniq.data, R (int)	19165, 2858, 0.0416
N <sub>ref</sub> , N <sub>par</sub>	3666, 224
S	1.040
Max. ans av. Shift/error	0.001, 0.000
Min. and max. resd. Dens (Å <sup>3</sup> )	-0.210, 0.274

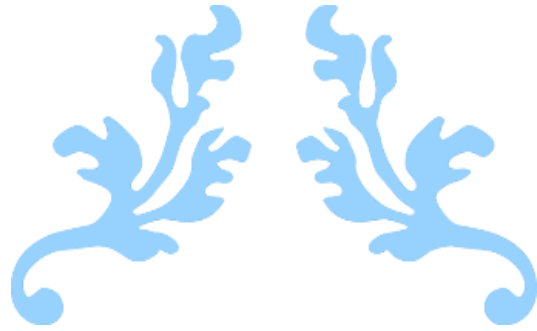
Table 3.9 Hydrogen bonds in (R,S)-PSA•PCA.

D-H...A	d(D-H) (Å)	d(H...A) (Å)	d(D...A) (Å)	D-H...A (°)	Symmetry operator
N17-H17A...O13	0.89	2.08	2.949	163.8	
O14-H14...O15	0.93	1.70	2.619	168.3	
O11-H11...O10	0.91	1.74	2.653	176.0	-x+1, -y+2, -z+1
C20-H20...N22	0.95	2.57	3.418	149.4	x+1, y, z
C23-H23...N19	0.95	2.57	3.419	148.8	x-1, y, z

## References

---

- <sup>1</sup> Ismael, M., Sahnoun, R., Suzuki, A., Koyama, M., Tsuboi, H., Hatakeyama, N., Endou, A., Takaba, H., Kubo, M., Shimizu, S., Del Carpio, C. & Miyamoto, A. 2009. *International Journal of Greenhouse Gas Control*, 3(5), 612-616.
- <sup>2</sup> Mondal, R. & Bhunia, M. 2008. *Journal of Chemical Crystallography*, 38(10), 787-792.
- <sup>3</sup> Jiang, H., Zhang, S. & Xu, Y. 2009. *Journal of Molecular Structure*, 919(1-3), 21-25.
- <sup>4</sup> Grothe, E., Meekes H., Vlieg E. ter Horst J. H. & de Gelder R. 2016. *Cryst. Growth Des.* 16, 3237–3243.
- <sup>5</sup> Gavezzotti, A. 1994. *Accounts of Chemical Research*, 27(10), 309-314.
- <sup>6</sup> Gavezzotti, A. & Filippini, G. 1994. *The Journal of Physical Chemistry*, 98(18), 4831-4837.

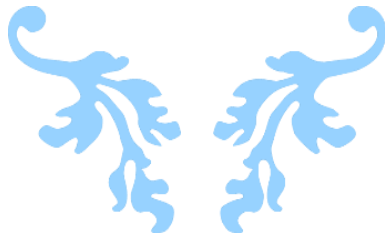


---

# CHAPTER IV

---

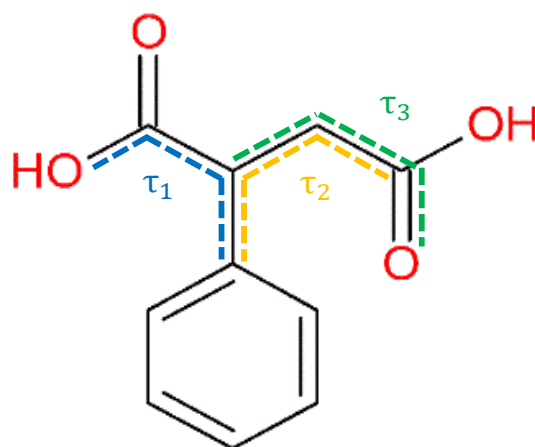
## BULK PROPERTY ANALYSIS



#### 4.1 Conformation analysis of the phenylsuccinic acid moiety

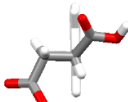
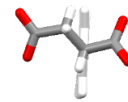
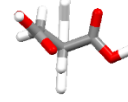
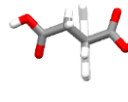
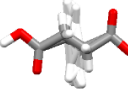
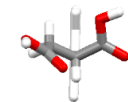
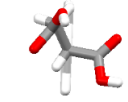
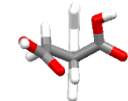
The PSA moiety showed a great variety of different conformations in the MCCs. To describe the conformations of the PSA, the following three torsion angles were considered:  $\tau_1$  ( $C_{\text{arom}}-C-C-O$ ),  $\tau_2$  ( $C_{\text{arom}}-C-C-C$ ) and  $\tau_3$  ( $C-C-C-O$ ) represented in Figure 4.1. In order to assess the distinctive conformations, a comparison was made by listing the torsion angles of PSA in each of the crystal structures in Table 4.1. The two typical conformations of PSA are based on the position of the succinic acid backbone and can be describe as ‘linear’ or ‘bent’. These were mentioned in the related structural descriptions because of their obviousness (see chapter 3). The independent rotation of the two carboxylic acid groups add an overtone to these basic conformations and creates a great variety of conformations of the PSA presented in the MCCs. The visual representation of this complex behaviour is shown in Table 4 (fourth column) by colouring the common aromatic rings white and positioning them to the back of the figure. The snapshots of the molecular conformations were taken looking down the  $C-C_{\text{arom}}$  bond, linking the aromatic ring and the backbone. The values of  $\tau_1$  varied from  $-64.15^\circ$  to  $-175.88^\circ$ , while  $\tau_2$  variation was from  $-70.57^\circ$  to  $176.14^\circ$  and  $\tau_3$ , with the largest variation, ranged from  $-160.12^\circ$  to  $164.75^\circ$ .

A recent study by Thompson and Day explained that molecules with large conformational flexibility often adopt high energy conformers when crystallising and compensate the energetically unfavoured conformation with the formation of inter- and intramolecular interactions.<sup>1</sup> The cases of PSA MCCs presented here are a great representation of this kind of behaviour.

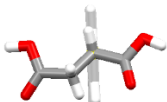
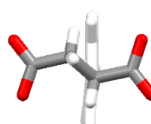
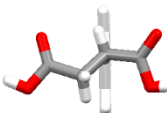
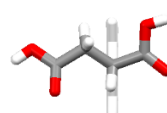
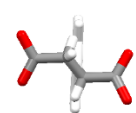
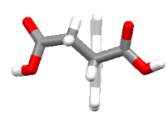
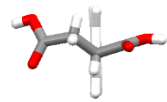
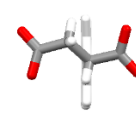
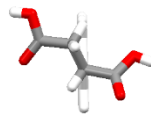
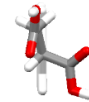


**Figure 4.1** Schematic representation of torsion angles of PSA.

**Table 4.1** Torsion angles and molecular conformations of PSA in MCCs

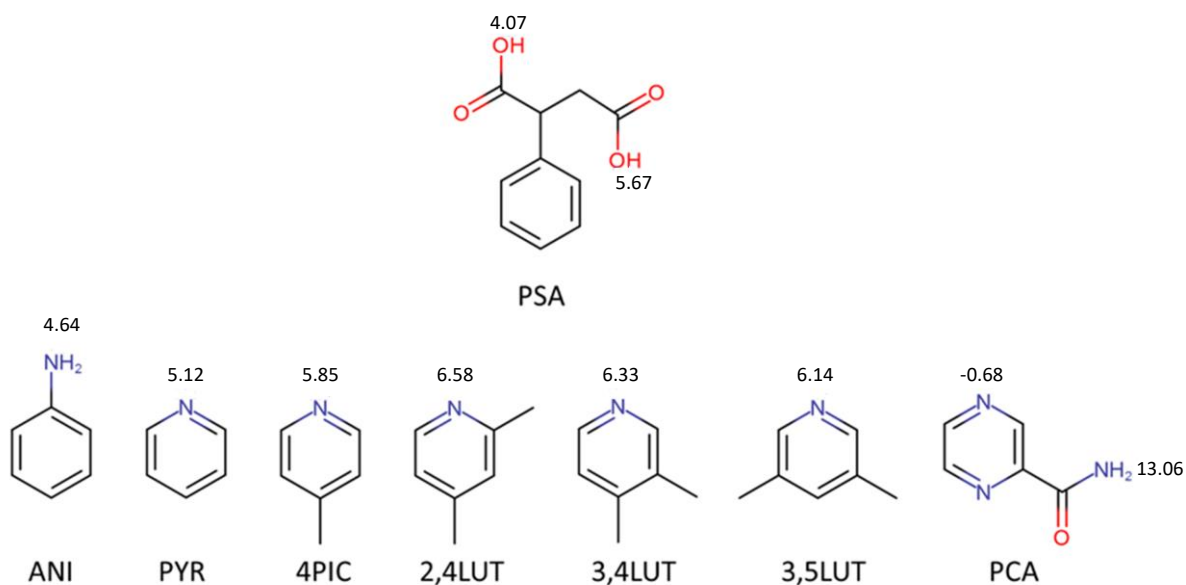
Crystal	$\tau_1(^{\circ})$	$\tau_2(^{\circ})$	$\tau_3(^{\circ})$	Conformation
[(R,S)-PSA] <sup>+</sup> [(ANI) <sup>+</sup> ]	-64.15	81.82	-130.86	
[(S)-PSA <sup>2-</sup> ][2ANI <sup>+</sup> ] $\cdot$ ANI	-105.83	56.68	-160.12	
(R,S)-PSA $\cdot$ 2PYR	-85.26	176.14	-6.65	
(R,S)-PSA $\cdot$ 2(4PIC)	-98.46	65.87	-159.22	
(R,S)-PSA $\cdot$ 2(2,4LUT)	-93.00	111.36	-11.73	
(R,S)-PSA $\cdot$ 2(3,4LUT)	-73.40	169.02	-6.36	
2(S-PSA) $\cdot$ 4(3,4LUT)	-113.11	165.80	-59.68	
	-75.46	171.77	-10.97	

**Table 4.1** Torsion angles and molecular conformations of PSA in MCCs (cont.)

Crystal	$\tau_1(^{\circ})$	$\tau_2(^{\circ})$	$\tau_3(^{\circ})$	Conformation
[(R,S)-PSA <sup>2-</sup> ] <sub>2</sub> [3,5LUT <sup>+</sup> ] <sub>2</sub> ·2(R,S)-PSA	-99.27	-49.03	-42.52	
	-93.93	60.12	-138.99	
	-71.72	-70.57	-31.28	
2[(S)-PSA <sup>2-</sup> ] <sub>4</sub> [3,5LUT <sup>+</sup> ] <sub>4</sub> ·4(S)-PSA	-78.14	70.06	-140.60	
	-117.66	76.08	164.75	
	-71.37	46.24	-130.48	
	-175.88	47.43	-117.61	
	-76.84	61.30	-140.35	
(R,S)-PSA·PCA	-127.54	64.23	154.65	
	-74.06	173.47	-18.10	

## 4.2 Protonation state of PSA and the cofomers in the multicomponent crystals

The prediction of a crystal structure to be a salt or a co-crystal is possible by evaluating the difference in the  $pK_a$  values of the acid-base pair that are included in the MCC. Therefore, the aqueous  $pK_a$  values for the co-crystallised compounds, PSA and amines, were calculated with Marvin<sup>2</sup> and are shown on Figure 4.2. The quantitative  $pK_a$  rule by Cruz Cabeza<sup>3</sup> was used to calculate the  $\Delta pK_a$  values for the acid-base pairs ( $\Delta pK_a = pK_a(\text{base}) - pK_a(\text{acid})$ , Table 4.2). As it was emphasised by the author, the quantitative  $pK_a$  rule was derived from “crystal structures in which one single proton was transferred, or the potential transfer of the most acidic proton of the acid to the most basic atom of the base, were considered (first ionisation constant only)”, therefore its application for the co-crystallisation of PSA, a diacid, should be evaluated with caution. The  $\Delta pK_a$  values were calculated with both the more acidic ( $pK_a = 4.07$ ) and the less acidic ( $pK_a = 5.67$ ) carboxylic acid group of the PSA for clarity, but it was noted that only the values based on the first ionisation constants should be discussed ( $\Delta pK_{a1}$ ). With the exception of the PCA, all cofomers are liquids and were used as a ‘solvent’ during the co-crystallisation experiments. This carries significance, hence the  $pK_a$  value of a compound depends significantly on the solvent used to dissolve it. The co-crystal of PSA and PCA was obtained from methanol. However, the study of Cruz Cabeza on  $pK_a$  did not cover the effect of different solvents, which acknowledgedly influence the values of the  $pK_a$ .<sup>4</sup> The quantitative  $pK_a$  rule states that co-crystals are expected to form if the  $\Delta pK_a$  is below -1 (zone 1), salt formation is expected if the  $\Delta pK_a$  is higher than 4 (zone 3) and, between these two boundaries lies the so called ‘salt-cocrystal continuum’ (zone 2)<sup>5</sup> where, around  $\Delta pK_a = 1$ , the formation of a salt or a co-crystal practically equal. The majority of the values, were found in zone 2, where the relative occurrence of ionised complexes increases linearly with increasing  $\Delta pK_a$  values. The obtained values for  $\Delta pK_{a1}$  varied from 0.57 to 6.35 and spread across the  $\Delta pK_a$  spectrum, with the majority lies in zone 2. It is unfortunate that none of the expectations that were based on the  $\Delta pK_a$  values were successfully fulfilled by the formed crystals. The five types of crystal emerged from these crystallisations (a true salt, a salt solvate, a solvate, a co-crystal and a co-crystal salt) emphasises further the complexity of zone 2 and this diversity points out again the importance of the recently published classification system for multicomponent crystals<sup>6</sup>.

Figure 4.2  $pK_a$  values of PSA and coformersTable 4.2  $\Delta pK_a$  values for PSA and selected coformers

Coformers	Acid	$\Delta pK_{a1}^*$	$\Delta pK_{a2}^*$	Expectation	Outcome
ANI	(R,S)-PSA	0.57	-1.03	Co-crystal > salt	True salt
ANI	(S)-PSA	0.57	-1.03	Co-crystal > salt	Salt solvate
PYR	(R,S)-PSA	1.05	-0.55	Co-crystal ~ salt	Solvate
4PIC	(R,S)-PSA	1.78	0.18	Co-crystal < salt	Solvate
2,4LUT	(R,S)-PSA	2.51	0.91	Co-crystal < salt	Solvate
3,4LUT	(R,S)-PSA	2.26	0.66	Co-crystal < salt	Solvate
3,4LUT	(S)-PSA	2.26	0.66	Co-crystal < salt	Solvate
3,5LUT	(R,S)-PSA	2.07	0.47	Co-crystal < salt	Co-crystal salt
3,5LUT	(S)-PSA	2.07	0.47	Co-crystal < salt	Co-crystal salt
PCA	(R,S)-PSA	6.35	4.75	Salt	Co-crystal

\*  $\Delta pK_a = pK_a(\text{base}) - pK_a(\text{acid})$



### 4.3 Z parameters of the multicomponent crystals

The discussed multicomponent crystal structures of PSA highlighted their structural complexity, but the complete description of the crystal structures cannot be finalised without the discussion of their full set of Z parameters. Due to the complexity of their nature it is crucial to define these parameters once again. The number of molecules in the entire unit cell is denoted as Z; the symbol Z' is defined as the number of molecules in the unit cell divided by the group multiplicity; the parameter Z'' is the sum of the components within the asymmetric unit, while Z' is the quantity of distinct kinds of chemical residues. It is important to note here, that enantiomers are not counted separately when Z' and Z' values are calculated. Based on the definition of Z', another problem arises too.

Since co-crystals and salts are differentiated by the proton transfer from the acid to the base, it is logical to consider the neutral PSA and the deprotonated PSA as two different types of molecules. If this is the case, therefore, new Z' values can be allocated for some of the crystals and they are shown in brackets following the original values (Table 4.3).

Steed and Steed stated that “There is no “driving force” toward  $Z' = 1$  or inherent preference for symmetry.” but they listed a series of scenarios when crystallisation may occur with  $Z' > 1$ . Two of the cases are (1) when compounds crystallise with resolved chirality and therefore the possible symmetry operators are limited and (2) when strong directional intermolecular interactions are formed between the molecules. In the case of the PSA crystals discussed here, both of these listed situations are apparent. Excellent examples to represent the complexity of the problem are the racemic and enantiopure pairs of 3,4LUT and 3,5LUT crystals (Table 4.3).

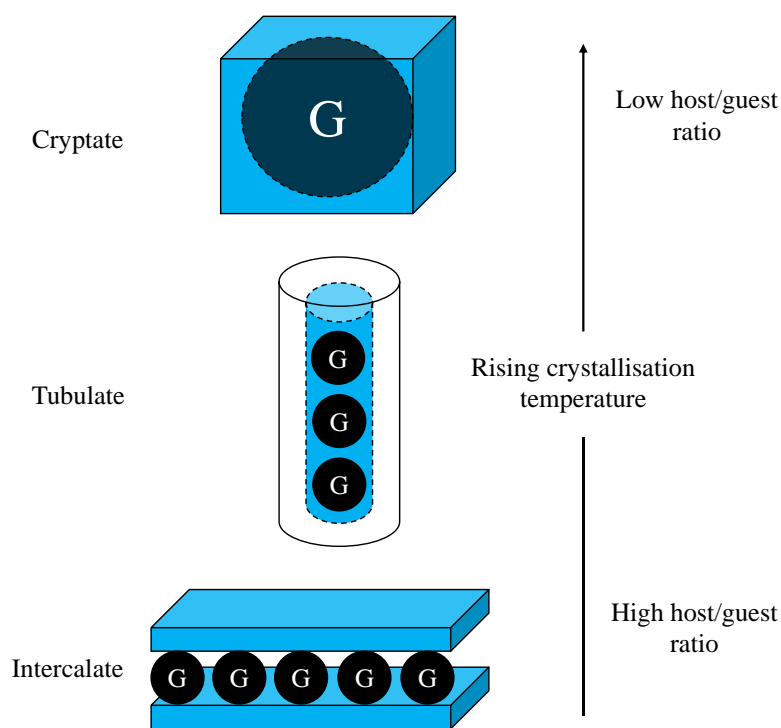
**Table 4.3** Z Space groups and parameters for PSA MCCs

Crystal	Space group	Z	Z'	Z''	Z'
[(R,S)-PSA·][ANI <sup>+</sup> ]	<i>Pn</i>	2	1	2	2
[(S)-PSA <sup>2-</sup> ][2ANI <sup>+</sup> ·ANI	<i>P2<sub>1</sub></i>	4	1	4	2 (3)
(R,S)-PSA·2PYR	<i>P<math>\bar{1}</math></i>	2	1	3	2
(R,S)-PSA·2(4PIC)	<i>P2<sub>1</sub>/c</i>	4	1	3	2
(R,S)-PSA·2(2,4LUT)	<i>P2<sub>1</sub>/c</i>	4	1	3	2
(R,S)-PSA·2(3,4LUT)	<i>P<math>\bar{1}</math></i>	2	1	3	2
2(S)-PSA·4(3,4LUT)	<i>P1</i>	2	2	6	2
[(R,S)-PSA <sup>2-</sup> ] <sub>2</sub> [3,5LUT <sup>+</sup> ] <sub>2</sub> ·2(R,S)-PSA	<i>P2<sub>1</sub>/c</i>	4	1	5	2 (3)
2[(S)-PSA <sup>2-</sup> ] <sub>4</sub> [3,5LUT <sup>+</sup> ] <sub>4</sub> ·4(S)-PSA	<i>P1</i>	1	2	10	2 (3)
(R,S)-PSA·PCA	<i>P<math>\bar{1}</math></i>	2	1	2	2

#### 4.4 Structure-property relationships in PSA crystals

Comparison of topology of inclusion compounds and how their physical chemical properties may be linked to this feature are in the centre of interest of the crystal engineering community.

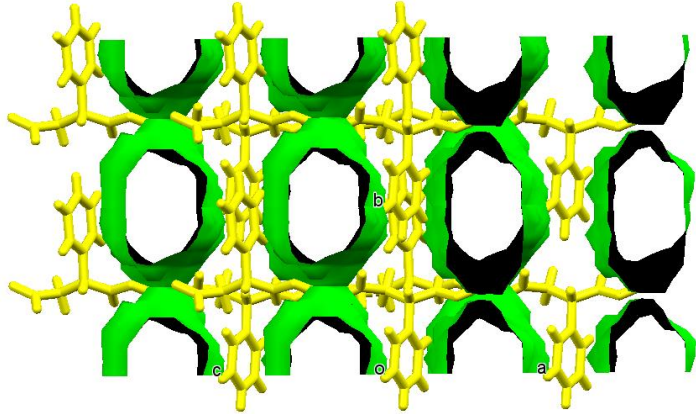
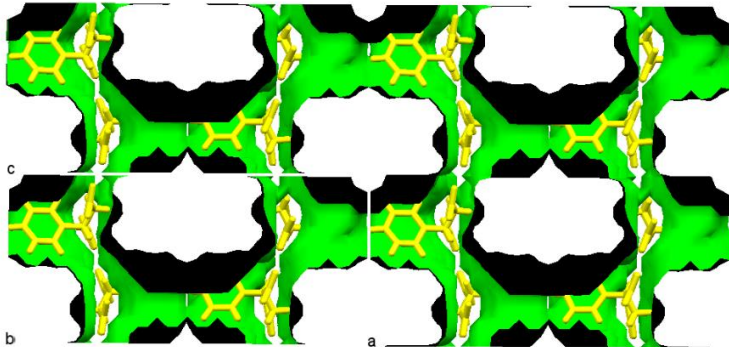
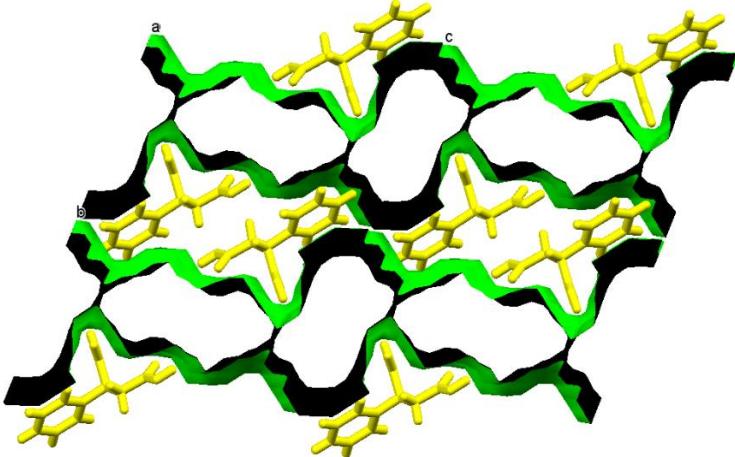
Ibragimov found correlation between the structures of host-guest complexes and their crystallisation temperatures and concluded that the crystallisation temperature increases with the decreasing host:guest ratio.<sup>7</sup> It was also noted that the different topologies of the crystalline material can be described as (1) intercalate, (2) tubulate, or (3) cryptate, according to decreasing host:guest ratios (Fig. 4.3).<sup>8</sup> To classify the PSA crystals according to this system, the bases were defined as the ‘guest’ and the PSA as the ‘host’.



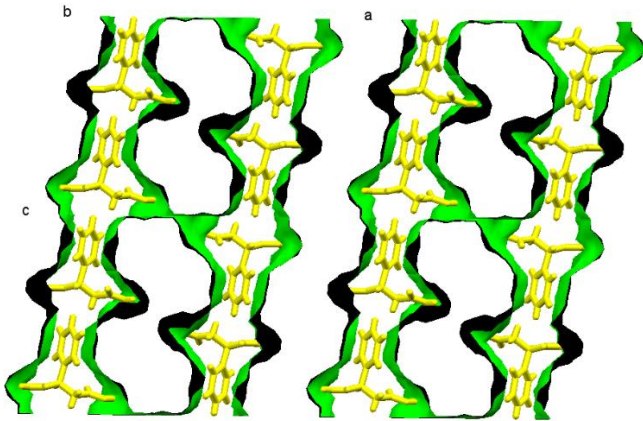
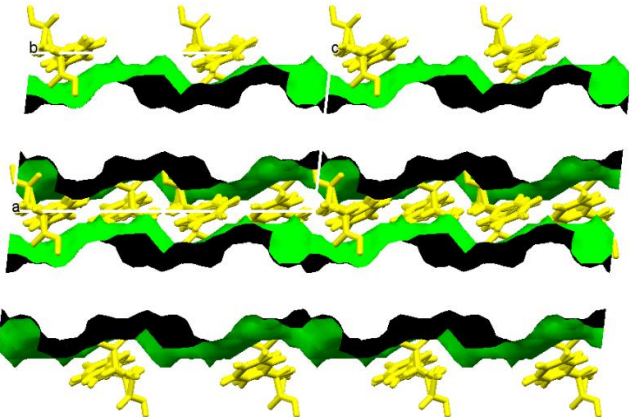
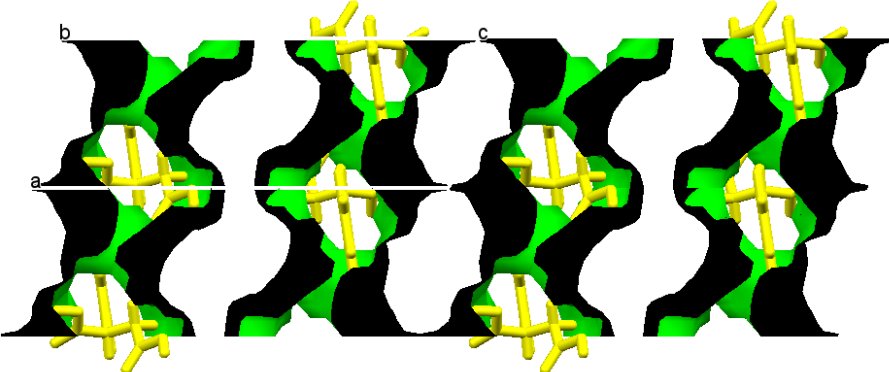
**Figure 4.3** Change in topology with crystallisation temperature

The bases (guest molecules) were removed from the structures and the volume of the created voids were calculated with the aid of Mercury (the probe size and the grid spacing were 1.2Å and 0.7Å, respectively). The graphical representation of the ‘empty’ host structures, the classification of the crystals, their calculated densities and the % void space are listed in Table 4.4. Channels and layers were observed with the void percentage varying from 28.8% to 63.3%, while the densities are ranging from 1.221 to 1.341 g.cm<sup>-3</sup>.

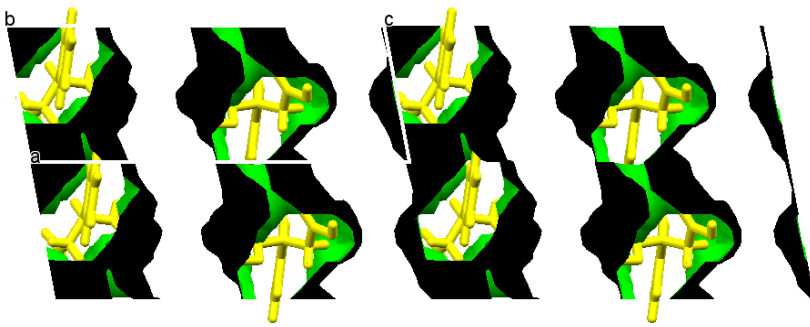
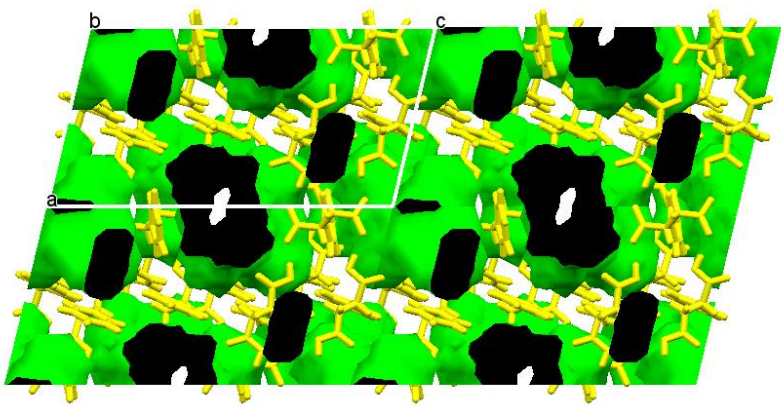
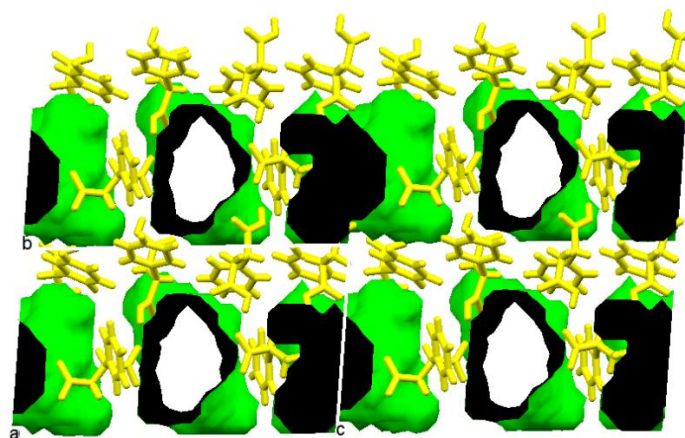
**Table 4.4** Densities, voids, solvent percentages for PSA MCCs

Crystal	Density	%Base	H:G ratio	Type
$[(R,S)\text{-PSA}^+][\text{ANI}^+]$	1.314 g.cm <sup>-3</sup>	36.5%	1:1	Tubulate
				
$[(S)\text{-PSA}^{2-}][2\text{ANI}^+]\cdot\text{ANI}$	1.221 g.cm <sup>-3</sup>	63.3%	1:3	Tubulate
				
$(R,S)\text{-PSA}\cdot 2\text{PYR}$	1.341 g.cm <sup>-3</sup>	44.6%	1:2	Intercalate
				

**Table 4.4** Densities, voids, solvent percentages for PSA MCCs (cont.)

Crystal	Density	%Base	H:G ratio	Type
(R,S)-PSA·2(4PIC)	1.272 g.cm <sup>-3</sup>	55.5%	1:2	Intercalate
				
(R,S)-PSA·2(2,4LUT)	1.223 g.cm <sup>-3</sup>	54.6%	1:2	Intercalate
				
(R,S)-PSA·2(3,4LUT)	1.255 g.cm <sup>-3</sup>	59.1%	1:2	Intercalate
				

**Table 4.4** Densities, voids, solvent percentages for PSA MCCs (cont.)

Crystal	Density	%Base	H:G ratio	Type
<b>2(S)-PSA·4(3,4LUT)</b>	1.227 g.cm <sup>-3</sup>	58.1%	2:4	Intercalate
				
<b>[(R,S)-PSA<sup>2-</sup>] 2[3,5LUT<sup>+</sup>]<b>·</b>2(R,S)-PSA</b>	1.298 g.cm <sup>-3</sup>	33.5%	2:3	Tubulate
				
<b>2[(S)-PSA<sup>2-</sup>] 4[3,5LUT<sup>+</sup>]<b>·</b>4(S)-PSA</b>	1.296 g.cm <sup>-3</sup>	28.8%	4:6	Tubulate
				

Thermogravimetry analysis (TGA) and differential scanning calorimetry (DSC) were used to monitor the thermal behaviour of the PSA MCCs under thermal stress. The TGA results were used to obtain accurate PSA:base % ratios and DSC was applied to record accurate melting temperatures and melting enthalpies of the PSA crystals. The results for the pure PSA (racemic and S-enantiomer) and the PSA:base crystals are summarised in Table 4.5 while the TGA and DSC curves for the multicomponent crystals are presented in the Appendix.

The TGA and DSC curves reveal congruent melting process for all the multicomponent crystals. Congruent melting occurs typically when a multicomponent compound melts and the composition of the melt (liquid) that forms is the same as the composition of the solid, i.e. there is no distinguishable step on the TGA curve that can be related undoubtedly to the release of the guest and thus subsequently, the DSC curve shows only one endotherm.<sup>9,10</sup> The congruent melting observed in all of the MCC's is due to the good solubility of the PSA in the bases used for the co-crystallisations. For example, the decomposition of the [(R,S)-PSA<sup>2-</sup>]<sub>2</sub>[3,5LUT<sup>+</sup>]<sub>2</sub>·2(R,S)-PSA and 2[(S)-PSA<sup>2-</sup>]<sub>4</sub>[3,5LUT<sup>+</sup>]<sub>4</sub>·4(S)-PSA crystals produced a TGA curve with one step, thus the calculation of the % base ratio was impossible for the bulk material. For some of the crystals we were able to guess the step related to the release of the base by using the first derivative of the TGA curve but even in these crystals significant differences were found between the measured and the theoretical % mass losses that are ranging from 1.57% to 32.74%.

**Table 4.5** Thermoanalytical data for PSA MCCs

Acid	Cofomer	TGA					DSC			
		% DECOMPOSITION			H:G ratio		MELTING POINT			
		Measured %	Theoretical %	Difference %	TGA	SCXRD	Onset °C	Peak °C	ΔH J/g	ΔT °C
(R,S)-PSA	-	n/a	n/a	n/a	n/a	n/a	170.15	171.97	146.37	n/a
(S)-PSA	-	n/a	n/a	n/a	n/a	n/a	172.05	177.54	140.15	n/a
PCA	-	n/a	n/a	n/a	n/a	n/a	189.09	191.34	194.54	n/a
(R,S)-PSA	ANI	30.84	32.41	-1.57	1:1	1:1	135.28	137.79	135.66	77.02
(S)-PSA	ANI	48.01	59.00	-10.99	1:2.4	1:3	61.00	63.55	108.30	78.92
(R,S)-PSA	PYR	34.01	44.89	-10.88	1:1.5	1:2	62.17	70.07	97.13	91.05
(R,S)-PSA	4PIC	20.95	48.96	-28.01	1:0.9	1:2	65.72	69.76	92.76	77.02
(R,S)-PSA	3,4LUT	30.61	59.07	-28.46	1:1	1:2	84.99	88.32	146.95	7.15
(S)-PSA	3,4LUT	36.08	68.82	-32.74	2:2.1	2:4	55.46	63.46	80.25	9.05
(R,S)-PSA	3,5LUT	97.32	62.34	n/a	n/a	2:3	134.76	138.78	110.21	1.15
(S)-PSA	3,5LUT	95.51	76.80	n/a	n/a	4:6	97.12	103.19	71.79	3.05
(R,S)-PSA	PCA	97.21	55.91	n/a	n/a	1:2	125.27	130.21	109.97	n/a

\*Thermoanalytical results for (R,S)-PSA·2.4LUT were not performed due to lack of sample.

\* $\Delta T = T_{onset} - T_{boiling (base)}$

The melting endotherms recorded by DSC show that the starting materials (R,S-PSA and S-PSA), have higher melting temperatures ( $T_{\text{on, R,S-PSA}} = 170.15\text{ }^{\circ}\text{C}$  and  $T_{\text{on, S-PSA}} = 172.05\text{ }^{\circ}\text{C}$ ) compared to all the inclusion compounds, as well as the pharmaceutical co-crystal. It is also interesting to note that the chiral acid has higher melting point than the racemic counterpart. This is an interesting observation because, based on Wallach's rule<sup>11</sup>, the melting point of a racemic crystal expected to be higher than its chiral counterpart, but PSA clearly does not fulfil this expectation.

The melting temperatures of the MCCs are presented on a bar chart for clarity (Figure 4.4, for systematic comparison, the pharmaceutical co-crystal was excluded from the bar chart) and the bars are coloured according to the MCC classification system discussed in Chapter 1. The lower melting points relate to the solvates, while co-crystal salts or true salts have higher melting points. Comparison of the melting points of the racemic-chiral crystal pairs reveals that in all three cases (inclusion of ANI, 3,4LUT and 3,5LUT) the racemic crystals have significantly higher melting point than the chiral counterpart and, thus here Wallach's rule is fulfilled.

It is interesting to note that while the hydrogen bonding ability of the chiral and the racemic PSA is the same when exposed to aromatic amines, i.e. the same acid-base heterosynthion is expected to be formed, the crystal packing can differ significantly. It is understood that the crystal packing is a results of many more factors than the hydrogen bond formation between the acid and the base but it is intriguing how significant the effect of chirality can be on the packing and physical chemical properties of the multicomponent crystals.

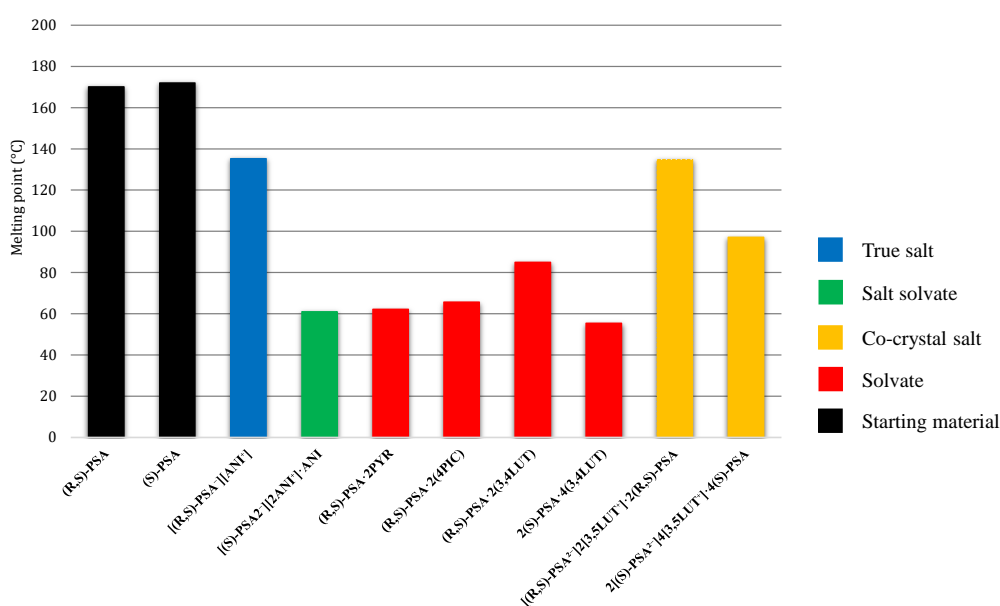


**Figure 4.4** Colour coded bar chart of melting points of PSA MCCs

#### 4.5 Occurrence of the $R_2^2(7)$ heterosynthon between carboxylic acid and aromatic amine moieties

The formation of the  $R_2^2(7)$  heterosynthon is an important crystal engineering tool. It is expected that this synthon forms when carboxylic acids hydrogen bond to aromatic amines. The formation of this synthon can happen when both the acid and the base stay neutral or the same graph set descriptor may be used to describe the synthon if proton transfer happens between the moieties and two charged molecular ions are interacting (Figure 4.5). The PSA MCCs discussed here are good examples for the formation of the  $R_2^2(7)$  heterosynthon of both types. To understand how common these motifs occur, with a special focus on its formation in chiral and racemic crystals too, a CSD analysis was carried out (Cambridge Structural Database, Nov 2018) with the aid of ConQuest (version 2.0.2, build 246535). General search filters were applied: 3D coordinates determined,  $R < 10\%$ , no errors, non-polymeric structures, and only single crystal structures were included. Organics were analysed separately and also subsets were created that include both organics and organometallics for completeness. The results of the organics are discussed here, and the results that contain both organics and organometallics are presented in the Appendix.

The  $R_2^2(7)$  heterosynthon may be formed between (1) a carboxylic acid and a pyridine moiety or (2) a carboxylate group and a pyridinium cation (Figure 4.5). The neutral (typically found in co-crystals) and the charged (typically found in salts) arrangements were investigated separately to compare the possible differences on the occurrence of the motifs. The results of the search are presented in Fig. 4.6 and 4.7.



**Figure 4.5** The  $R_2^2(7)$  heterosynthon formed in co-crystals and salts



The subset of carboxylic acid and pyridine moieties gave 2500 hits, out of which 710 (28.4%) present the  $R_2^2(7)$  heterosynthon only, and 40 hits (5.6%) crystallised in space groups that allow the crystallisation of enantiopure compounds. The majority of the 710 hits crystallised in centrosymmetric space groups (623 hits, 87.7%). In case of hydrogen transfer, i.e. when the  $R_2^2(7)$  heterosynthon forms between carboxylate and pyridinium moieties, the outcome of the analysis is similar. The subset of carboxylate and pyridinium moieties gave 1025 hits, out of which 256 (24.9%) present the  $R_2^2(7)$  heterosynthon. 24 hits (9.37%) represents structures that crystallised in space groups that allow enantiopure compounds. The majority of the 256 hits crystallised in centrosymmetric space groups (217, 84.7%). It is interesting to note, that crystals with ‘double motifs’, i.e. when both charged and non-charged  $R_2^2(7)$  heterosynthons occur in the same crystal, are very rare. Only 9 hits of this kind were found in the CSD and all of them crystallised in centrosymmetric space groups.

Four of the PSA MCCs presented in this work ((R,S)-PSA·2PYR, (R,S)-PSA·2(4PIC), (R,S)-PSA·2(2,4LUT) and (R,S)-PSA·2(3,4LUT)) form neutral  $R_2^2(7)$  heterosynthons and crystallised in centrosymmetric space groups. The 2(S)-PSA·4(3,4LUT) also forms the  $R_2^2(7)$  heterosynthon but, obviously, crystallises in a non-centrosymmetric space group. Interestingly, the inclusion compounds [(R,S)-PSA<sup>2-</sup>]<sub>2</sub>[3,5LUT<sup>+</sup>]<sub>2</sub>·2(R,S)-PSA and 2[(S)-PSA<sup>2-</sup>]<sub>4</sub>[3,5LUT<sup>+</sup>]<sub>4</sub>·4(S)-PSA did not form the ‘expected’  $R_2^2(7)$  heterosynthon but the hydrogen bonds are similar in nature in both the chiral and the enantiopure crystals. In the crystal of (R,S)-PSA·PCA the acid-amide synthon was observed instead of the  $R_2^2(7)$  heterosynthon.

To summarise, the statistical analysis showed that the occurrence of the formation of the  $R_2^2(7)$  heterosynthon when both carboxylic acid/carboxylate and pyridine/pyridinium moieties are presented in the same crystal structure is around 25-30%. The formation of this synthon is less possible in the case of crystallising enantiopure crystals because the limitations of the packing of chiral compounds adds an extra constraint to the crystallisation step. Recently it was shown that molecules with large conformational flexibility may adopt high energy conformers when crystallising and, to compensate the energetically unfavoured conformation additional inter- and intramolecular interactions are formed.<sup>1</sup> This scenario is especially valid for the crystallisation of enantiopure compounds. In a reverse logic, it is equally possible, that molecules will ‘sacrifice’ strong intermolecular interactions in favour of close packing during crystallisation.

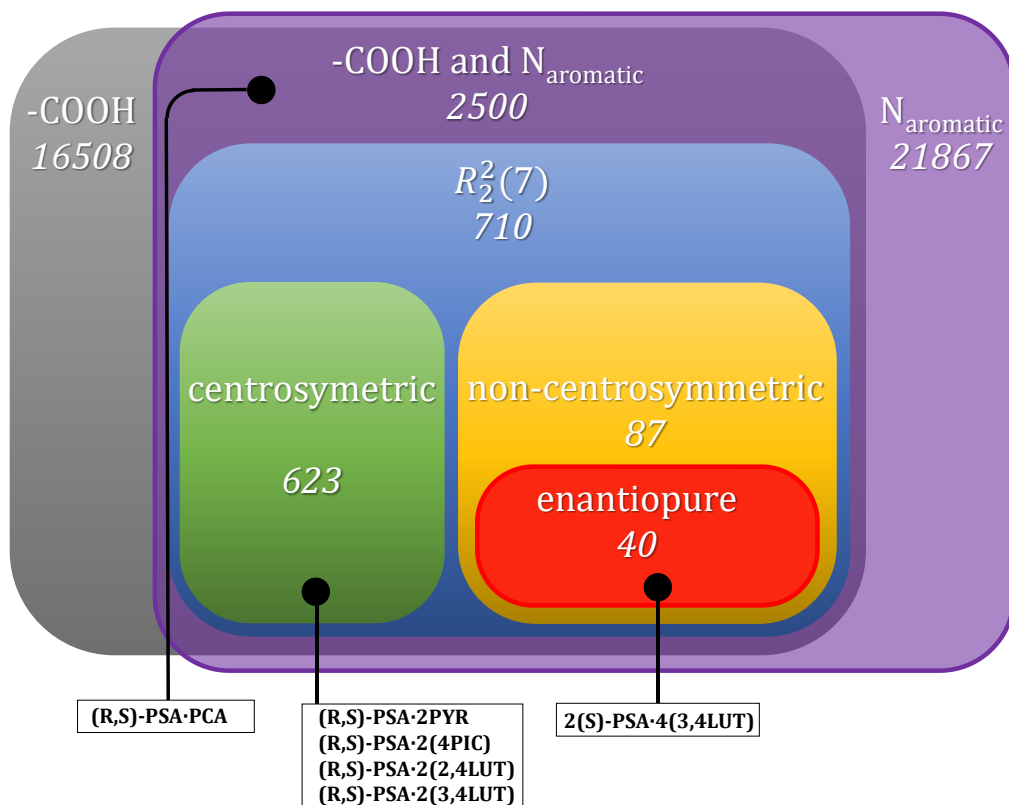


**Figure 4.6** Occurrence of carboxylic acid and pyridine moieties, and their combination in the CSD

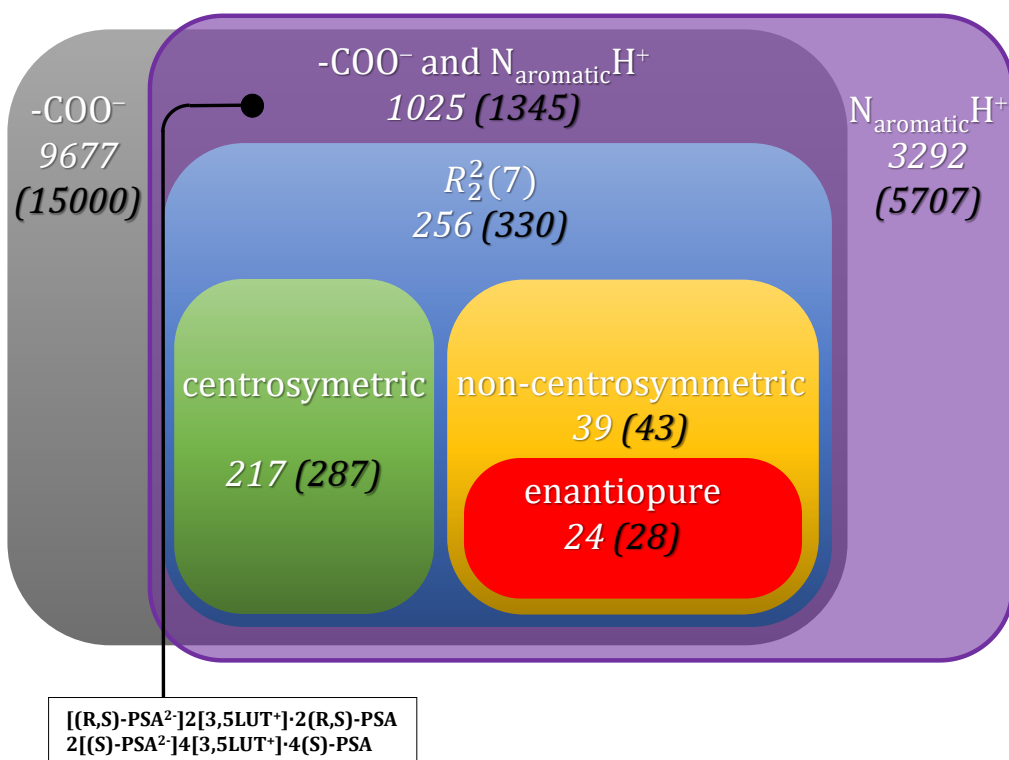
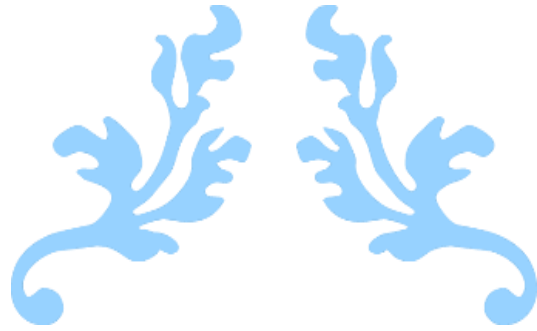


**Figure 4.7** Occurrence of carboxylate and pyridinium moieties, and their combination in the CSD

## References

- 
- <sup>1</sup> Thompson H. P. G. & Day G. M. 2014. *Chem. Sci.* 5, 3173-3182.
  - <sup>2</sup> Calculator Plugins were used for structure property prediction and calculation, Marvin 16.4.25.0, 2016, ChemAxon, (<http://www.chemaxon.com>)
  - <sup>3</sup> Cruz-Cabeza, A. J. 2012. *CrystEngComm*, 14: 6362-6365.
  - <sup>4</sup> Black S. N., Collier E. A., Davey R. J. & Roberts R. J. 2007. *J. Pharm. Sci.* 96, 1053-1068.
  - <sup>5</sup> Childs S. L., Stahly G. P. & Park A. 2011. *Mol. Pharm.*, 4, 323-338.
  - <sup>6</sup> Grothe, E., Meekes H., Vlieg E. ter Horst J. H. & de Gelder R. 2016. *Cryst. Growth Des.* 16, 3237-3243.
  - <sup>7</sup> Ibragimov, B. T. 1999. *Macrocyclic Chem.* 34, 345-353
  - <sup>8</sup> Nassimbeni L. 2003. *Acc. Chem. Res.* 36, 631-637
  - <sup>9</sup> White, M. & Perry, R. 1994. *Chemistry of Materials*, 6(5), 603-610.
  - <sup>10</sup> Greenwood, J. & Hess, P. 1998. *Journal of Geophysical Research: Solid Earth*, 103(B12), 29815-29828.
  - <sup>11</sup> Brock, C. P., Schweizer, W. B. & Dunitz, J. D. 1991. *J. Am. Chem. Soc.* 113, 9811-9820.

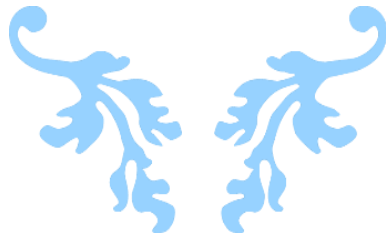


---

# CHAPTER V

---

## SUMMARY & CONCLUSION



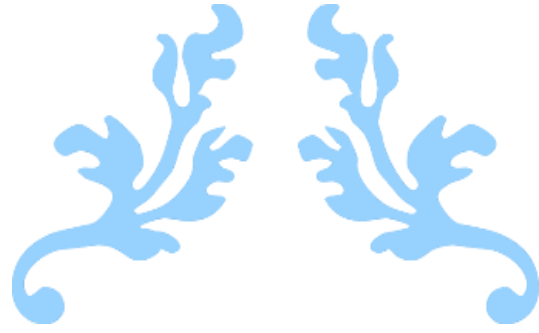
Chiral molecules are known to contrast in their physical and chemical properties relying upon whether they are available as the racemate or the pure enantiomer. Thus, the design and production of the chiral and racemic crystalline materials with desired properties remain a difficult task. The primary aim of this research was to design and synthesise a series of (i) multicomponent crystals of phenylsuccinic acid, which have limited options for auxiliary interactions with added conformational flexibility, while the co-crystallising compounds (primary and aromatic amines) were varied systematically; and (ii) a series of pharmaceutical multicomponent crystals using pyrazine carboxamide while the co-crystallising compound or cofomer was phenylsuccinic acid. The acid was used in a racemic mixture form and in an optical active enantiomer (*S* form), for both model and pharmaceutical multicomponent crystals. The dicarboxylic acid was chosen to explore the formation of the O–H···N hydrogen bonding and the synthon arrangement in the inclusion compounds to enlighten the effect of chirality on the crystal packing, while the choice of the bases was due to the position and quantity of the methyl groups around the pyridine moiety. Eleven new crystalline materials were synthesised by combining phenylsuccinic acid (PSA, racemate or the *S*-enantiomer), with primary or aromatic amines (aniline, ANI, pyridine, PYR, 4-picoline, 4PIC, 2,4-lutidine, 2,4LUT, 3,4-lutidine, 3,4LUT and 3,5-lutidine, 3,5LUT) and the drug pyrazinecarboxamide (PCA). The multicomponent crystals formed were examined by differential scanning calorimetry, thermogravimetric analysis, powder and single crystal X-ray diffraction and Fourier transform infrared spectroscopy for their complete characterisation. Ten out of the eleven novel crystal structures resulted in multicomponent crystals with the expected composition, i.e. both the acid and the base were included in the crystal. Co-crystallisation of (R,S)-PSA with *tert*-butylamine (tBa) under atmospheric conditions produced crystals with unexpected chemical composition. The amine reacted with the atmospheric CO<sub>2</sub> and formed a carbonate salt [2tBa<sup>+</sup>][COO<sup>2-</sup>]. The successful co-crystallisations resulted in a variety of different crystal forms: five solvates ((R,S)-PSA·2PYR, (R,S)-PSA·2(4PIC), (R,S)-PSA·2(2,4LUT), (R,S)-PSA·2(3,4LUT), 2(S)-PSA·4(3,4LUT), two co-crystal salts ([ (R,S)-PSA<sup>2-</sup> ]<sub>2</sub>[3,5LUT<sup>+</sup>]<sub>2</sub>·2(R,S)-PSA and 2[(S)-PSA<sup>2-</sup>]<sub>4</sub>[3,5LUT<sup>+</sup>]<sub>4</sub>·4(S)-PSA), one salt ([ (R,S)-PSA<sup>-</sup> ][ANI<sup>+</sup>]), one salt-solvate ([ (S)-PSA<sup>2-</sup> ][2ANI<sup>+</sup>]<sub>2</sub>·ANI) and a co-crystal (R,S)-PSA·PCA) were identified. Grinding was successfully used to reproduce the multicomponent crystals obtained via slow evaporation method with the exception of [(S)-PSA<sup>2-</sup>]<sub>2</sub>[2ANI<sup>+</sup>]<sub>2</sub>·ANI. The task to obtain chiral crystals was extremely challenging. Only three bases (ANI, 3,4LUT and 3,5LUT) were successfully co-crystallised with (*S*)-phenylsuccinic acid. The phenylsuccinic acid showed great conformational variety and the acid:base ratios varied significantly in the

obtained crystals: 1:1 in the co-crystal, 1:2 in the solvates, 2:3 in the co-crystal salts, and 1:1 and 1:3 in the salt and salt solvate, respectively. The analysis of the crystal packing ( $Z$  and related parameters, void analysis, etc.) highlighted the complexity of the packing of the multicomponent crystals and the significant differences between the racemic multicomponent crystals and their chiral counterparts. Values of  $Z' > 1$  were observed exclusively in the chiral structures of 2(S)-PSA·4(3,4LUT) and 2[(S)-PSA<sup>2-</sup>]<sub>4</sub>[3,5LUT<sup>+</sup>]<sub>4</sub>·4(S)-PSA).

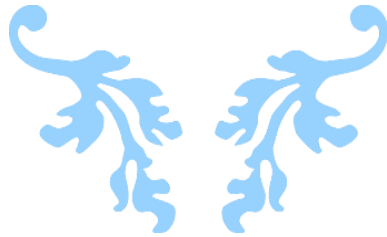
The thermoanalysis of the multicomponent crystals revealed congruent melting due to the good solubility of the acid in the base; the decomposition curve showed no mass loss that could be associated to the release of the solvent/base. The melting points of the crystals revealed that the enantiopure crystals had lower melting points than their racemic counterparts which agrees well with the common observation that enantiopure structures pack less efficiently, indicated by the relatively lower densities, and therefore are expected to be less stable under thermal stress.

The acid-base heterosynthon, depicted as  $R_2^2(7)$ , was formed between the carboxylic acid and the pyridine moiety only in five of the multicomponent crystals: (R,S)-PSA·2PYR, (R,S)-PSA·2(4PIC), (R,S)-PSA·2(2,4LUT), (R,S)-PSA·2(3,4LUT) and 2(S)-PSA·4(3,4LUT). Interestingly, in the co-crystal of (R,S)-PSA·PCA the carboxylic acid formed hydrogen bonds via the amide functional group of the PCA instead of via the aromatic nitrogen atom. In [(R,S)-PSA<sup>2-</sup>]<sub>2</sub>[3,5LUT<sup>+</sup>]<sub>2</sub>·2(R,S)-PSA, 2[(S)-PSA<sup>2-</sup>]<sub>4</sub>[3,5LUT<sup>+</sup>]<sub>4</sub>·4(S)-PSA, [(R,S)-PSA<sup>-</sup>] [ANI<sup>+</sup>] and [(S)-PSA<sup>2-</sup>]<sub>2</sub>[2ANI<sup>+</sup>] the expected acid-amine heterosynthon was not formed. The occurrence of the  $R_2^2(7)$  synthon was investigated on a statistically more significant dataset with the aid of the Cambridge Structural Database and the analysis revealed that the heterosynthon is formed only in 25-30% of the cases. It was also concluded that formation of the  $R_2^2(7)$  synthon is less expected when crystallising enantiopure compounds because the limitations of the packing of chiral compounds adds an extra constraint to the packing of the crystal.

We believe that the results presented here are important contributions to the field of crystal engineering and the supramolecular chemistry of chiral vs racemic formulations and, generate potential interest in the field of pharmaceutical formulations in the future.



# APPENDIX



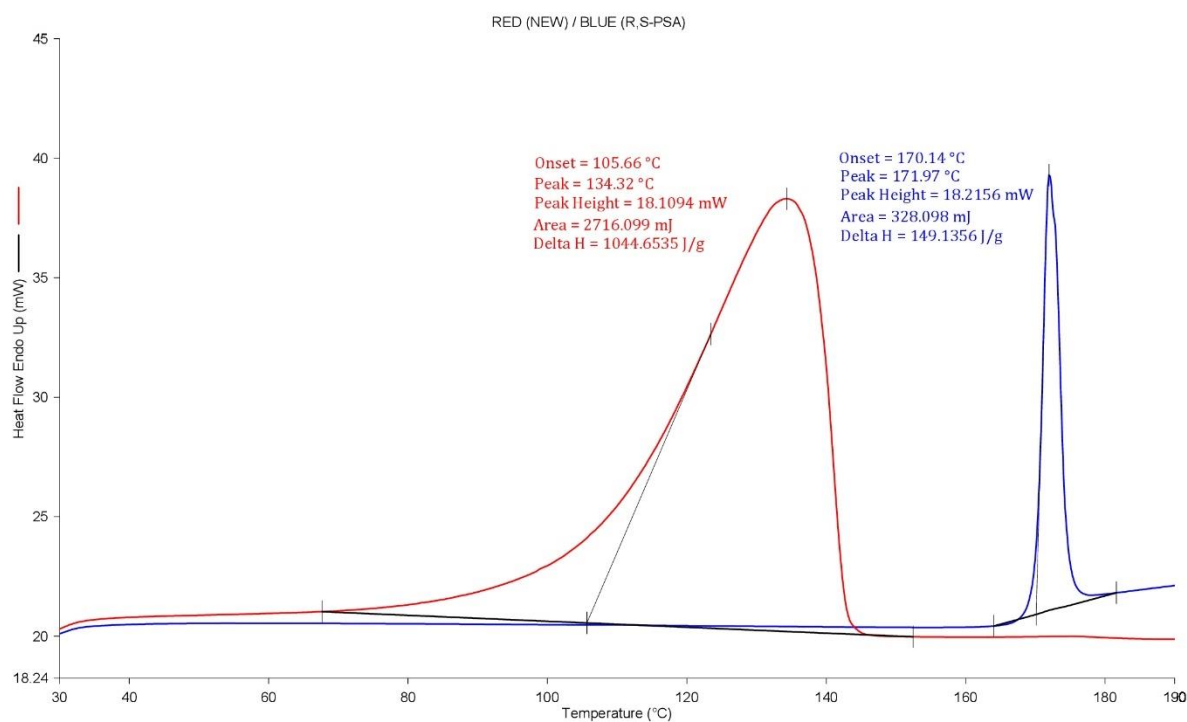


Figure A.1 DSC curve of  $[2tBa^+][COO^{2-}]$  and the starting material.

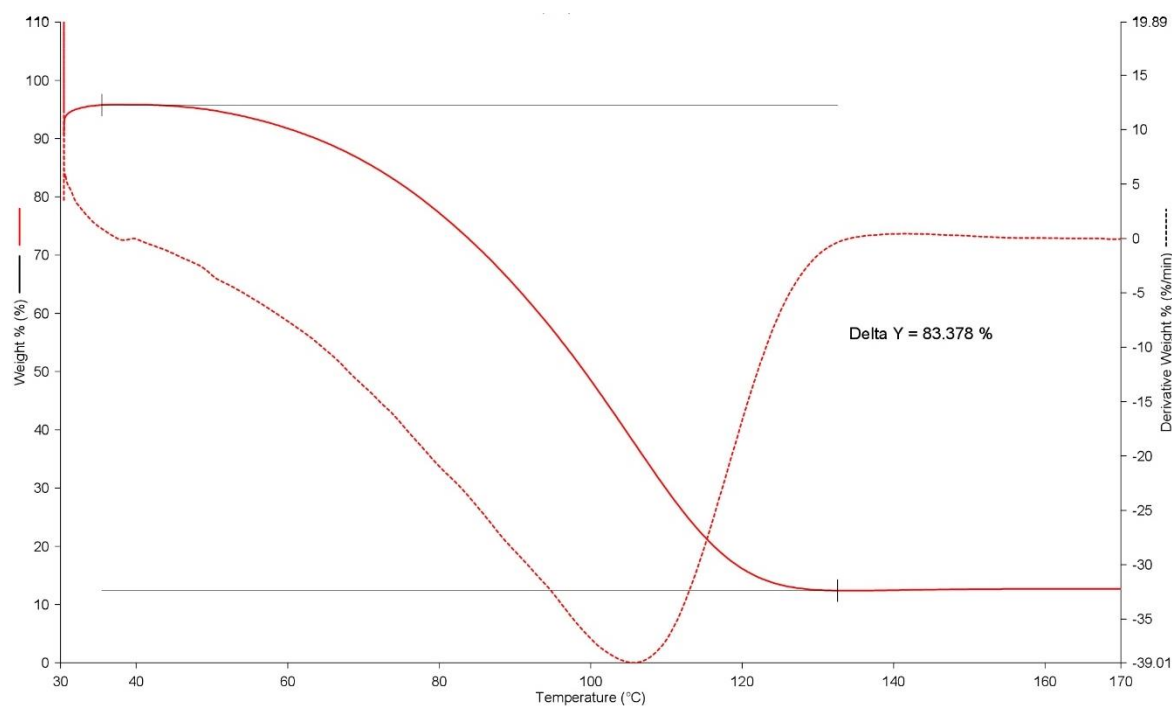
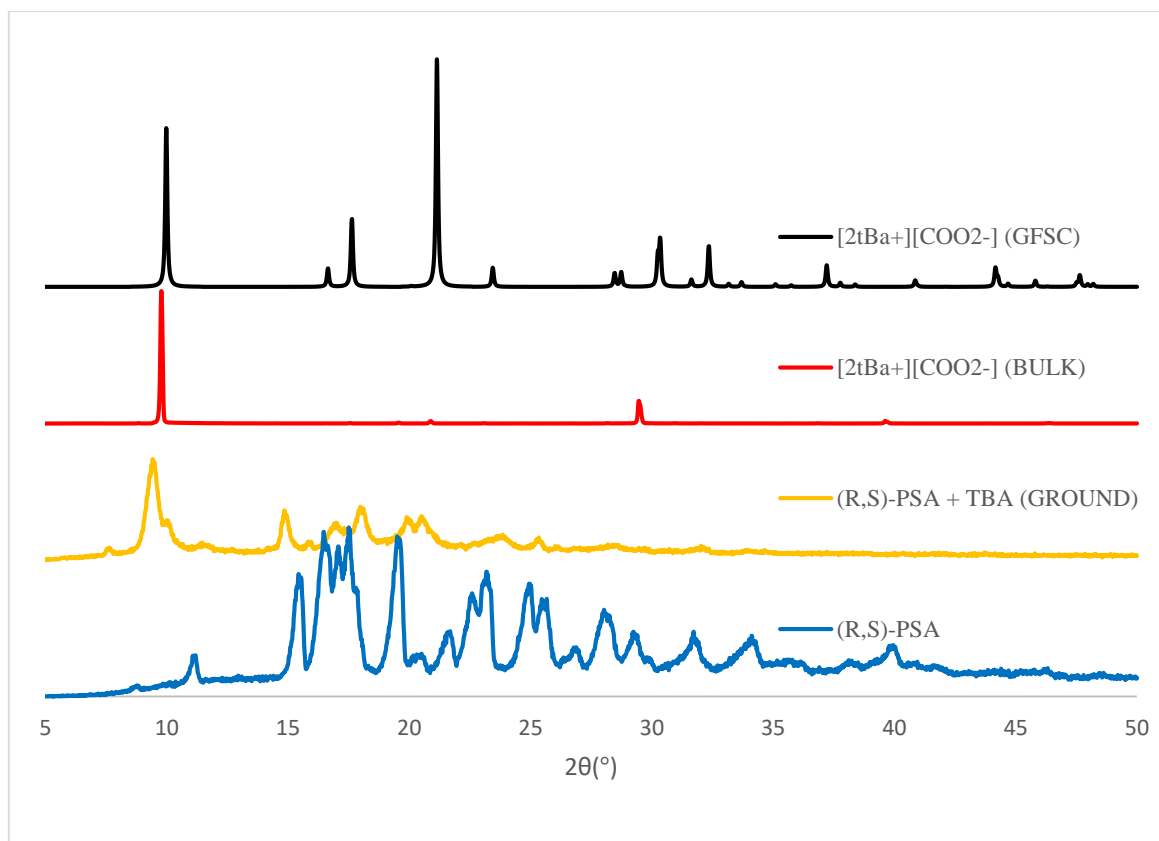
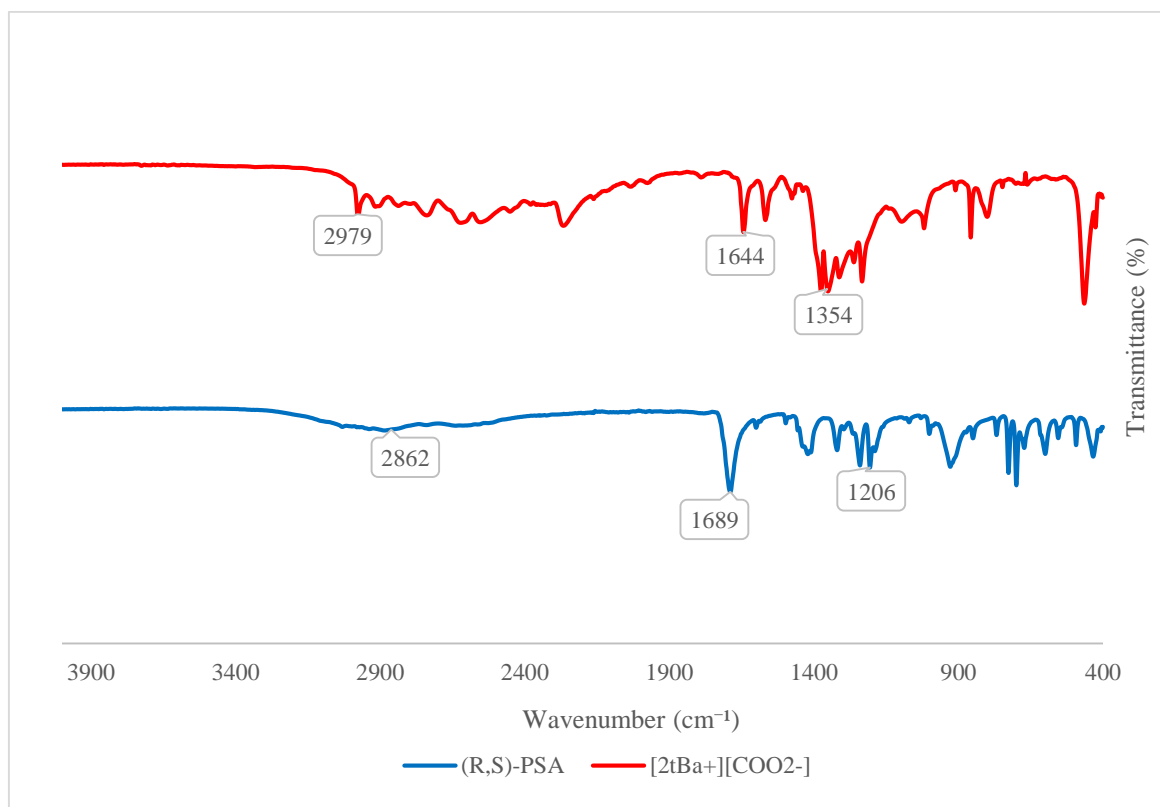


Figure A.2 TG curve of  $[2tBa^+][COO^{2-}]$ .

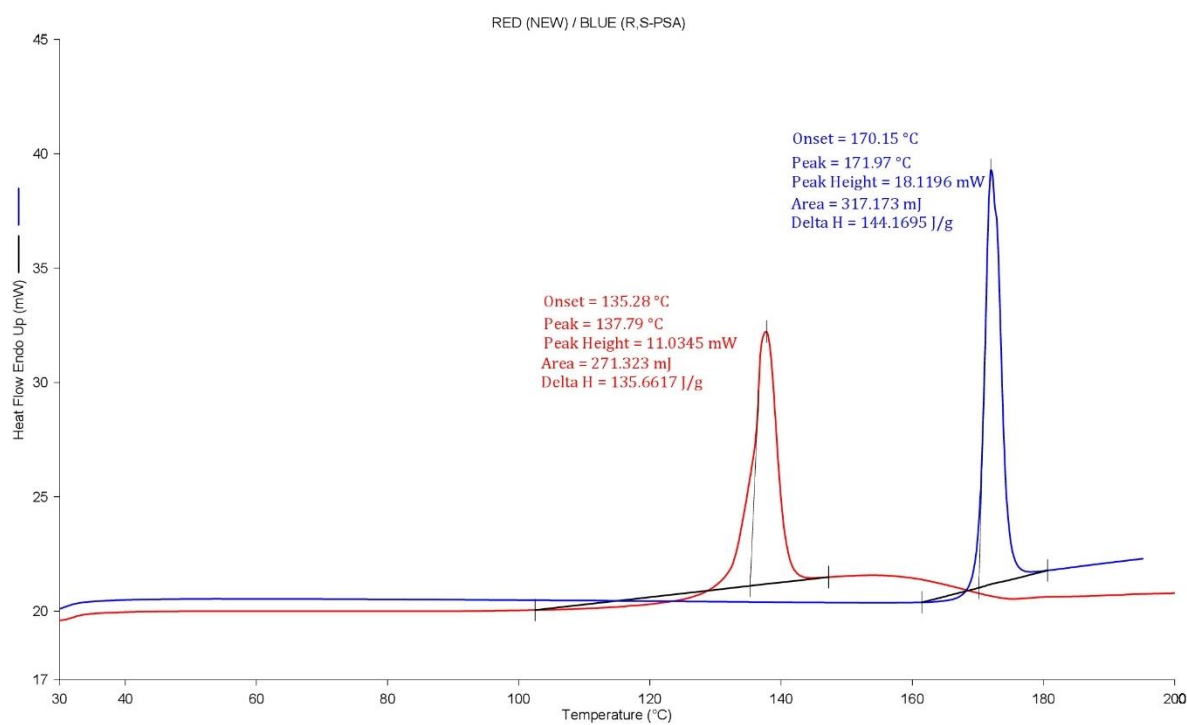
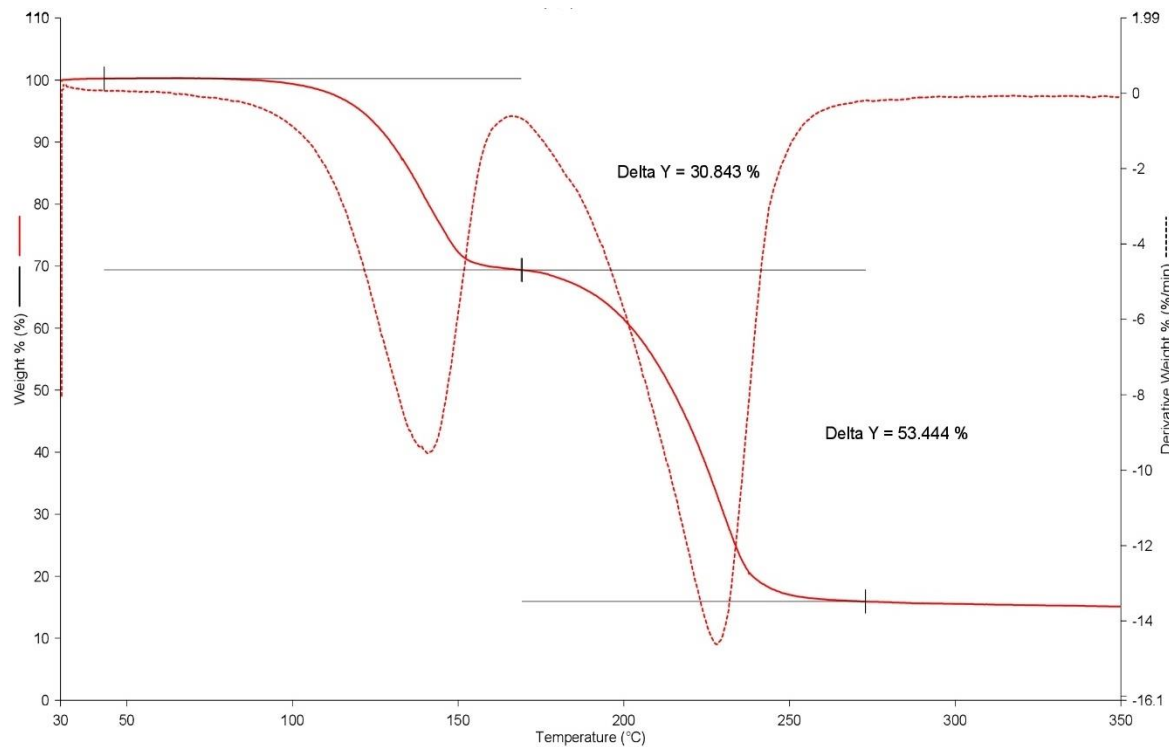


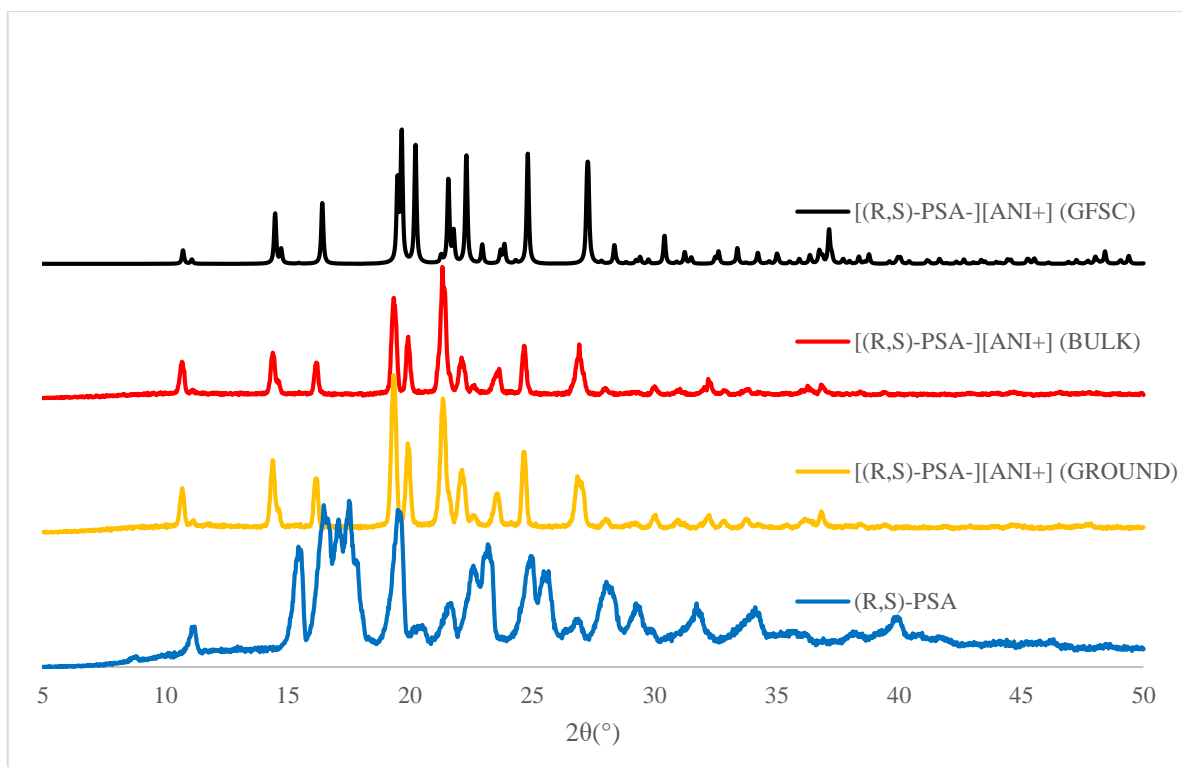


**Figure A.3** PXRD curve of [2tBa<sup>+</sup>][COO<sup>2-</sup>] and the starting material.

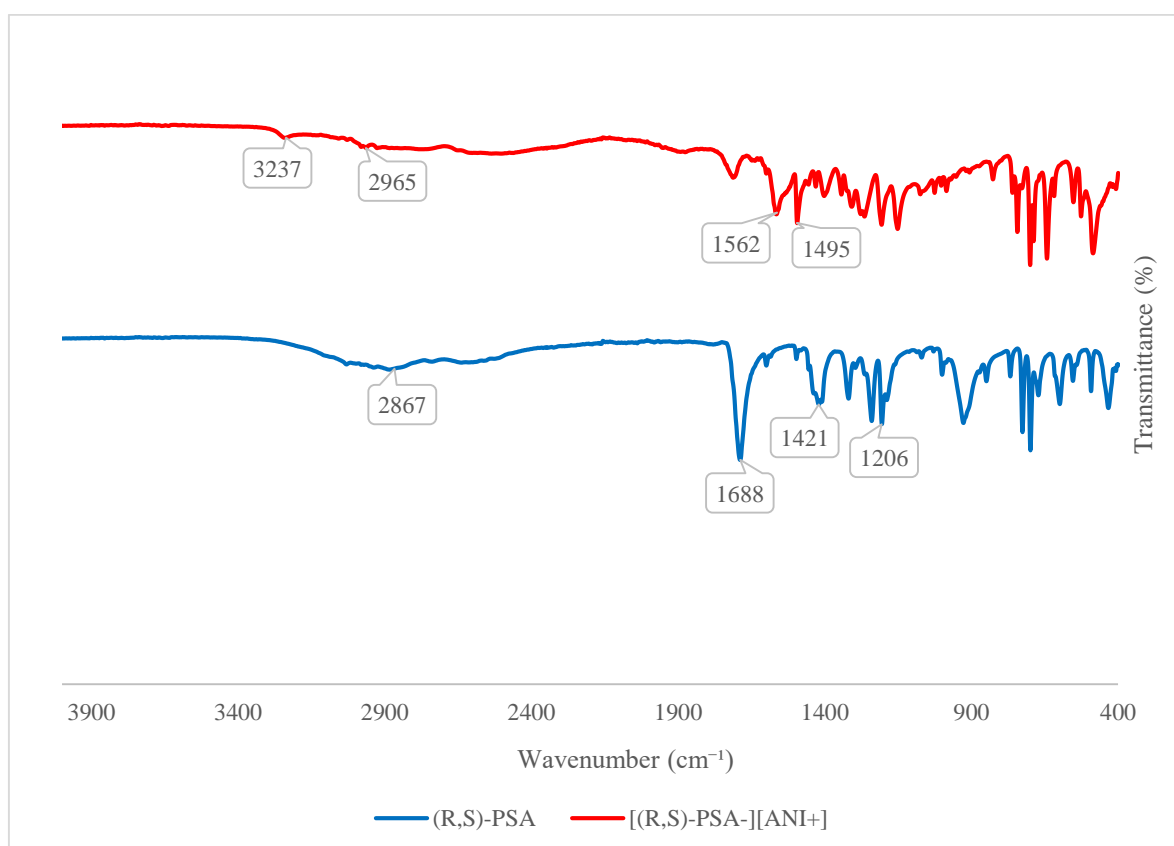


**Figure A.4** IR curve of [2tBa<sup>+</sup>][COO<sup>2-</sup>] and the starting material.

**[(R,S)-PSA<sup>-</sup>][ANI<sup>+</sup>]****Figure B.1** DSC curve of [(R,S)-PSA<sup>-</sup>][ANI<sup>+</sup>] and the starting material.**Figure B.2** TG curve of [(R,S)-PSA<sup>-</sup>][ANI<sup>+</sup>]

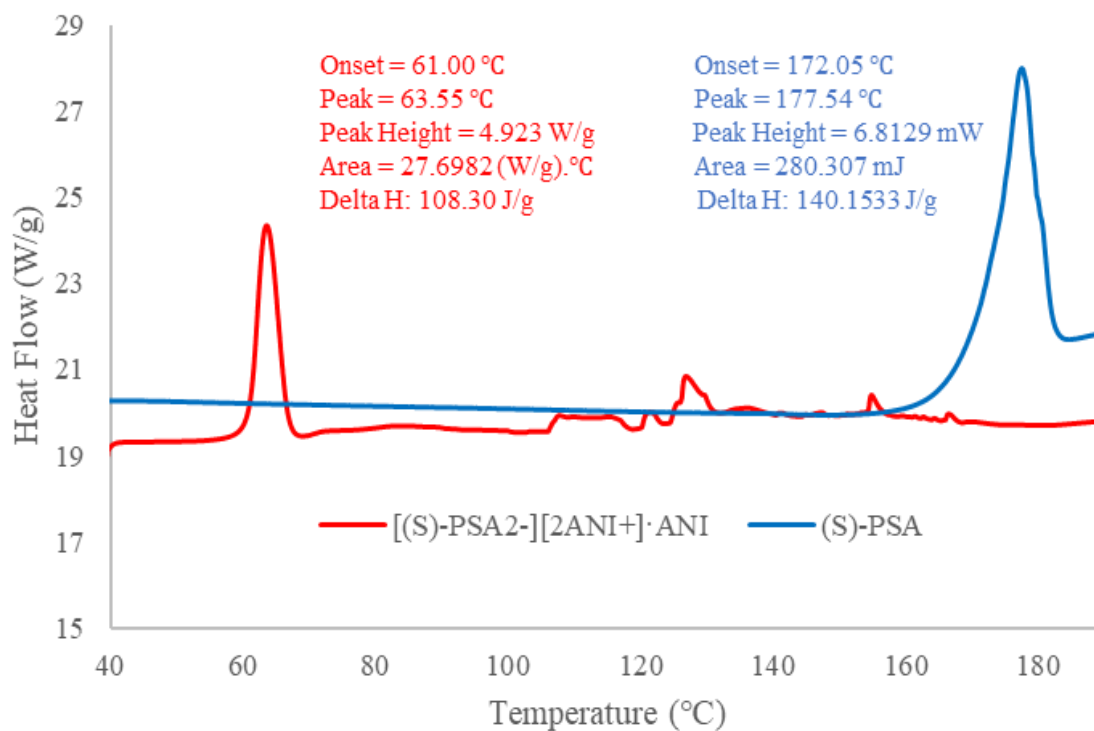


**Figure B.3** PXR D curve of [(R,S)-PSA<sup>-</sup>][ANI<sup>+</sup>] and the starting material.

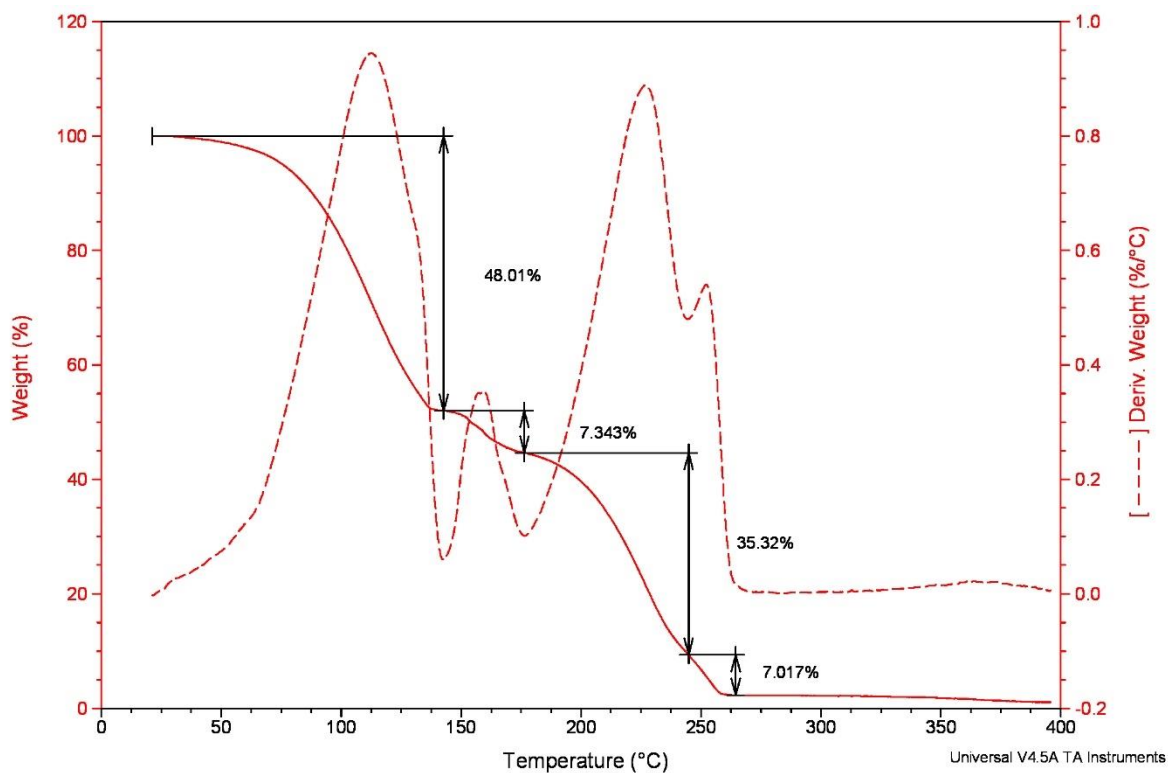


**Figure B.4** IR curve of [(R,S)-PSA<sup>-</sup>][ANI<sup>+</sup>] and the starting material.

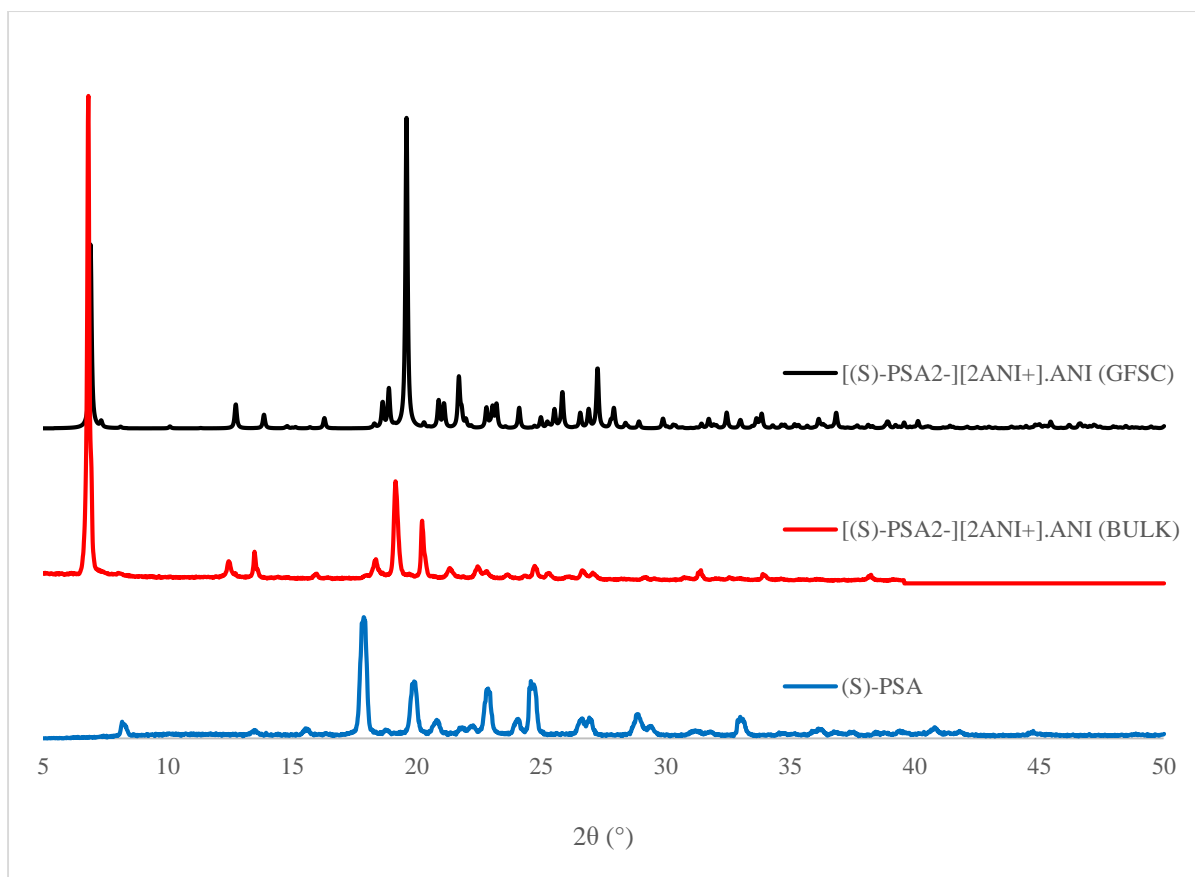
**[(S)-PSA<sup>2-</sup>] [2ANI<sup>+</sup>]·ANI**



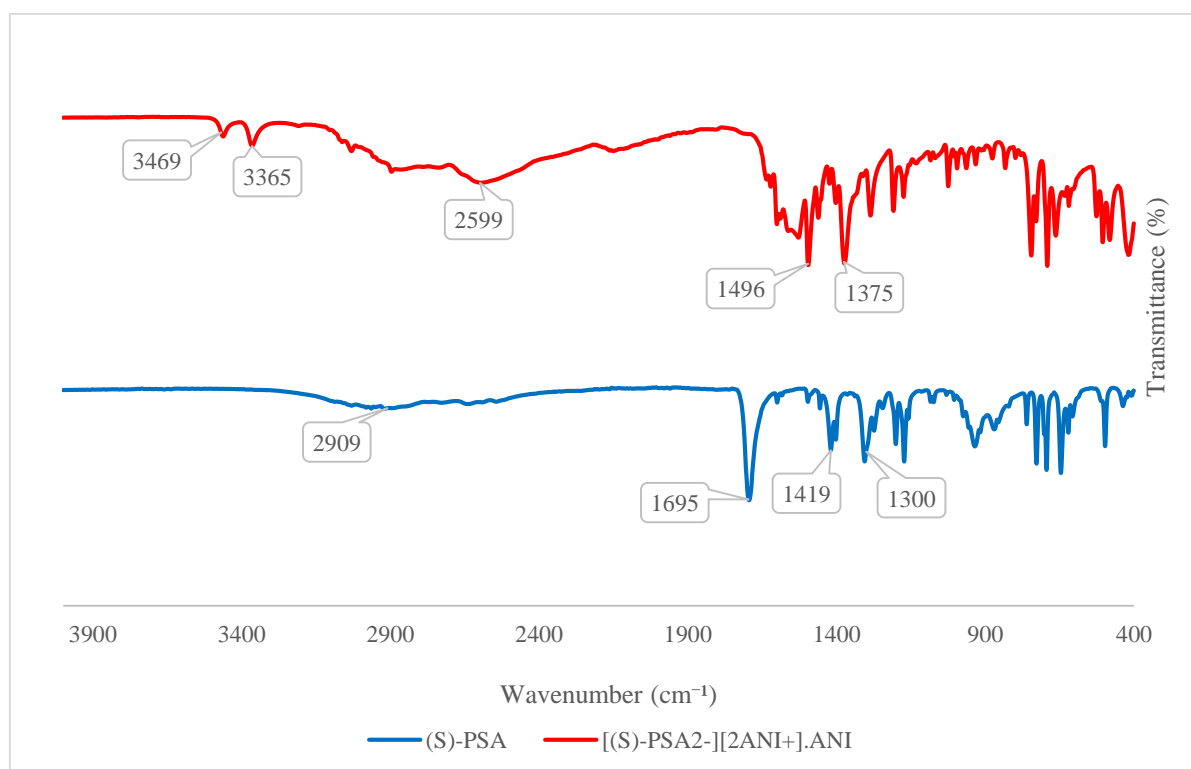
**Figure C.1** DSC curve of [(S)-PSA<sup>2-</sup>] [2ANI<sup>+</sup>]·ANI and the starting material.



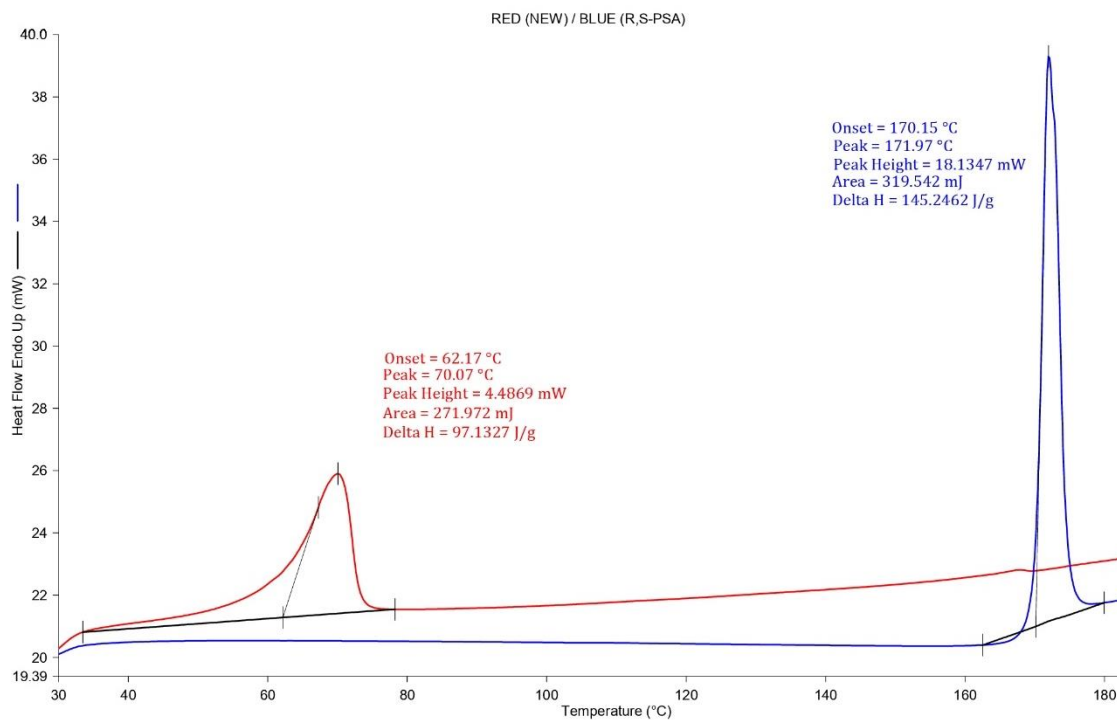
**Figure C.2** TG curve of [(S)-PSA<sup>2-</sup>] [2ANI<sup>+</sup>]·ANI.



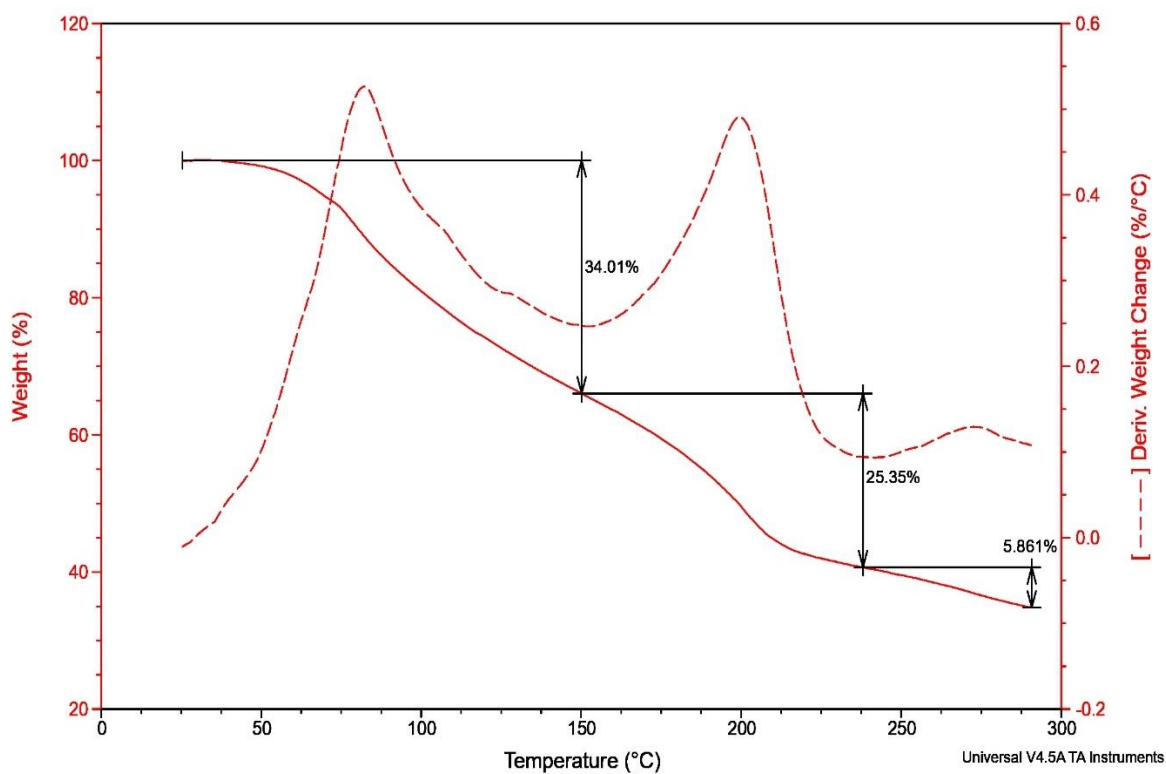
**Figure C.3** PXR D curve of [(S)-PSA<sup>2-</sup>][2ANI<sup>+</sup>]·ANI and the starting material.



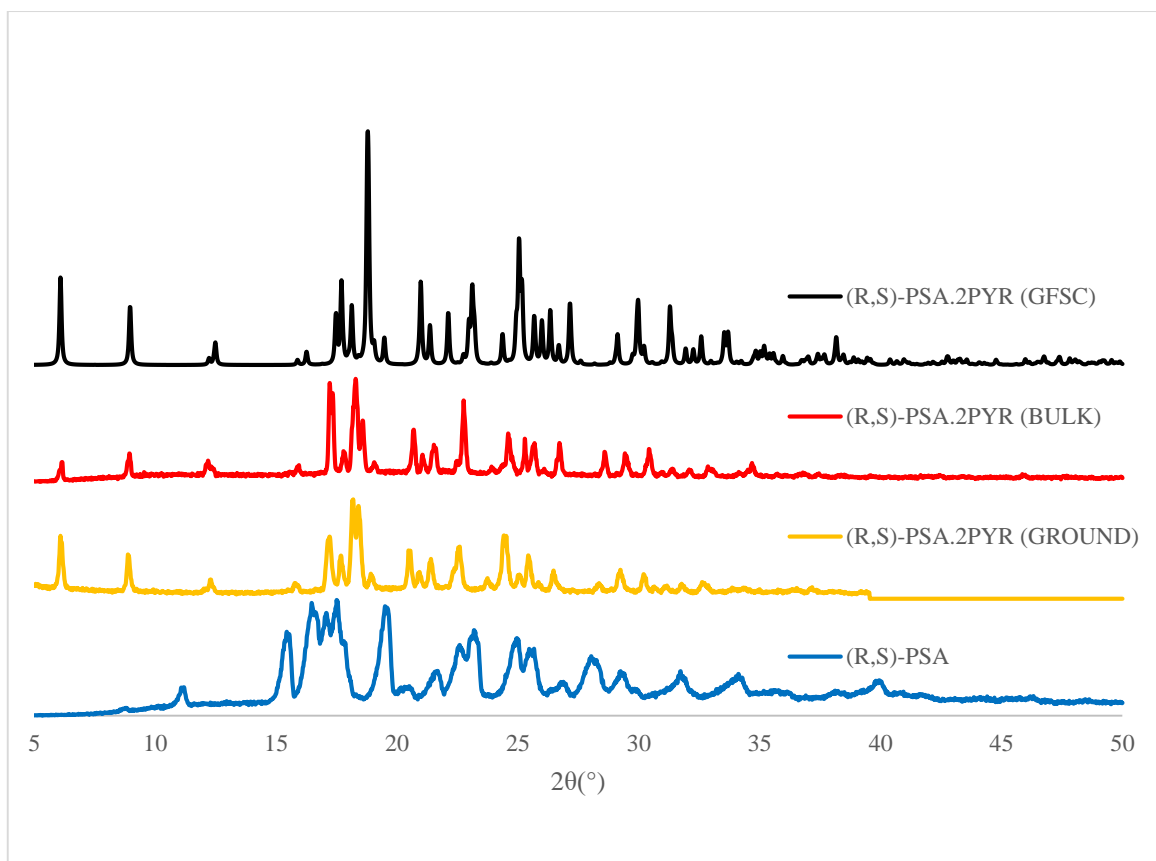
**Figure C.4** IR curve of [(S)-PSA<sup>2-</sup>][2ANI<sup>+</sup>]·ANI and the starting material.

**(R,S)-PSA·2PYR**

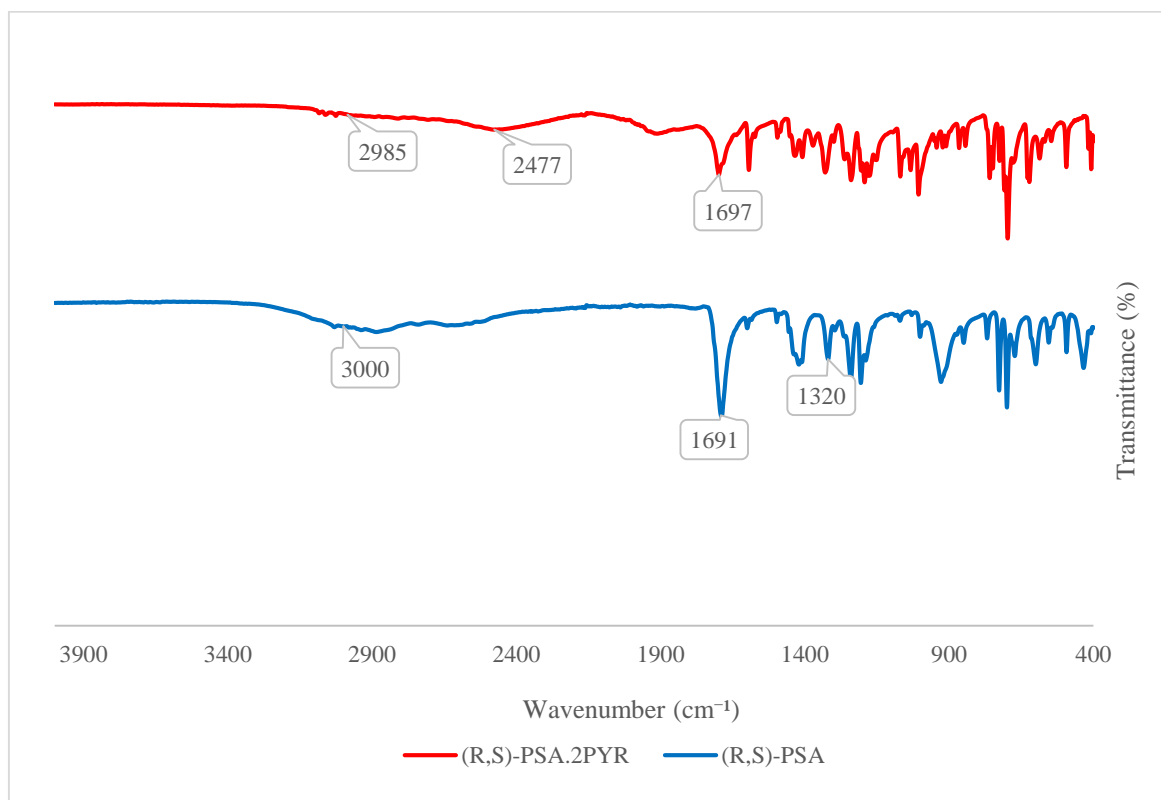
**Figure D.1** DSC curve of (R,S)-PSA·2PYR and the starting material.



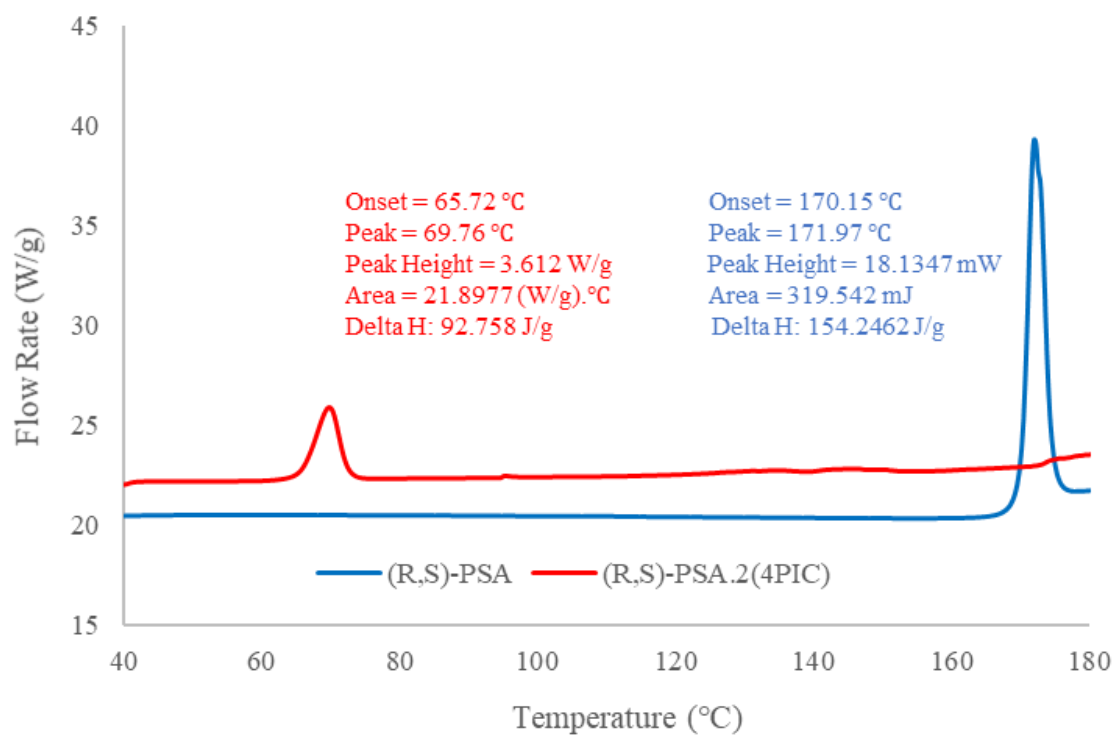
**Figure D.2** TG curve of (R,S)-PSA·2PYR.



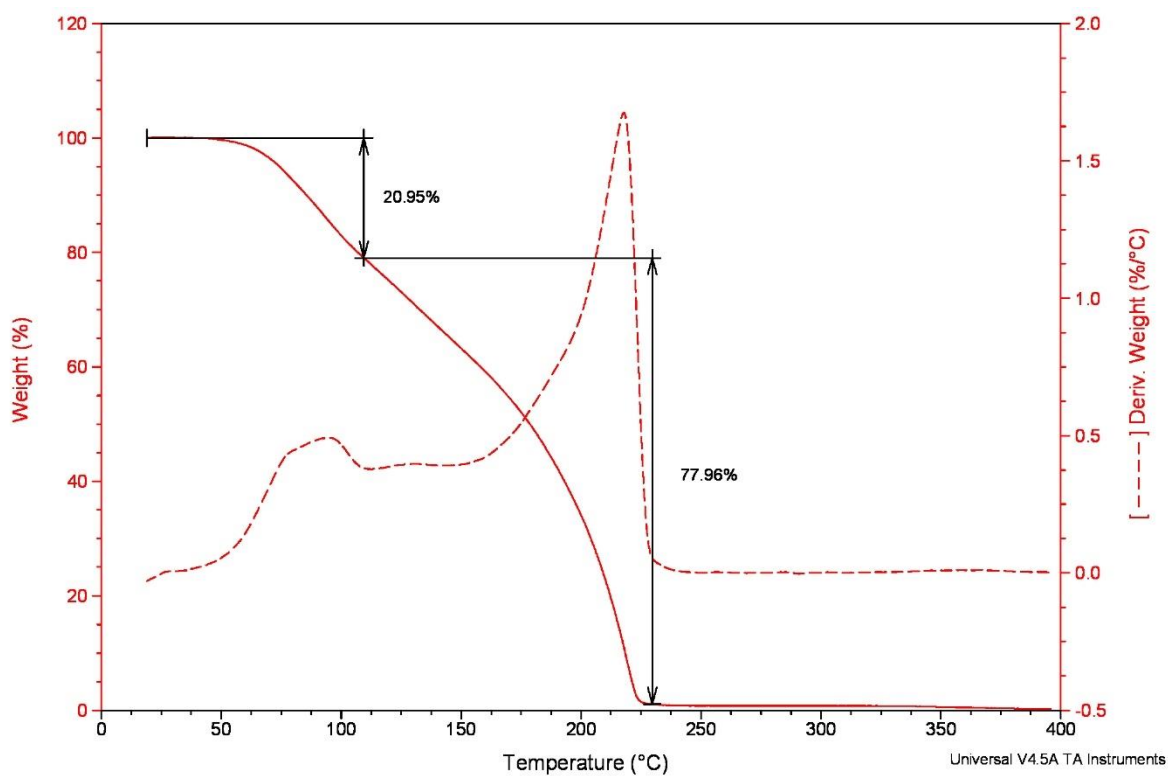
**Figure D.3** PXRD curve of (R,S)-PSA·2PYR and the starting material.



**Figure D.4** IR curve of (R,S)-PSA·2PYR and the starting material

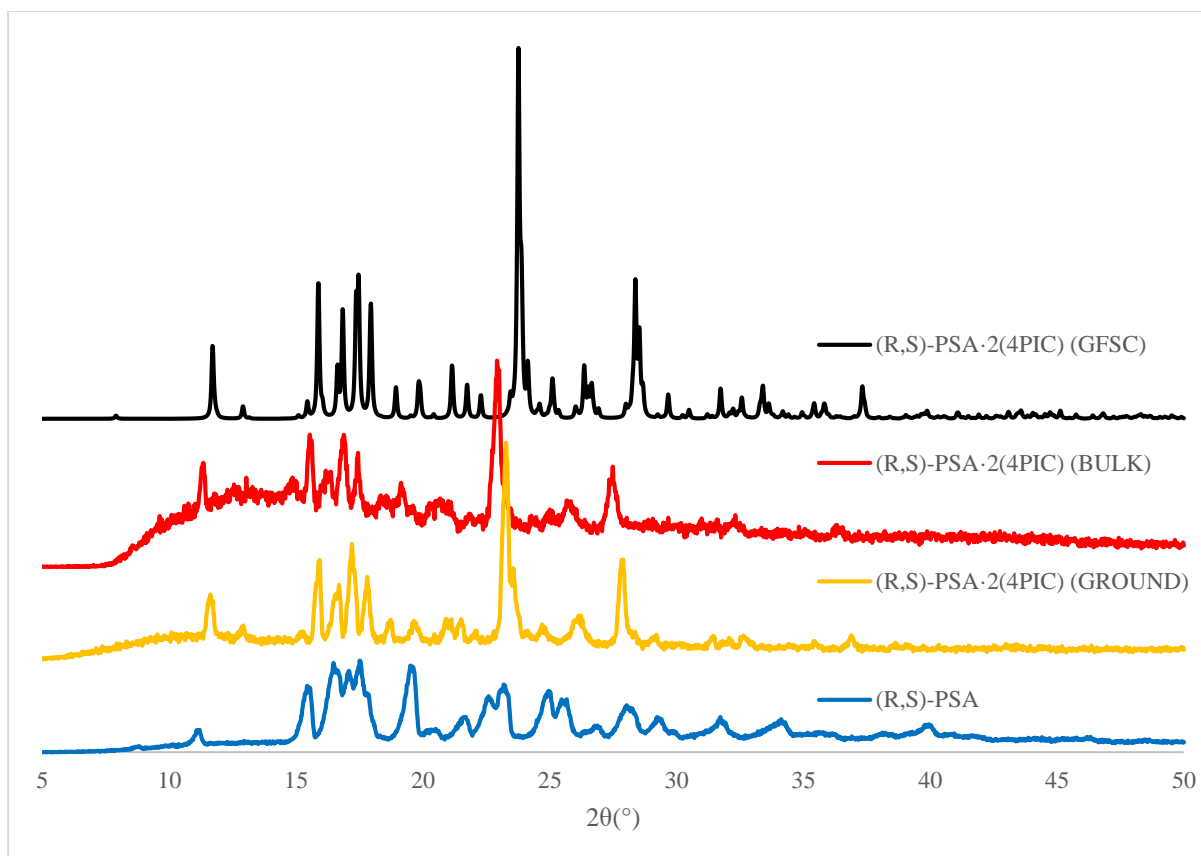
**(R,S)-PSA·2(4PIC)**

**Figure E.1** DSC curve of (R,S)-PSA·2(4PIC) and the starting material.

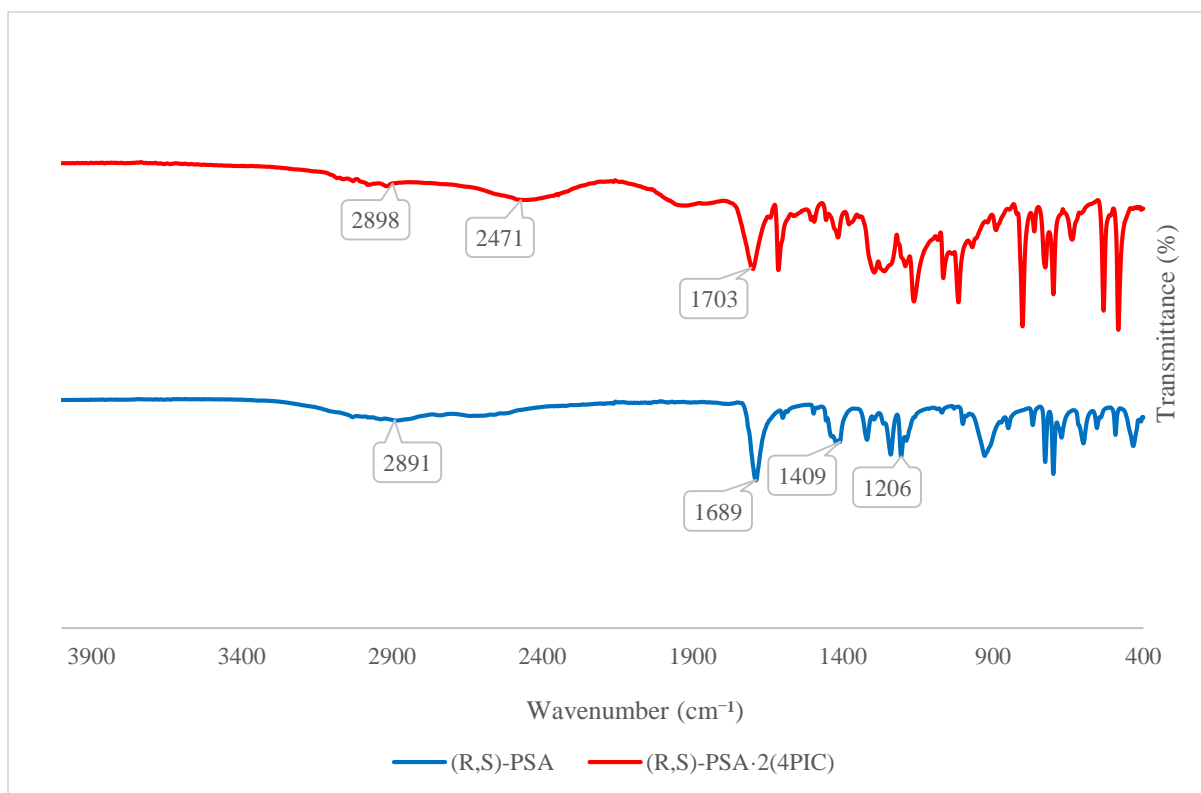


**Figure E.2** TG curve of (R,S)-PSA·2(4PIC).

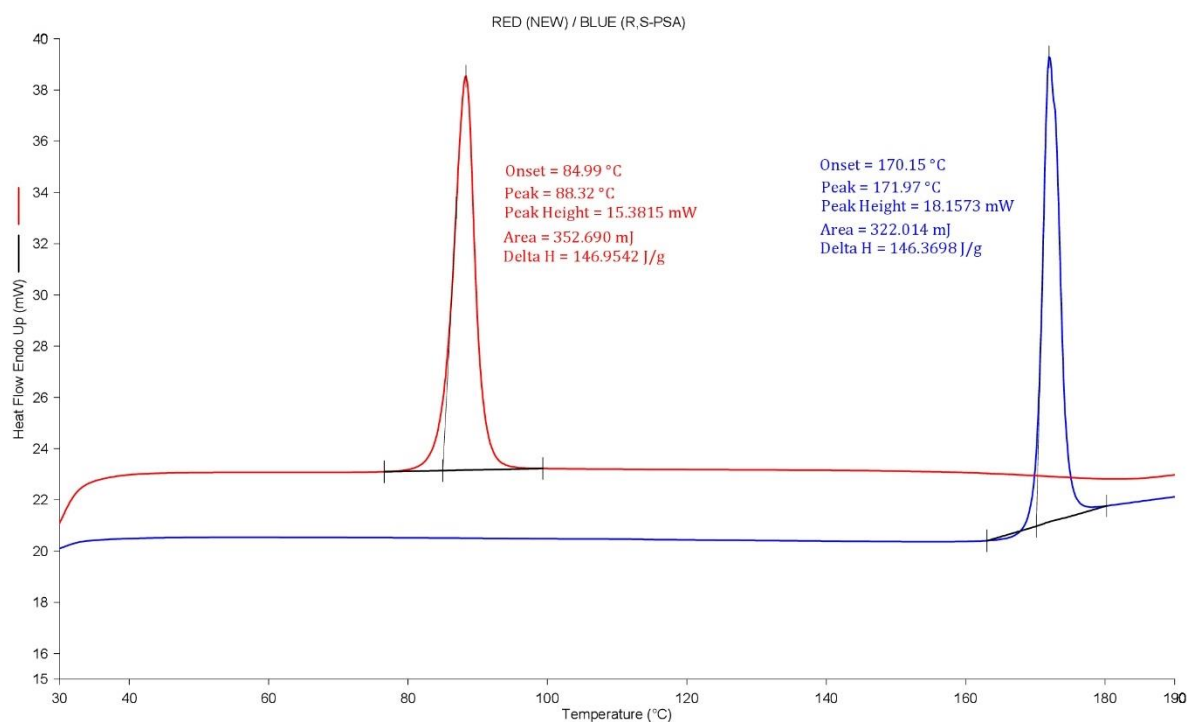
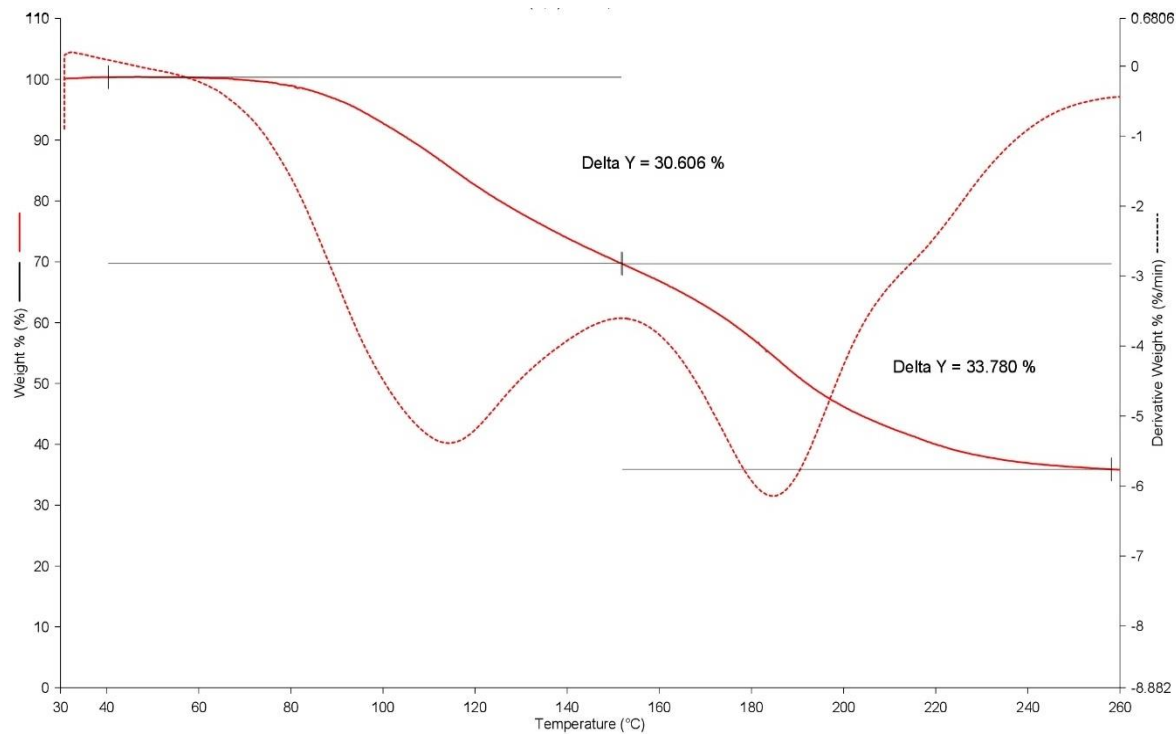


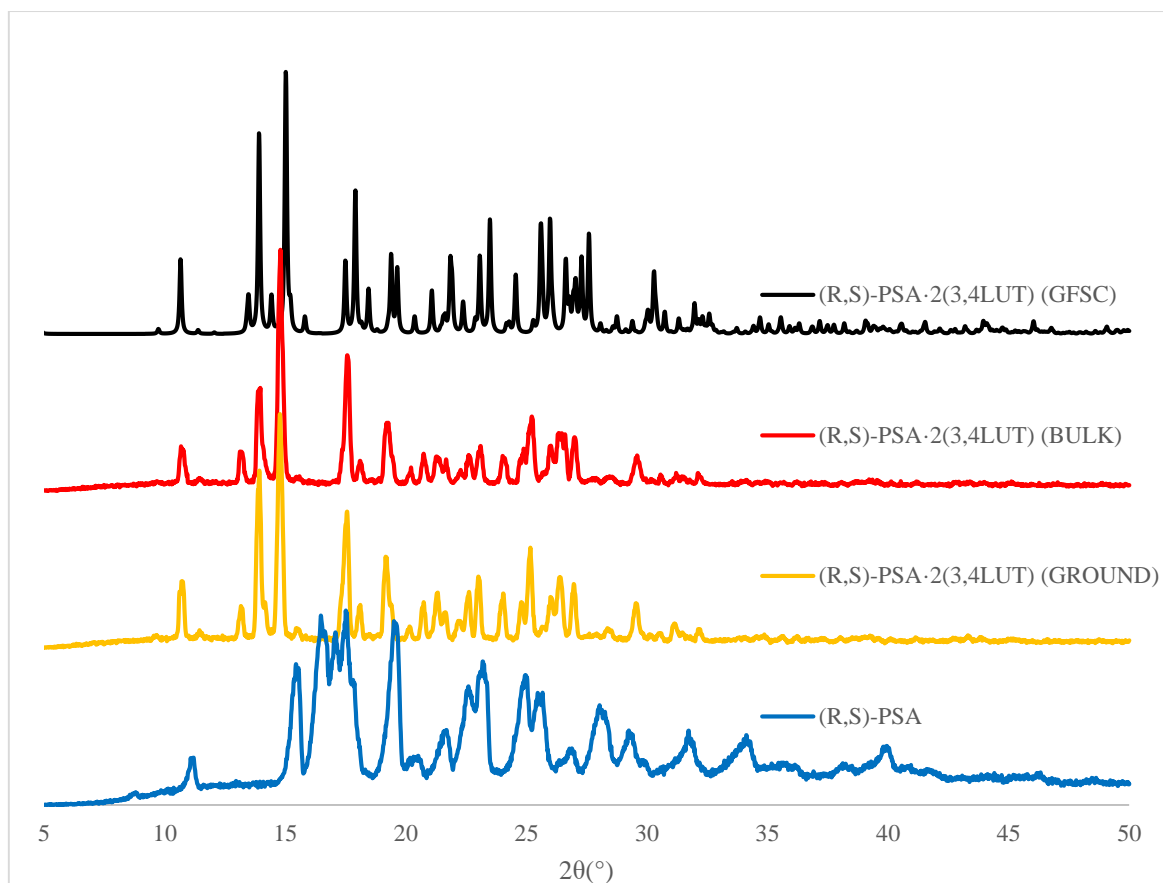


**Figure E.3** PXRD curve of (R,S)-PSA·2(4PIC) and the starting material.

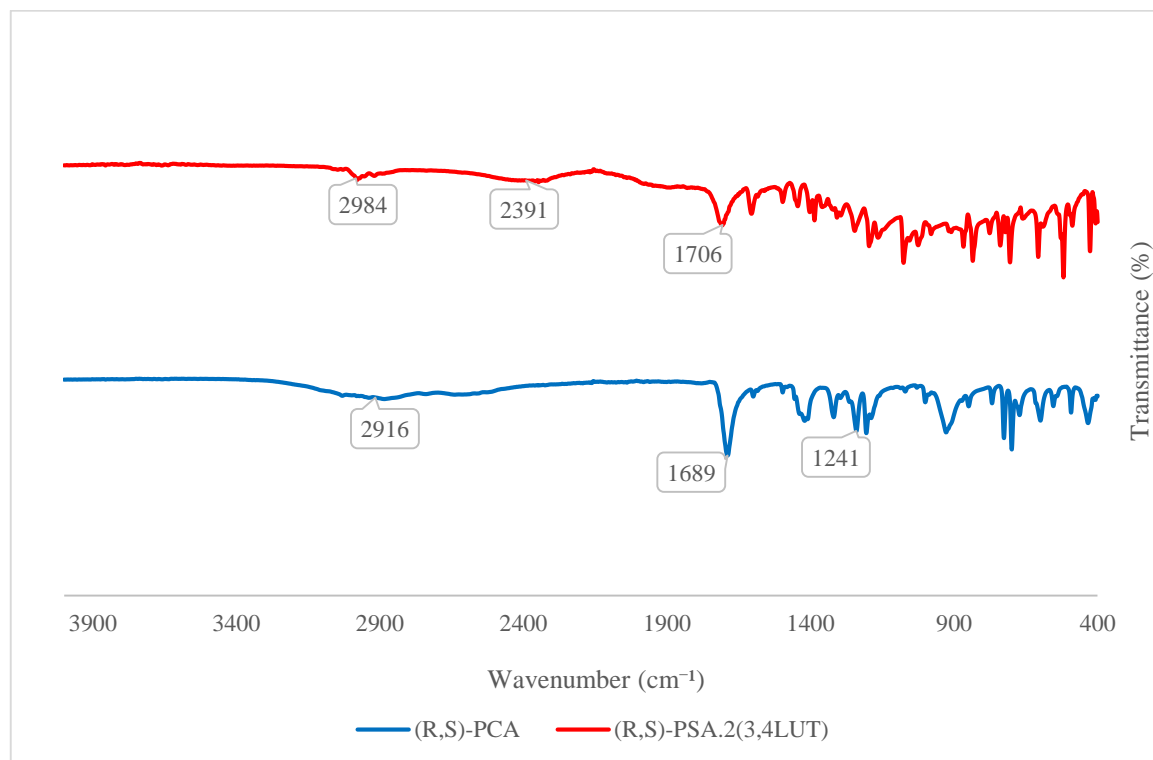


**Figure E.4** IR curve of (R,S)-PSA·2(4PIC) and the starting material.

**(R,S)-PSA·2(3,4LUT)****Figure F.1** DSC curve of (R,S)-PSA·2(3,4LUT) and the starting material.**Figure F.2** TG curve of (R,S)-PSA·2(3,4LUT)

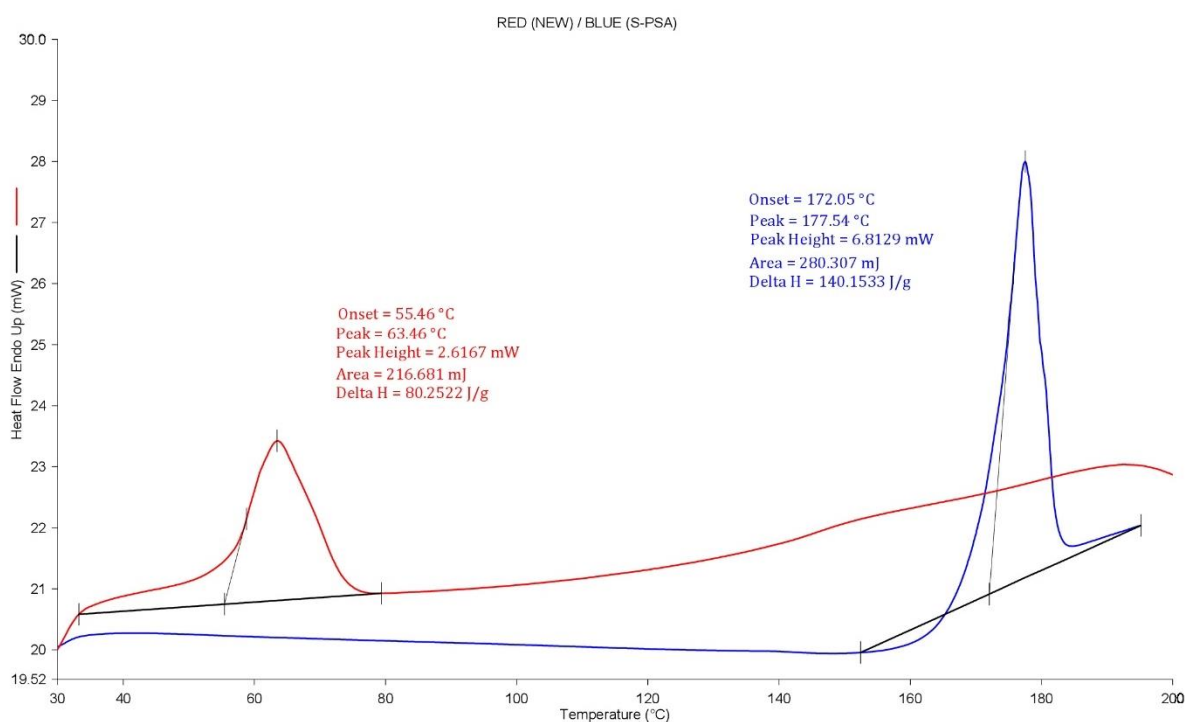


**Figure F.3** PXRD curve of (R,S)-PSA·2(3,4LUT) and the starting material.

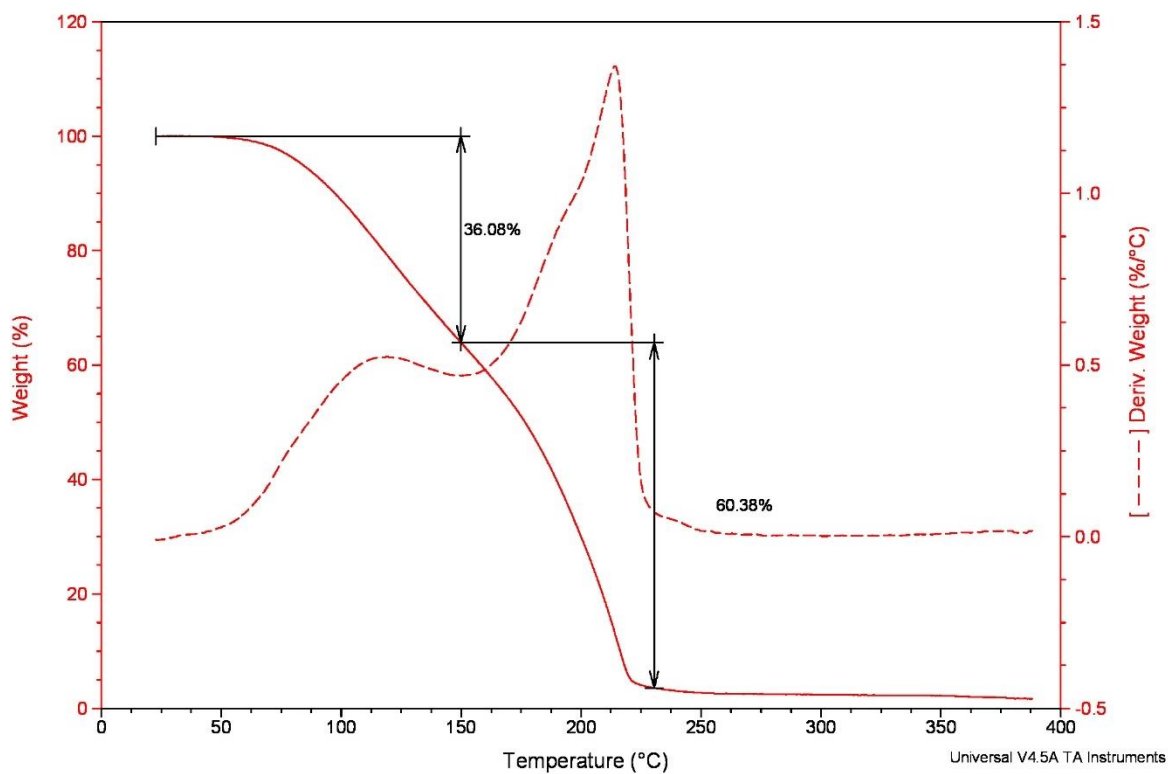


**Figure F.4** IR curve of (R,S)-PSA·2(3,4LUT) and the starting material.

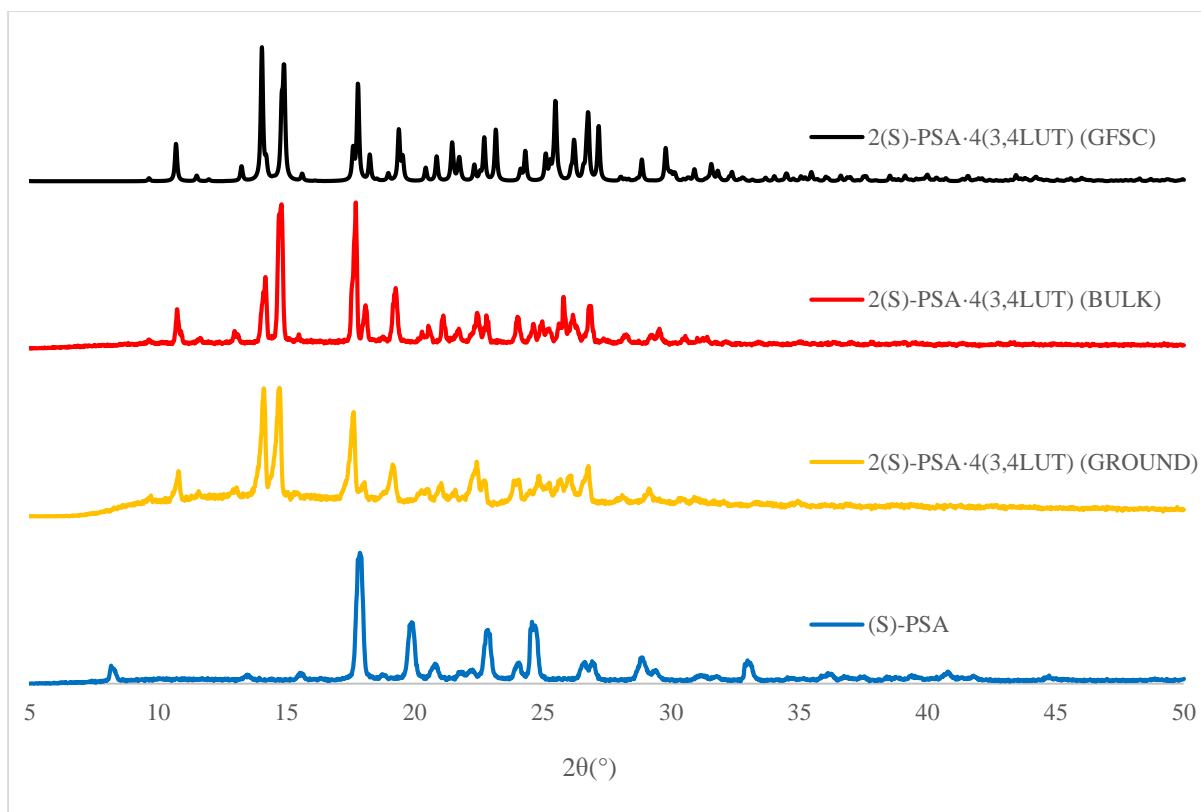
## 2(S)-PSA·4(3,4LUT)



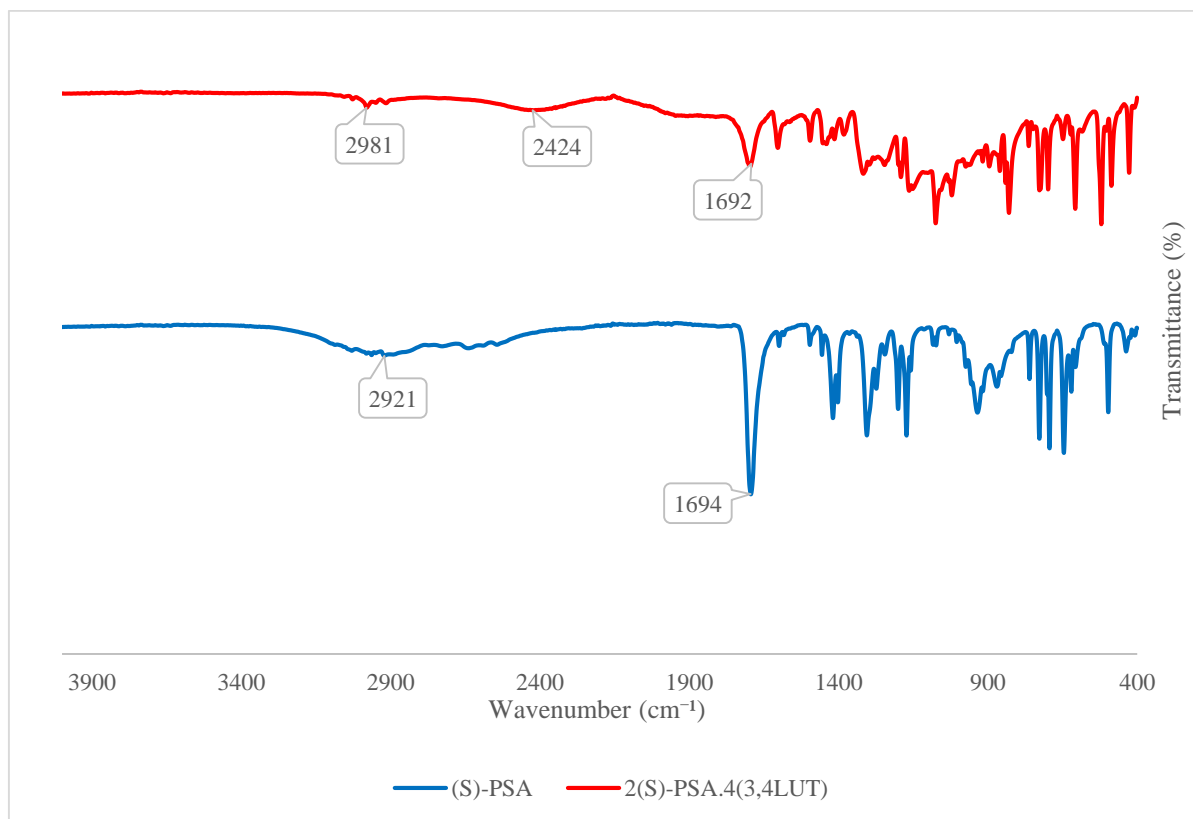
**Figure G.1** DSC curve of 2(S)-PSA·4(3,4LUT) and the starting material.



**Figure G.2** TG curve of 2(S)-PSA·4(3,4LUT)

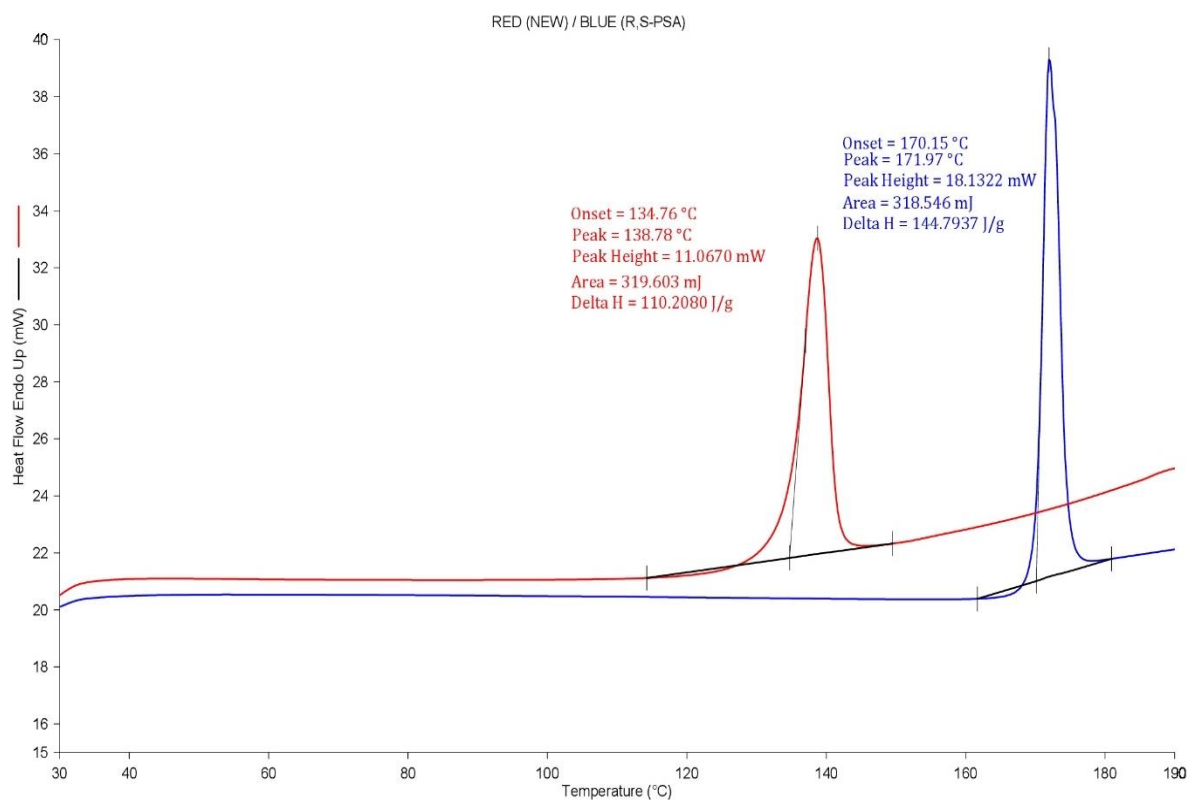


**Figure G.3** PXRD curve of 2(S)-PSA·4(3,4LUT) and the starting material.

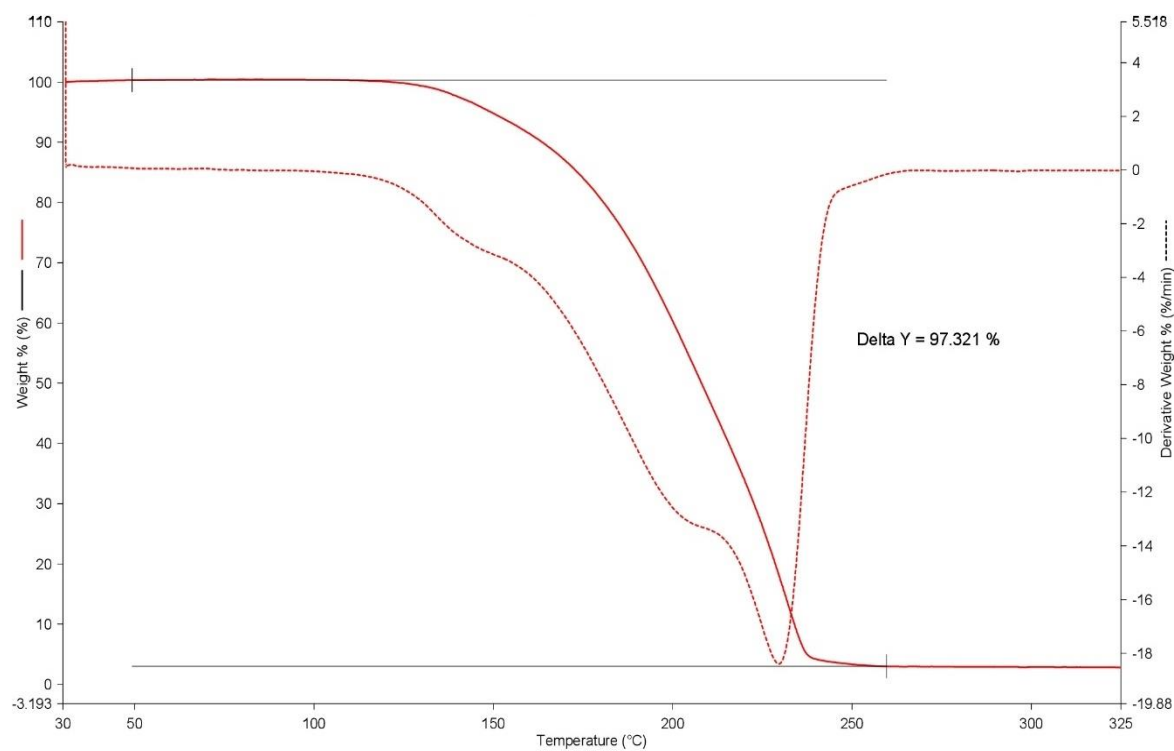


**Figure G.4** IR curve of 2(S)-PSA·4(3,4LUT) and the starting material.

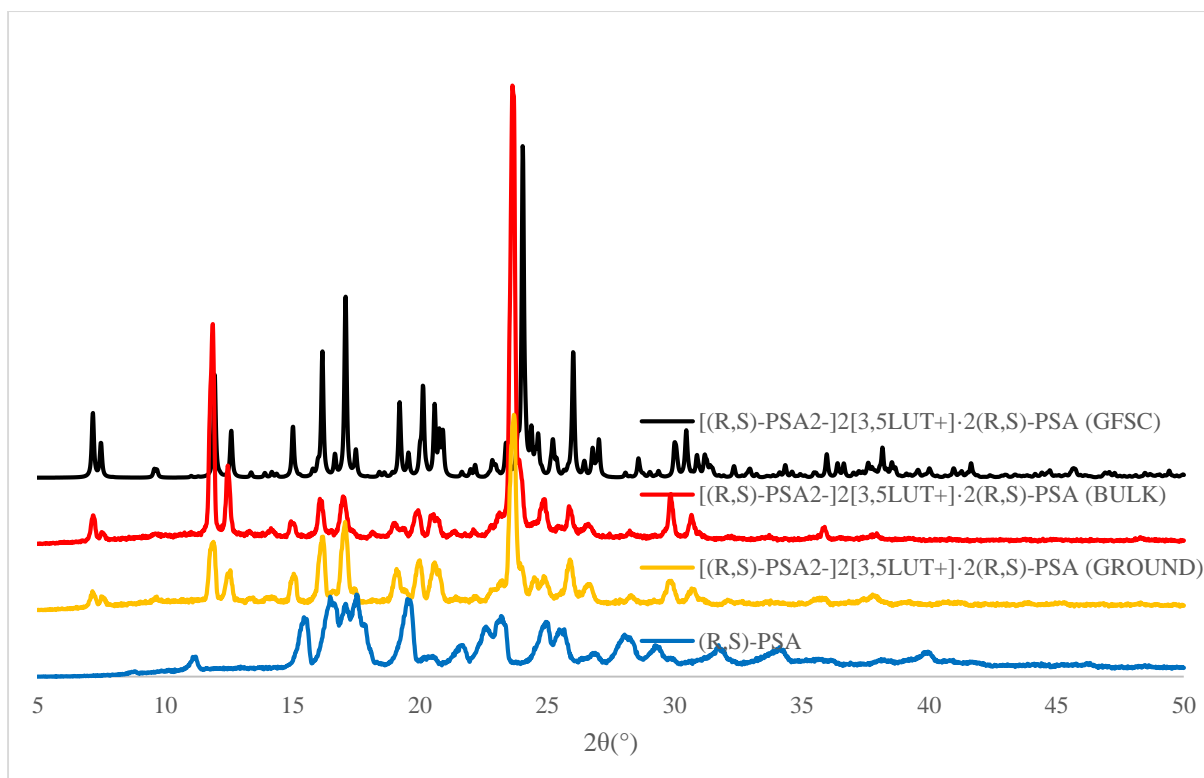
**[(R,S)-PSA<sup>2-</sup>] 2[3,5LUT<sup>+</sup>]·2(R,S)-PSA**



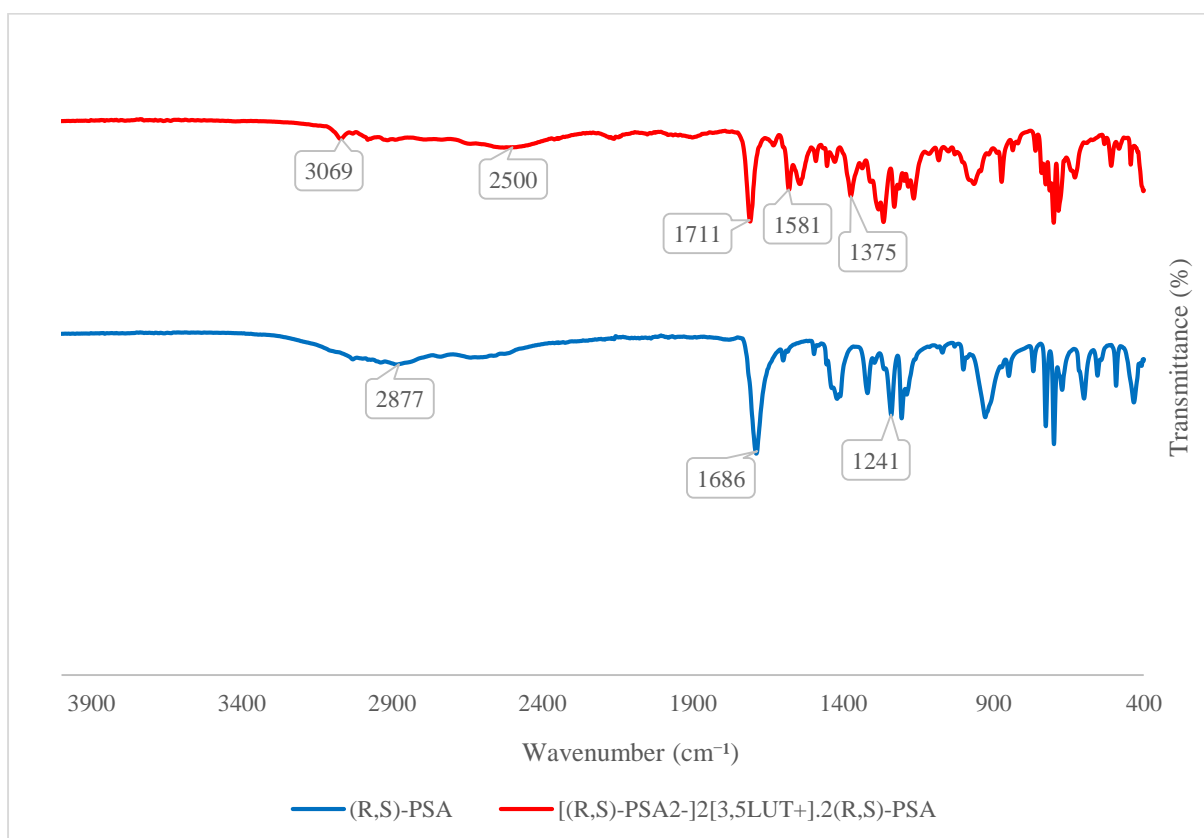
**Figure H.1** DSC curve of [(R,S)-PSA<sup>2-</sup>] 2[3,5LUT<sup>+</sup>]·2(R,S)-PSA and the starting material.



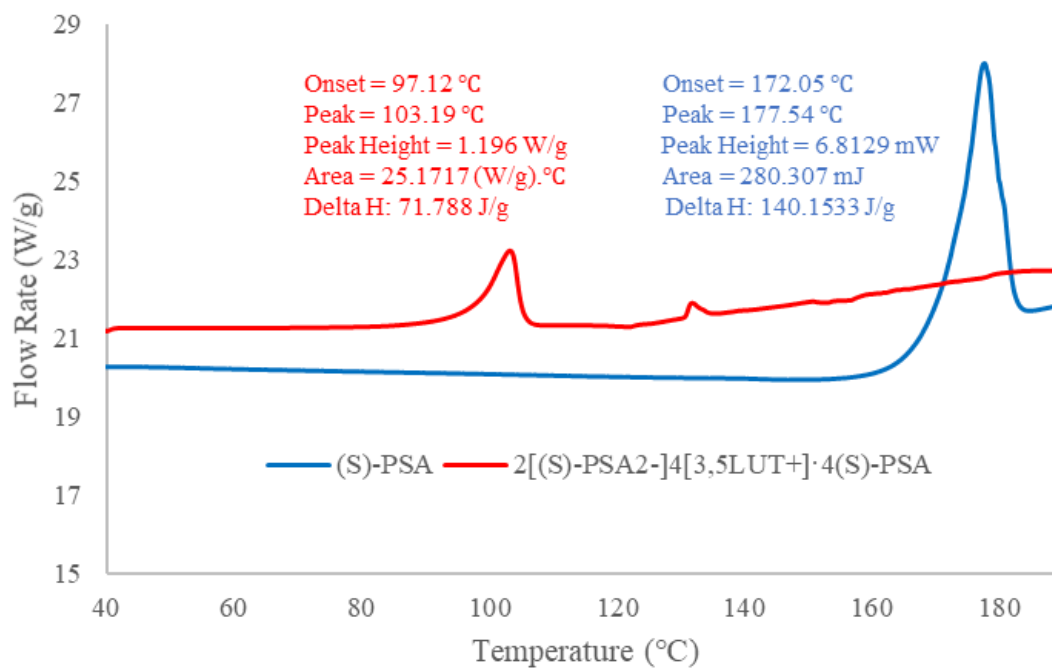
**Figure H.2** TG curve of [(R,S)-PSA<sup>2-</sup>] 2[3,5LUT<sup>+</sup>]·2(R,S)-PSA.



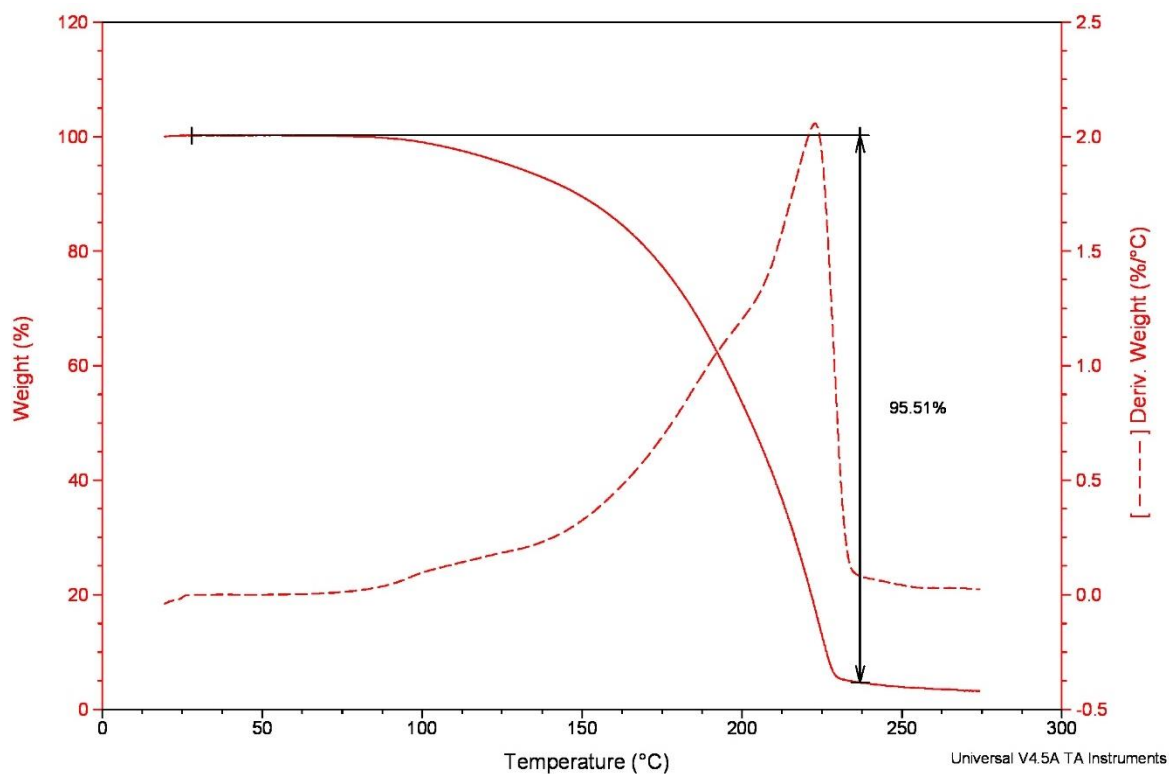
**Figure H.3** PXRD curve of  $[(R,S)\text{-PSA}_2\text{-}]_2[3,5\text{LUT}^+]\cdot 2(R,S)\text{-PSA}$  and the starting material.



**Figure H.4** IR curve of  $[(R,S)\text{-PSA}_2\text{-}]_2[3,5\text{LUT}^+]\cdot 2(R,S)\text{-PSA}$  and the starting material.

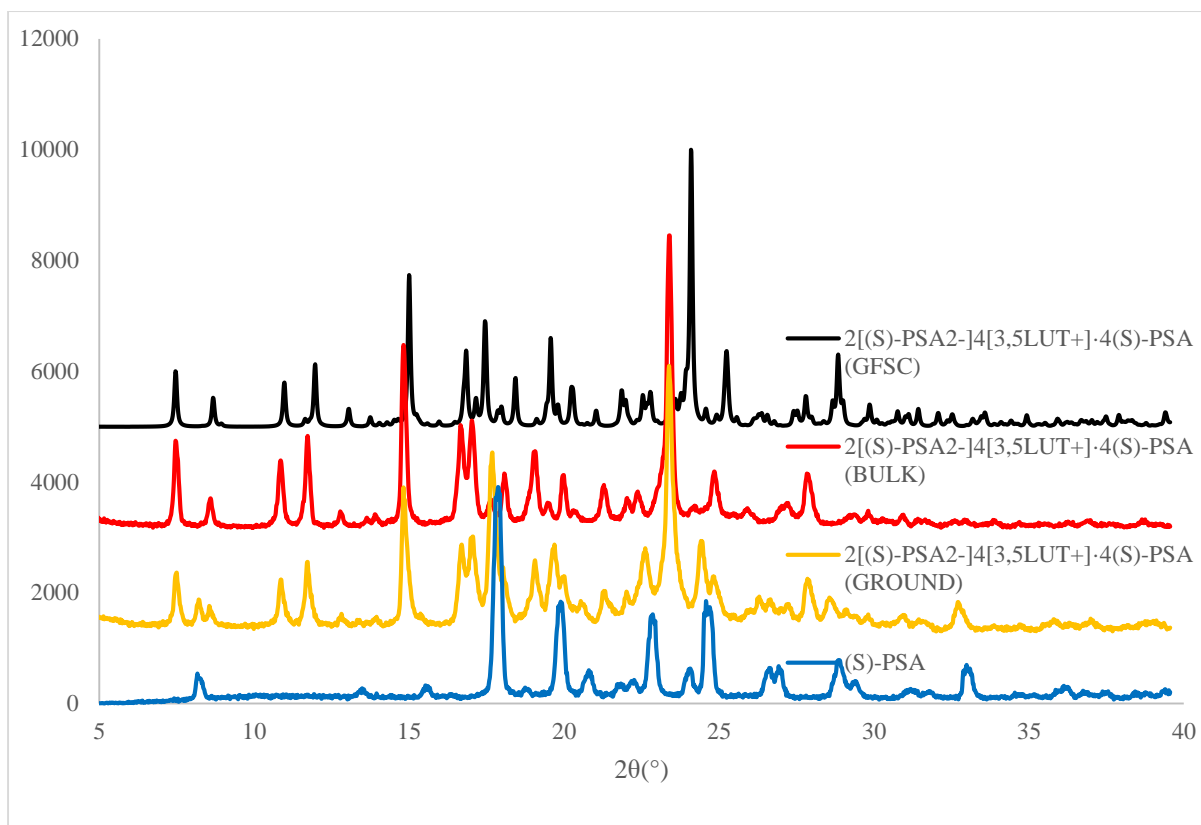
$2[(S)\text{-PSA}^2]_4[3,5\text{LUT}^+]_4(S)\text{-PSA}$ 


**Figure I.1** DSC curve of  $2[(S)\text{-PSA}^2]_4[3,5\text{LUT}^+]_4(S)\text{-PSA}$  and the starting material.

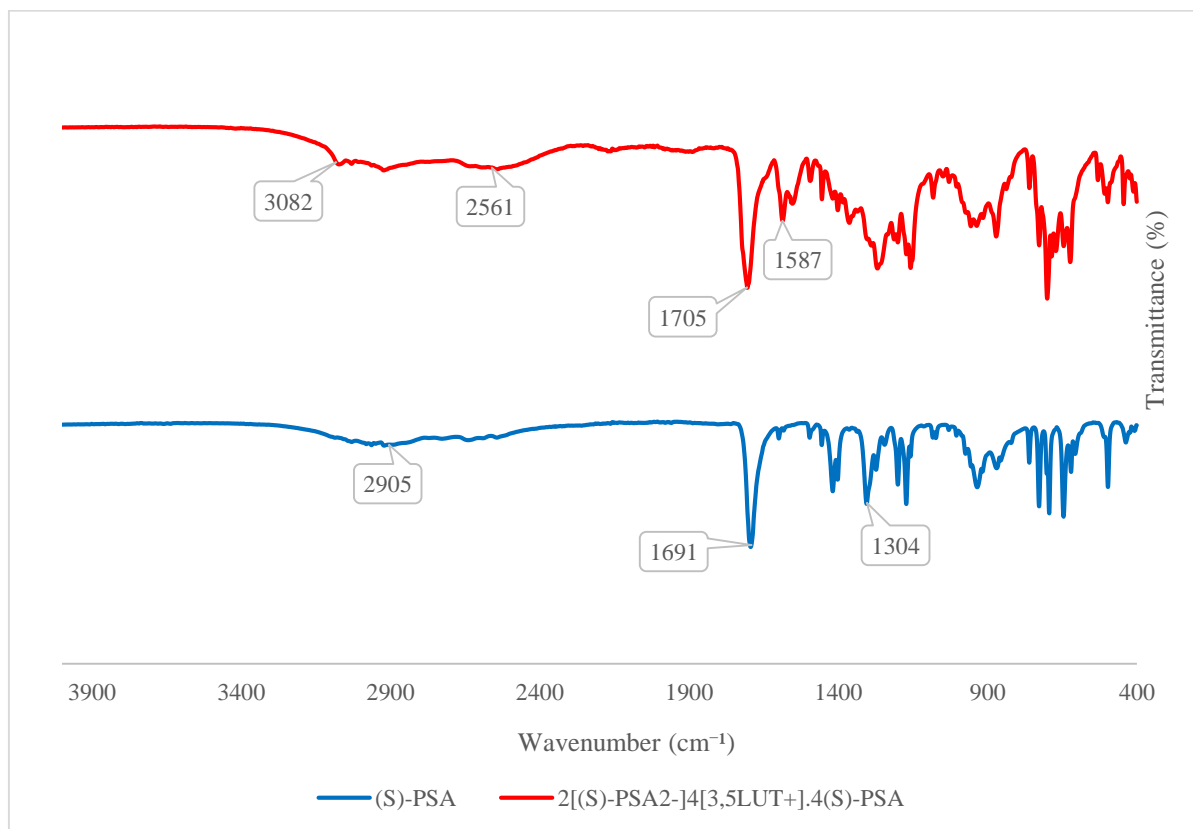


**Figure I.2** TG curve of  $2[(S)\text{-PSA}^2]_4[3,5\text{LUT}^+]_4(S)\text{-PSA}$

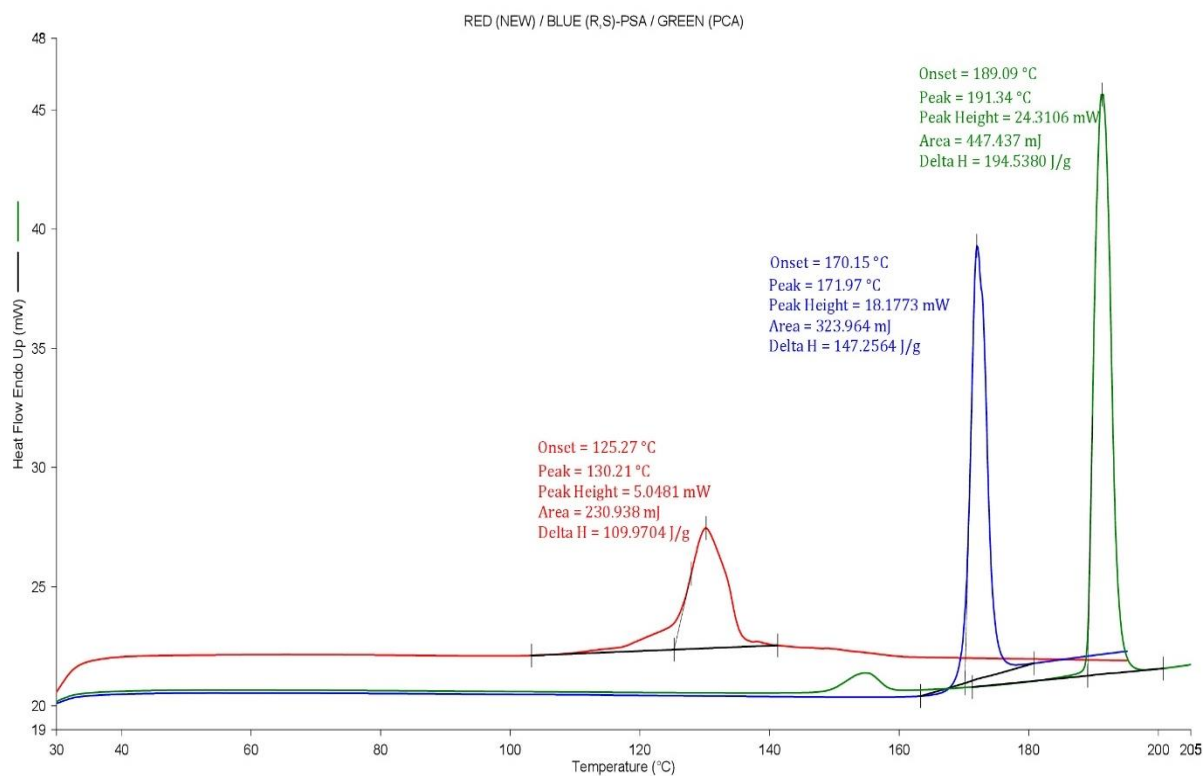




**Figure I.3** PXRD curve of  $2[(S)\text{-PSA}_2\text{-}]_4[3,5\text{LUT}^+] \cdot 4(S)\text{-PSA}$  and the starting material.



**Figure I.4** IR curve of  $2[(S)\text{-PSA}_2\text{-}]_4[3,5\text{LUT}^+] \cdot 4(S)\text{-PSA}$  and the starting material.

**(R,S)-PSA·PCA**

**Figure J.1** DSC curve of (R,S)-PSA·PCA and the starting materials.

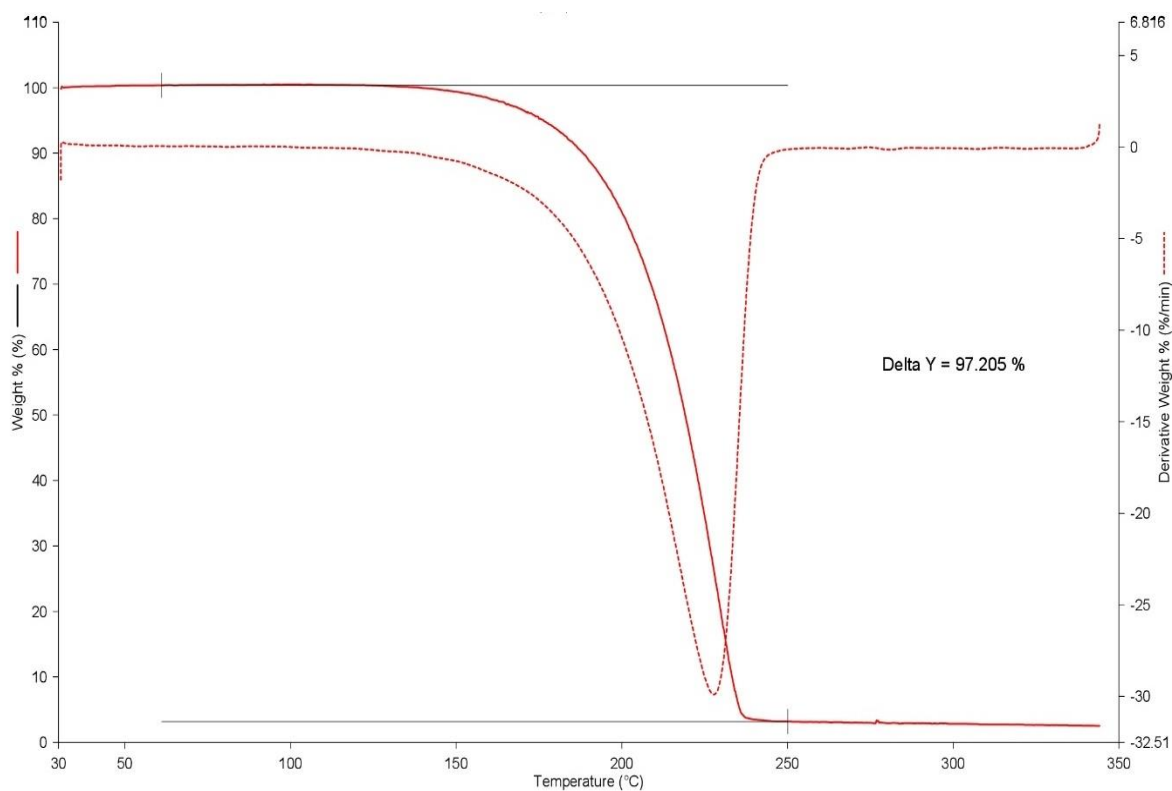


**Figure J.2** TG curve of (R,S)-PSA·PCA

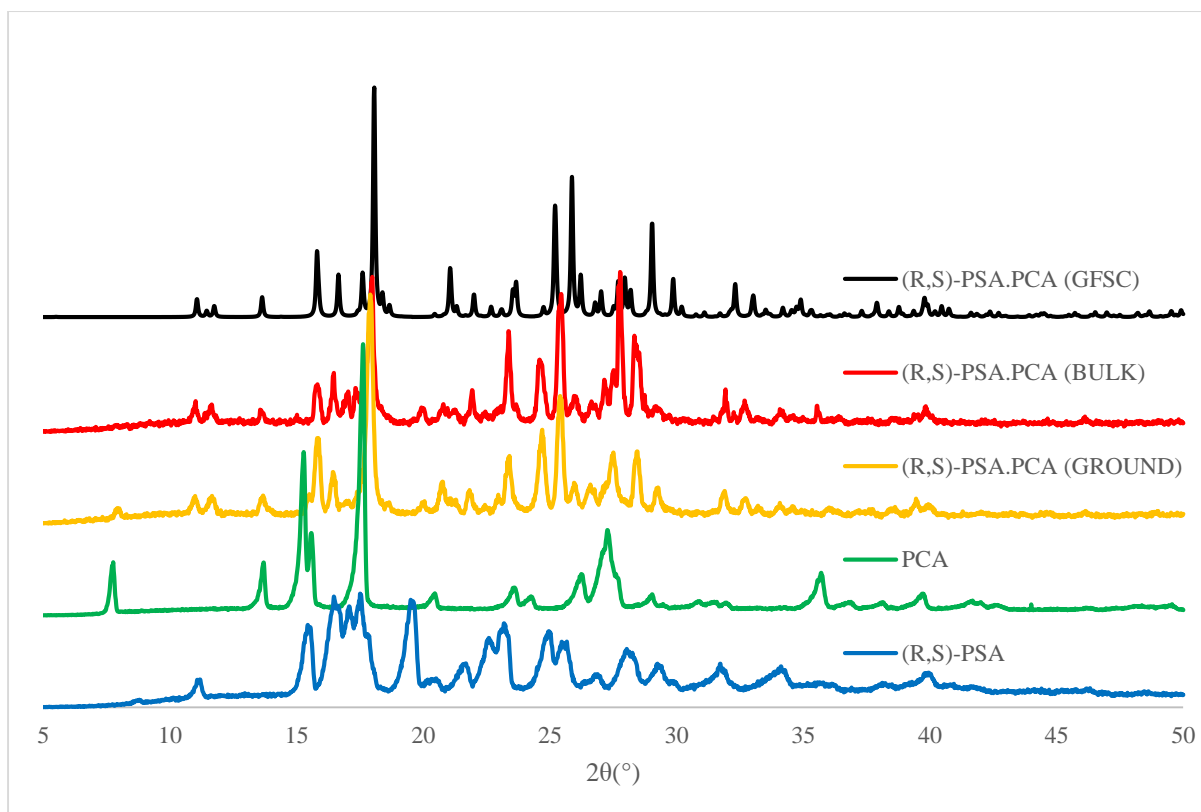


**Figure J.3** PXR D curve of (R,S)-PSA·PCA and the starting materials.

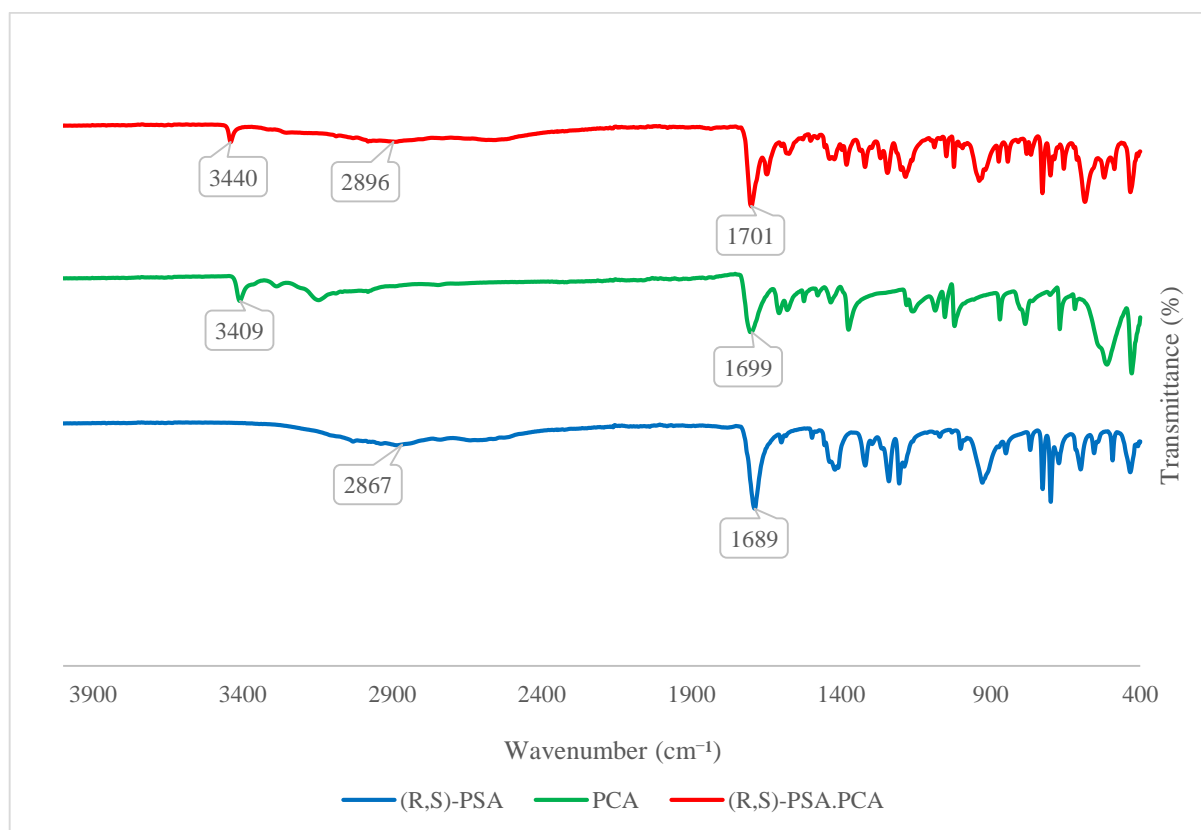


**Figure J.4** IR curve of (R,S)-PSA·PCA and the starting materials.

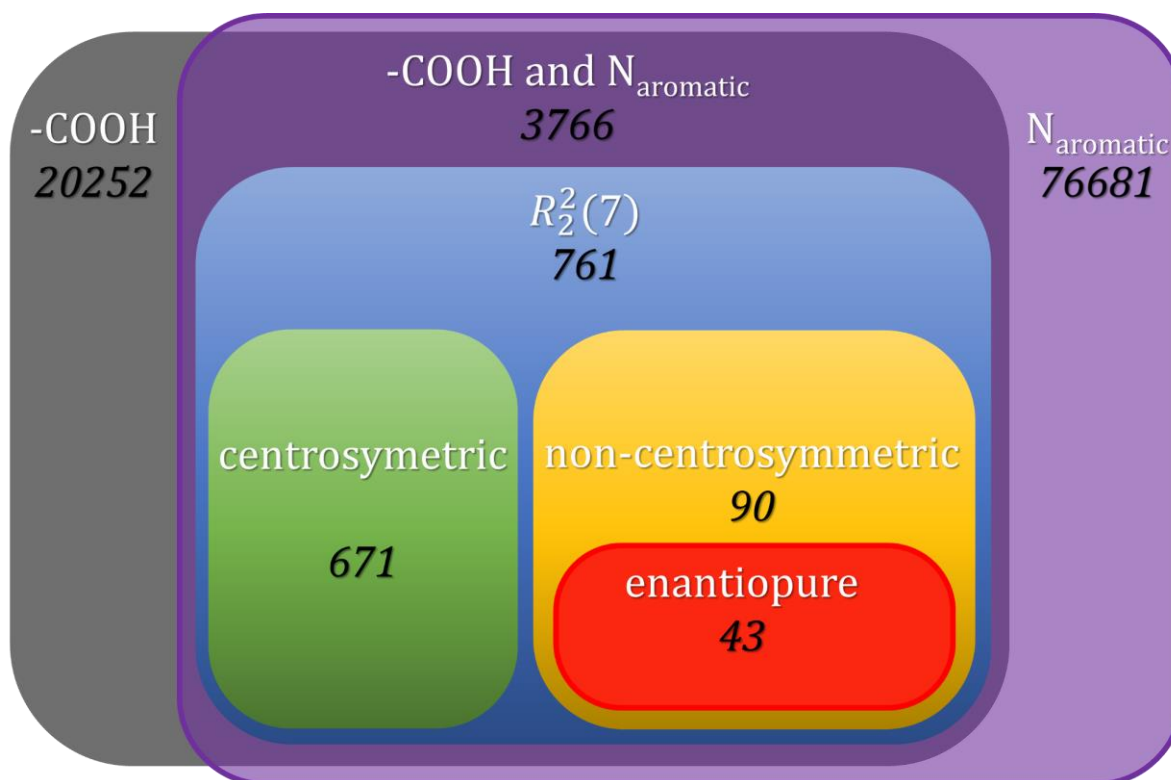


**Figure K.1** Occurrence of carboxylic acid and pyridine moieties, and their combination in the CSD (Organic & Inorganic)

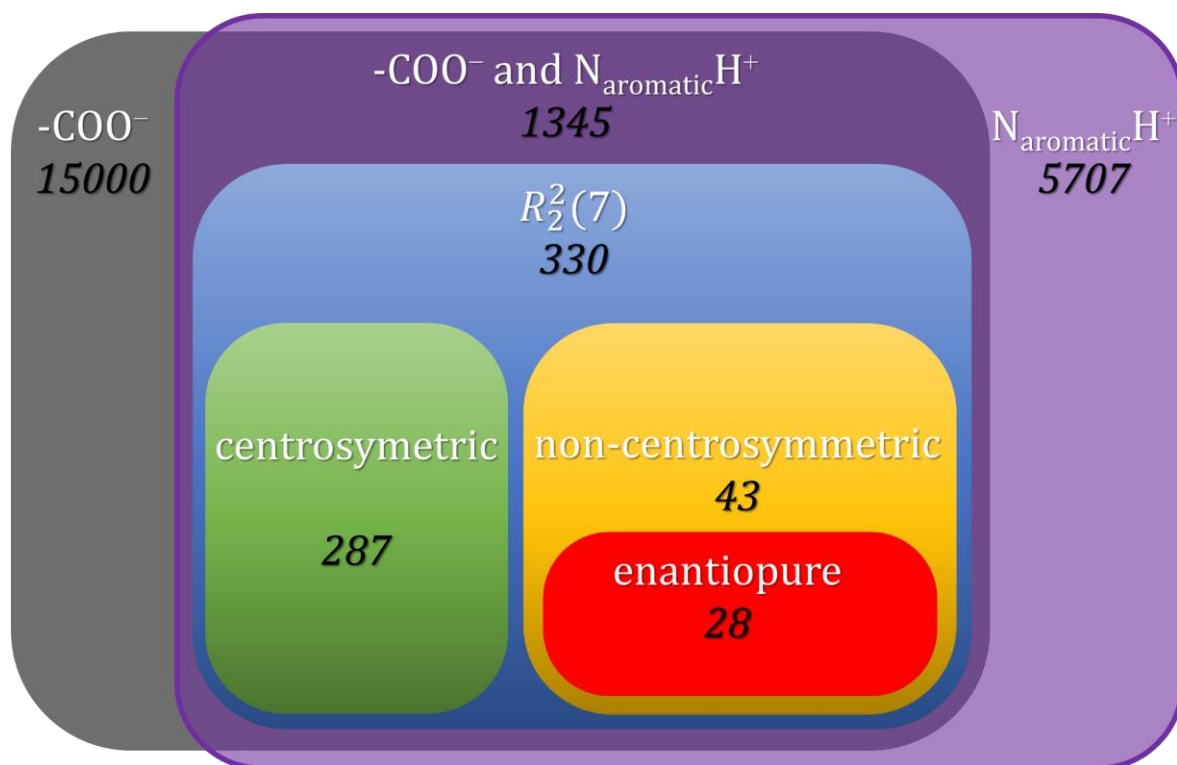


**Figure K.2** Occurrence of carboxylate and pyridinium moieties, and their combination in the CSD (Organic & Inorganic)